

## **Copyright Warning & Restrictions**

The copyright law of the United States (Title 17, United States Code) governs the making of photocopies or other reproductions of copyrighted material.

Under certain conditions specified in the law, libraries and archives are authorized to furnish a photocopy or other reproduction. One of these specified conditions is that the photocopy or reproduction is not to be “used for any purpose other than private study, scholarship, or research.” If a user makes a request for, or later uses, a photocopy or reproduction for purposes in excess of “fair use” that user may be liable for copyright infringement,

This institution reserves the right to refuse to accept a copying order if, in its judgment, fulfillment of the order would involve violation of copyright law.

**Please Note: The author retains the copyright while the New Jersey Institute of Technology reserves the right to distribute this thesis or dissertation**

Printing note: If you do not wish to print this page, then select “Pages from: first page # to: last page #” on the print dialog screen

The Van Houten library has removed some of the personal information and all signatures from the approval page and biographical sketches of theses and dissertations in order to protect the identity of NJIT graduates and faculty.

## **ABSTRACT**

### **RODENT TESTING DEVICE SURROGATE FOR SHOCKWAVE BLAST TESTING**

**by**

**Anthony C. Misistia**

Many laboratories around the world are conduct shockwave blast injury tests on rodents to simulate blast traumatic brain injury (TBI). Each of these laboratories has different techniques for creating the shockwave blasts as well as positioning the rats. There is no device to determine whether or not the rodent animal models actually experiences a true blast wave in a given set up. This device was developed as a method for verifying rodents undergoing true shockwave blasts through biometrics, instrumentation and the basic biomechanical responses a rodent experiences during such tests. Since the goal of shockwave blast testing is to replicate the live-fire conditions, it is important to have loads of biomechanical authenticity.

A rodent test device (RTD) is developed to simulate the loading conditions of rats under shockwave blasts. At the most basic level the RTD is the same size and shape as a Sprawgue-Dawley rat so that it can be easily placed into a given laboratory set up that conducts shockwave blast research on rodents. Fidelity to the shape, size, weight and fundamental mechanics of a rat were important considerations in the development process given the range of diversity found in different laboratories.

**RODENT TESTING DEVICE SURROGATE  
FOR SHOCKWAVE BLAST TESTING**

**by**

**Anthony C. Misistia**

**A Thesis  
Submitted to the Faculty of the  
New Jersey Institute of Technology  
in Partial Fulfillment of the Requirements for the Degree of  
Master of Science in Biomedical Engineering**

**Department of Biomedical Engineering**

**January 2016**

**Approval Page**

**RODENT TESTING DEVICE SURROGATE  
FOR SHOCKWAVE BLAST TESTING**

**Anthony C. Misistia**

---

Dr. Namas Chandra, Thesis Advisor Date  
Director of NJIT Center for Biomechanics, Materials and Medicine;  
Professor of Biomedical Engineering, NJIT

---

Dr. Bryan Pfister, Committee Member Date  
Department Chair of Biomedical Engineering, NJIT

---

Dr. Maciej Skotak, Committee Member Date  
Assistant Research Professor, NJIT

## **BIOGRAPHICAL SKETCH**

**Author:** Anthony C. Misistia

**Degree:** Master of Science

**Date:** January 2016

### **Undergraduate and Graduate Education:**

- Master of Science in Biomedical Engineering  
New Jersey Institute of Technology, Newark, NJ 2016
- Bachelor of Science in Biomedical Engineering  
New Jersey Institute of Technology, Newark, NJ 2012

**Major:** Biomedical Engineering

*This is dedicated to my family. Thank you for your love, support and faith in me.  
The confidence and strength you gave me were just as important as good data  
was to complete this project.*

## **ACKNOWLEDGMENT**

Thanks to my advisor Dr. Namas Chandra for his guidance and tutelage in the subjects of traumatic brain injury mechanics and shockwave blast mechanics. Also I would like to express my gratitude to my committee Dr. Bryan Pfister and Dr. Maciej Skotak who provided me with endless insight into the world of hands on scientific investigation. I would like to thank Dr. Aravind Sundaramurthy for his technical advice and my peers in the lab Matthew Kuriakose, Eren Alay, Sudepto Kahali, Brian Swenson, Praveenkumarbaba Siddabattuni, and also Daniel Younger for lending me a hand with conducting the tests and fine tuning technical issues. Thank you.



## TABLE OF CONTENTS

Chapter		Page
1	INTRODUCTION.....	1
1.1	Objective.....	1
1.2	Background.....	1
2	DEVICE REQUIREMENTS .....	6
3	DESIGN METHODOLOGY.....	6
3.1	Design Overview .....	7
3.2	Head.....	7
3.2.1	Obtaining Sample Head .....	8
3.2.2	Deconstruction.....	11
3.2.3	Adaption for Instrumentation.....	14
3.3	Body.....	17
3.3.1	Obtaining Body Geometry Samples.....	19
3.3.2	Establishing Normal Geometry.....	22
3.3.3	Designing 50 <sup>th</sup> Percentile Body.....	24
3.3.4	Designing 90 <sup>th</sup> Percentile Body.....	27
3.3.5	Designing 95 <sup>th</sup> Percentile Body.....	29
3.4	Mass.....	31
3.4.1	Obtaining Mass Samples.....	31
3.4.2	Establishing Normality.....	32
3.4.3	Finding 50 <sup>th</sup> , 90 <sup>th</sup> , 95 <sup>th</sup> Percentile Mass.....	33
3.4.4	Reconciling Difference in Mass.....	34

<b>Chapter</b>	<b>TABLE OF CONTENTS (Continued)</b>	<b>Page</b>
4	Prototype Development.....	36
4.1	Manufacturing.....	36
4.1.1	Material Selection.....	37
4.1.2	Mold Design.....	40
4.1.3	Casting.....	42
4.1.4	Compiling Parts.....	43
4.2	Instrumentation.....	43
5	Testing.....	47
6	Conclusion .....	51
6.1	Results.....	51
6.1.1	Peak Overpressures.....	51
6.1.2	Impulses.....	54
6.1.3	Accelerations.....	56
6.1.4	Velocities.....	58
6.2	Summary.....	61
6.3	Future.....	62
	APPENDIX A RAW GEOMETRIC DATA OF THE RODENT BODY.....	63
	APPENDIX B COLLECTED AND SORTED RODENT MASS DATA.....	86
	APPENDIX C NORMALITY DATA.....	88
	APPENDIX D PRESSURE AND TIME RAW DATA.....	99

## LIST OF TABLES

<b>Table</b>	<b>Page</b>
3.1 Lengths between points of interest in the head form.....	<b>12</b>
3.2 Heights and widths at points of interest in the head form.....	<b>12</b>
3.3 50 <sup>th</sup> percentile rat dimensions.....	<b>25</b>
3.4 90 <sup>th</sup> percentile rat dimensions.....	<b>27</b>
3.5 95 <sup>th</sup> percentile rat dimensions.....	<b>29</b>
3.6 Masses expected for 50 <sup>th</sup> , 90 <sup>th</sup> , and 95 <sup>th</sup> percentile.....	<b>34</b>
3.7 Calculated Void Volumes of RTD Body .....	<b>35</b>
4.1 Properties of Polyurethane.....	<b>39</b>
A.1 Length in millimeters between points raw data.....	<b>63</b>
A.2 Length in millimeters between base of neck and end of neck with outliers removed.....	<b>64</b>
A.3 Length in millimeters between neck and shoulder outliers removed.....	<b>65</b>
A.4 Length between shoulder and last rib in millimeters outliers removed.....	<b>66</b>
A.5 Length in millimeters between last rib and pelvis outliers removed.....	<b>67</b>
A.6 Length in millimeters between pelvis and thigh outliers removed.....	<b>68</b>
A.7 Length in millimeters between thigh and tail base, outliers removed.....	<b>69</b>
A.8 Height at varying points in the body raw data .....	<b>70</b>
A.9 Height at base of neck in millimeters with outliers removed.....	<b>71</b>
A.10 Height at end of neck in millimeters with outliers removed.....	<b>72</b>

**LIST OF TABLES**  
**(Continued)**

A.11	Height at shoulder in millimeters with outliers removed.....	<b>73</b>
A.12	Height at last rib in millimeters with outliers removed.....	<b>74</b>
A.13	Height at pelvis in millimeters with outliers removed.....	<b>75</b>
A.14	Height at thigh in millimeters with outliers removed.....	<b>76</b>
A.15	Height at base of tail in millimeters with outliers removed.....	<b>77</b>
A.16	Width raw data at varying points in millimeters.....	<b>78</b>
A.17	Width in millimeters at the base of the neck with outliers removed	<b>79</b>
A.18	Width in millimeters at the end of the neck with outliers removed.	<b>80</b>
A.19	Width in millimeters at the shoulder with outliers removed.....	<b>81</b>
A.20	Width in millimeters at the last rib with outliers removed.....	<b>82</b>
A.21	Width in millimeters at the pelvis with outliers removed.....	<b>83</b>
A.22	Width in millimeters at the thigh with outliers removed.....	<b>84</b>
A.23	Width in millimeters at the base of the tail with outliers removed.	<b>85</b>
B.1	Masses of rats both raw data and outliers removed in grams.....	<b>86</b>

## LIST OF FIGURES

Figures		Page
1.1	Friedlander Wave of a shock front as depicted by a pressure versus time graph. The Sharp peak to the left represents the overpressure of the shockfront while the proceeding pressure that is on the decay represents the blast winds. The baseline is representing the atmospheric pressure. Pressures above the baseline are referred to as the overpressure and those under the baseline are the underpressure. There are three main ways to categorize an explosive blast wave's traits: shock intensity, duration and impulse. The shock intensity is characterized as the value of the peak overpressure. The duration of the blast wave is the value from the peak to the baseline pressure. The impulse is defined as the area beneath the shockwave from the point of the overpressure peak to the point where it decays to the baseline...	2
3.1	Digital three dimensional model of the rodent skin outer layer obtained from an original MRI scan of the animal into the form of a stereolithographic image file as seen here.....	10
3.2	Physical three dimensional models of three layers of a rat's head. From top to bottom they are the skin, the skull and the brain printed in white acrylonitrile butadiene styrene and used for physical measurements and size feasibility tests in the real world.....	11
3.3	Simplified solid model of rat head as a digital rendering made using the swept blend function through the ellipses drawn from the sample size at structurally significant parts of the head. The model was rendered in Creo Parametric 2.0 software.....	13
3.4	Simplified rat head model with instrumentation features included depicted as a digital, three-dimensional rendering. Front sensor hole is shown at the bottom left corner and the angled sensor cavity is shown above it. A section is cut away to view the hollow of the skull at the top where the cables will go through .....	16
3.5	Drawing of the first draft of the RTD body.....	18

<b>Chapter</b>	<b>LIST OF FIGURES (continued)</b>	<b>Page</b>
3.6	Drawing of reference ruler device for assisting in image analysis of rats. It was necessary to consider the natural way the body would lay upon the surface or up against a wall and how that would distort the measurements. As a result the ruler was given a solid floor but a wall with a large window cut out so that any extra mass from the thighs would not be impeded or squished up by a wall. The ruler was made in a bright color to contrast with the white fur of the rat so that it would be easier to spot certain landmarks against the background of red. Views from top left going clockwise are isometric, top, back, left.....	<b>20</b>
3.7	Photos of a rat resting upon the ruler device. Above is the bird's eye view and below is a side on view. This rat was anaesthetized and all of its muscles are relaxed. Its head is shaved on the top for easy instrumentation for another experiment.....	<b>21</b>
3.8	Figures of observed and expected data before and after outlier removal. The x axis depicts the z-values and the y axis is millimeters of length between two points in the body. After the outliers were removed, the data points followed a normal distribution much better as it was very close to the expected outcome line.....	<b>24</b>
3.9	50 <sup>th</sup> percentile Sprague-Dawley drawings with dimensions in millimeters. Views starting top right going clockwise are top, front and isometric.....	<b>26</b>
3.10	90 <sup>th</sup> percentile Sprague-Dawley drawings with dimensions in millimeters. Views starting top right going clockwise are top, front and isometric .....	<b>28</b>
3.11	95 <sup>th</sup> percentile Sprague-Dawley drawings with dimensions in millimeters. Views starting top right going clockwise are top, front and isometric.....	<b>30</b>
3.12	Figure of observed and expected data versus z-values with outliers removed. The two figures are consistent with shape and values.....	<b>30</b>
4.1	A demonstration of the build tank size of the 3D printer in the program Cura 2.0 used to arrange parts intended for printing.....	<b>37</b>

<b>Chapter</b>	<b>LIST OF FIGURES (Continued)</b>	<b>Page</b>
4.2	Drawing of half of the mold with views from top left: isometric, bottom, left .....	<b>42</b>
4.3	Schematic of a Kulite XCL-072 Pressure Sensor.....	<b>44</b>
4.4	Schematic of a Kulite XCL-152 Pressure Sensor.....	<b>44</b>
4.5	Endevco 7264C piezoresistive accelerometer schematic.....	<b>45</b>
5.1	The harness clockwise from top left: right, top, isometric and front.....	<b>47</b>
5.2	RTD inside the shock tube with a harness.....	<b>48</b>
5.3	Rat cadaver inside shock tube without harness.....	<b>49</b>
5.4	RTD unstrapped outside shock tube barrel.....	<b>50</b>
6.1	Overpressures at nose sensor.....	<b>52</b>
6.2	Overpressures at head sensor.....	<b>53</b>
6.3	Incident pressures.....	<b>54</b>
6.4	Nose Impulse.....	<b>55</b>
6.5	Head Impulse.....	<b>55</b>
6.6	Incident Impulse.....	<b>56</b>
6.7	Peak Positive Acceleration.....	<b>57</b>
6.8	Peak Negative Acceleration.....	<b>57</b>
6.9	Velocities for 2 membrane, inside shock tube, secured by strap...	<b>58</b>
6.10	Velocities for 2 membrane, inside shock tube, not secured by strap.....	<b>59</b>
6.11	Velocities for 2 membrane, outside shock tube, secured by a strap.....	<b>59</b>

<b>Chapter</b>	<b>LIST OF FIGURES (Continued)</b>	<b>Page</b>
6.12	Velocities for 2 membrane, outside shock tube, not secured by strap.....	60
6.13	Velocities for 4 membrane, inside shock tube, not secured by strap.....	60
C.1	Normality of data for percentile versus neck length in mm.....	88
C.2	Normality of data for percentile versus neck to shoulder length in mm.....	89
C.3	Normality of data for percentile versus shoulder to rib length in millimeters.....	89
C.4	Normality of data for percentile versus rib to pelvis length in millimeters.....	90
C.5	Normality of data for percentile versus pelvis to thigh length in millimeters.....	90
C.6	Normality of data for percentile versus thigh to tail base length in millimeters.....	91
C.7	Normality of data for percentile base of neck height in mm.....	91
C.8	Normality of data for percentile end of neck height in millimeters.	92
C.9	Normality of data for percentile shoulder height in millimeters.....	92
C.10	Normality of data for percentile rib height in millimeters.....	93
C.11	Normality of data for percentile pelvis height in millimeters.....	93
C.12	Normality of data for percentile thigh height in millimeters.....	94
C.13	Normality of data for percentile tail base height in millimeters.....	94
C.14	Normality of data for percentile base of neck width in millimeters.	95
C.15	Normality of data for percentile end of neck width in millimeters...	95
C.16	Normality of data for percentile shoulder width in millimeters.....	96



<b>Chapter</b>	<b>LIST OF FIGURES (Continued)</b>	<b>Page</b>
C.17	Normality of data for percentile rib width in millimeters.....	<b>96</b>
C.18	Normality of data for percentile pelvis width in millimeters.....	<b>97</b>
C.19	Normality of data for percentile thigh width in millimeters.....	<b>97</b>
C.20	Normality of data for percentile tail base width in millimeters.....	<b>98</b>
C.21	Mass normality.....	<b>98</b>
D.1	1535 acceleration versus time of shot .....	<b>100</b>
D.2	1535 pressure versus time of nose, head and incident sensors....	<b>100</b>
D.3	1536 acceleration versus time of shot. ....	<b>101</b>
D.4	1536 pressure versus time of nose, head and incident sensors...	<b>101</b>
D.5	1537 acceleration versus time of shot .....	<b>102</b>
D.6	1537 pressure versus time of nose, head and incident sensor.....	<b>102</b>
D.7	1538 Acceleration Versus Time of Shot 1535 .....	<b>103</b>
D.8	1538 pressure versus time of nose, head and incident sensors...	<b>103</b>
D.9	1539 acceleration versus time of shot 1535 .....	<b>104</b>
D.10	1539 pressure versus time of nose, head and incident sensors...	<b>104</b>
D.11	1540 acceleration versus time of shot 1535 .....	<b>105</b>
D.12	1540 pressure versus time of nose, head and incident sensors...	<b>105</b>
D.13	1541 acceleration versus time of shot .....	<b>106</b>
D.14	1541 pressure versus time of nose, head and incident sensors...	<b>106</b>
D.15	1542 acceleration versus time of shot .....	<b>107</b>
D.16	1542 pressure versus time of nose, head and incident sensors...	<b>107</b>
D.17	1543 acceleration versus time of shot .....	<b>108</b>

<b>Chapter</b>	<b>LIST OF FIGURES (Continued)</b>	<b>Page</b>
D.18	1543 pressure versus time of nose, head and incident sensors...	<b>108</b>
D.19	1544 acceleration versus time of shot 1535 .....	<b>109</b>
D.20	1544 pressure versus time of nose, head and incident sensors...	<b>109</b>
D.21	1545 acceleration versus time of shot 1535 .....	<b>110</b>
D.22	1545 pressure versus time of nose, head and incident sensors...	<b>110</b>
D.23	1546 acceleration versus time of shot 1535 .....	<b>111</b>
D.24	1546 pressure versus time of nose, head and incident sensors ...	<b>111</b>
D.25	1547 acceleration versus time of shot .....	<b>112</b>
D.26	1547 pressure versus time of nose, head and incident sensors...	<b>112</b>
D.27	1548 acceleration versus time of shot .....	<b>113</b>
D.28	1548 pressure versus time of nose, head and incident sensors...	<b>113</b>
D.29	1549 acceleration versus time of shot .....	<b>114</b>
D.30	1549 pressure versus time of nose, head and incident sensors...	<b>114</b>
D.31	1550 acceleration versus time of shot 1535 .....	<b>115</b>
D.32	1550 pressure versus time of nose, head and incident sensors...	<b>115</b>
D.33	1551 acceleration versus time of shot .....	<b>116</b>
D.34	1551 pressure versus time of nose, head and incident sensors...	<b>116</b>
D.35	1552 acceleration versus time of shot .....	<b>117</b>
D.36	1552 pressure versus time of nose, head and incident sensors...	<b>117</b>
D.37	1553 acceleration versus time of shot .....	<b>118</b>

<b>Chapter</b>	<b>LIST OF FIGURES (Continued)</b>	<b>Page</b>
D.38	1553 pressure versus time of nose, head and incident sensors ...	<b>118</b>
D.39	1554 acceleration versus time of shot 1535 .....	<b>119</b>
D.40	1554 pressure versus time of nose, head and incident sensors...	<b>119</b>
D.41	1555 acceleration versus time of shot 1535 .....	<b>120</b>
D.42	1555 pressure versus time of nose, head and incident sensors...	<b>120</b>
D.43	1556 acceleration versus time of shot 1535 .....	<b>121</b>
D.44	1556 pressure versus time of nose, head and incident sensors...	<b>121</b>
D.45	1557 acceleration versus time of shot .....	<b>122</b>
D.46	1557 pressure versus time of nose, head and incident sensors...	<b>122</b>
D.47	1558 acceleration versus time of shot .....	<b>123</b>
D.48	1558 pressure versus time of nose, head and incident sensors...	<b>123</b>
D.49	1559 acceleration versus time of shot .....	<b>124</b>
D.50	1559 pressure versus time of nose, head and incident sensors...	<b>124</b>
D.51	1560 acceleration versus time of shot 1535 .....	<b>125</b>
D.52	1560 pressure versus time of nose, head and incident sensors...	<b>125</b>
D.53	1561 acceleration versus time of shot 1535 .....	<b>126</b>
D.54	1561 pressure versus time of nose, head and incident sensors...	<b>126</b>
D.55	1562 acceleration versus time of shot 1535 .....	<b>127</b>
D.56	1562 pressure versus time of nose, head and incident sensors...	<b>127</b>
D.57	1563 acceleration versus time of shot .....	<b>128</b>
D.58	1563 pressure versus time of nose, head and incident sensors...	<b>128</b>

<b>Chapter</b>	<b>LIST OF FIGURES (Continued)</b>	<b>Page</b>
D.60	1564 pressure versus time of nose, head and incident sensors...	<b>129</b>
D.61	1565 acceleration versus time of shot .....	<b>130</b>
D.62	1565 pressure versus time of nose, head and incident sensors...	<b>130</b>
	REFERENCES.....	<b>131</b>

## **Chapter 1**

### **INTRODUCTION**

#### **1.1 Objective**

The objective of this thesis is to develop a device that measures and validates the biomechanical loading conditions presence experienced by live rodent models during shockwave blast test conditions including pressures, velocities, and acceleration.

#### **1.2 Background Information**

The nature of warfare in recent times has become drastically different. New types of firepower have been added to the clash and as a result, many unexpected complications have arisen. Specifically, firepower in the form of explosives such as improvised explosive devices (IED) and heavy artillery has led to a significantly higher amount of exposures to blast shockwaves. These numbers of exposures have been especially significant with the recent and continuing military operations abroad where United States military personnel encounters the detonations of many different kinds of IED which could produce a variety of bodily harm.

A blast wave is formed when a volume of gases, that form as a result of the chemical reactions within a chemical explosive such as those found in IEDs, expand around and this expansion effectively pushes back the atmosphere surrounding an explosion. The high pressure portion of the atmosphere moves faster than that which hasn't been compressed by the expansion wave from the initial gases. As this blast wave approaches a sudden peak value of pressure it

then is followed by an immediate decay. (Kinney and Graham) A typical blast wave in the form of a pressure vs. time graph is featured in Figure 1.1. This standard wave pattern is known as a Friedlander Wave.

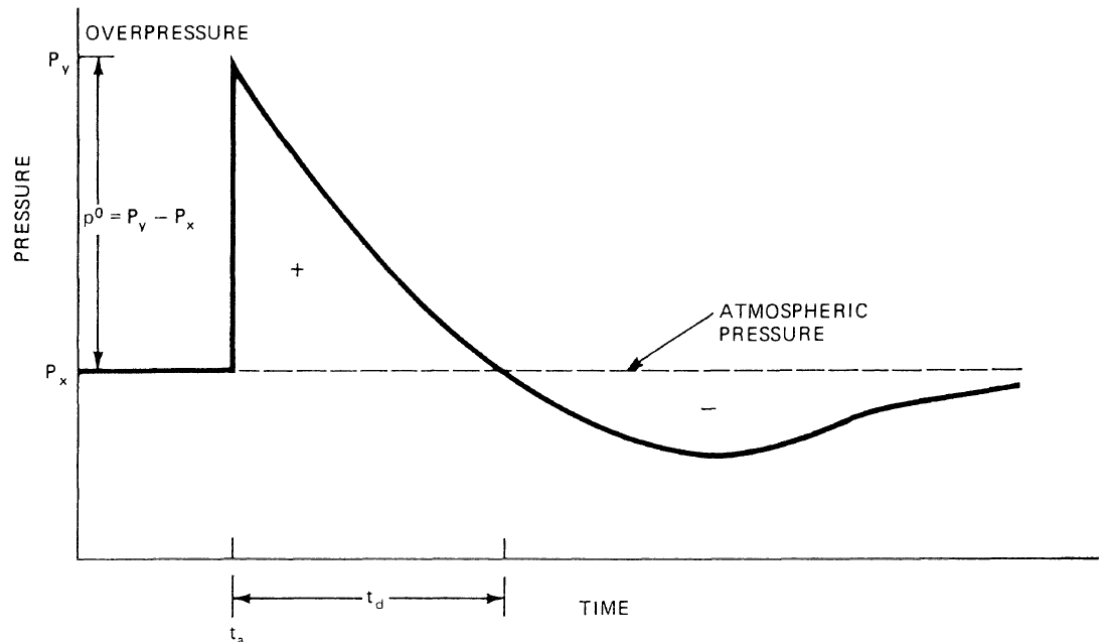


**Figure 1.1** Friedlander Wave of a shock front as depicted by a pressure versus time graph. The Sharp peak to the left represents the overpressure of the shockfront while the proceeding pressure that is on the decay represents the blast winds. The baseline is representing the atmospheric pressure. Pressures above the baseline are referred to as the overpressure and those under the baseline are the underpressure. There are three main ways to categorize an explosive blast wave's traits: shock intensity, duration and impulse. The shock intensity is characterized as the value of the peak overpressure. The duration of the blast wave is the value from the peak to the baseline pressure. The impulse is defined as the area beneath the shockwave from the point of the overpressure peak to the point where it decays to the baseline.

Source: Kinney, Gilbert Ford and Kenneth Judson Graham. *Explosive Shocks in Air*. New York: Springer Science + Business Media, 1985. pp. 91.

The field effects of a shockwave blast on our military personnel are linked to a growing number of negative long and short term health effects. These effects include but are not limited to mild traumatic brain injury (TBI), moderate TBI and

pulmonary injury (S.T. Ahlers). These injuries are caused by not only the extreme pressures experienced during a blast wave but also by the damaging effects of involuntary acceleration of the head and neck experienced during the blast winds during the non-linear decay phase of the blast following the shock front (S.T. Ahlers).

It is difficult to use actual explosions in the laboratory for reasons of safety, expense and lack of repeatability (Sundaramurthy and Chandra). One popular method of simulating field conditions of an explosion without using actual explosions is the use of a compressed gas based shock tube. In its most basic form, a compressed gas shock tube is composed of a driver section and a driven section. The driver section is the location where the gas is compressed into before being released manually or by rupture of a barrier that is containing it. The driven section is the area where the atmosphere would in theory be compressed by the rapidly expanding gases coming out of the driver section (Sundaramurthy and Chandra). This compressed atmosphere will then theoretically form the shockwave blast. Certain labs also employ other specific features in shock tubes to theoretically optimize the ability to generate and fine tune the properties of a shockwave blast. Such features include a transitional section to help form the wave structure when going from driver to driven section.

Due to the rapidly growing incidents of blast exposures faced by men and women everyday around the world, there is an increased demand for understanding of the mechanisms and effects of shockwave blasts on a model. In order to conduct research on the exact physiological effects of shockwave

blasts, researchers seek to replicate the conditions of field blasts on smaller mammalian models such as rats and mice. Some negative health conditions in rodent models include loss of coordination, behavioral changes, retardation of spatial learning and acquisition of data impairment, amnesia (S.T. Ahlers) as well as post-concussive syndromes that has overlapping symptoms as PTSD such as fatigue, poor sleep, irritability, and impaired concentration in humans (Elder and Cristian).

Be it for an acceleration test on the mechanics of a rat or the pressures registered at the skull of a rodent, there are countless studies put out in recent time that implement some form or another of placing a rodent model into a plethora of different rigs that are believed to replicate field conditions of a blast as well as position the rat in such a way that would be an analog for the humans who are the ultimate goal of understanding the effects of physiologically. Hundreds of laboratories around the world are conducting what they claim to be shockwave blast injury tests on rodents.

Each of these labs has different techniques for creating the blasts as well as a different location and position for the rat to experience it. The sizes and shapes of the shock tubes vary greatly in many cases. The driven sections have been listed as small and cylindrical as having a 22.62cm<sup>2</sup> circumference (Budde, Shah and McCrea) to as large as a 71.12cmx71.12cm square profile (Sundaramurthy and Chandra). There is also different philosophy to what could be customized to lead to certain desired characteristics per outcome. For example in the case of shock intensity, many labs will employ a thicker barrier



between the driver and driven sections by adding more or thicker membranes (Sundaramurthy and Chandra). In other cases, some researchers sought the same results by simply moving the specimen further from the breach between the driver and driven sections (Budde, Shah and McCrea). There is also a distinction in each lab whether the test subject needs to be inside the shock tube driven section (Cernak) or somewhere outside of the shock tube (Budde, Shah and McCrea).

There has yet to be a universal method or device to determine whether or not the rat actually experiences a true blast wave in a given set up. Because of this, there have been a number of papers published regarding injury mechanisms during a blast that have been considered founded on the false premises of true shockwave presence. Many of the studies show a lack of instrumentation close enough to the rodent, optimally on the rodent itself, to confidently confirm the presence of a Friedlander wave actually being present in the study. As a result the resulting data regarding the effects of a shockwave cannot be satisfactorily accepted because it isn't necessarily clear if there was in fact a shockwave's presence that could have been the insult to the injury.

## **CHAPTER 2**

### **DEVICE REQUIREMENTS**

The ultimate goal of the device is to verify rodents going through a true shockwave blast in a given experimental set up. These experiments have the aim of blast testing to replicate the live-fire conditions. In order to be a proper surrogate for rodent models that are undergoing these experiments, there are three main concerns that will be addressed in every portion of the design process.

The first requirement is biofidelity with respect to mechanics. The device needs to be true to the size, shape, geometry and mass distribution as would be found in the live rat model. This is because size and shape could affect the way that the shock front interacts with a given body. Mass could also affect acceleration factors. The second is the ability to be instrumented. Specifically this refers to sensors that measure pressure, acceleration or anything else that may serve to quantify the loading conditions that the model may experience. The final design consideration is the ability to be durable. The device is not meant to be disposable or single use. It would be most useful as something that could be used many times before needing to be replaced.

## **CHAPTER 3**

### **DESIGN METHODOLOGY**

#### **3.1 Design Overview**

The design method can be broken down into several portions. The first is the head. The design was gleaned from data from a real rat model. This was then simplified and given small design features that allow for it to be instrumented. The next portion was the body. The dimensions of the body were found using real rat models and the data was normalized and found at the different relevant body percentile sizes along the normal curve. The design was also made to include adaptations to facilitate instrumentation. The final section was the mass of the rat. This is where real data of rat masses were obtained and organized to account for the different percentiles size rats.

#### **3.2 Head Design**

The process of designing a head had several key focuses. These were biofidelity in shape, prototype manufacture feasibility and also the ability to be properly instrumented and adapted to fit multiple types of sensors. Geometric biofidelity was an incredibly important consideration due to the angles a surface presents itself to a blast wave having a significant effect on the way the wave will act upon the body. It determines the amount of stagnation pressure a body will encounter as opposed to purely static pressure.

The head portion of the design was accomplished by obtaining the proper model, sampling the geometry, deconstructing the shape into a simpler form,

producing a series of sensors and experimenting with several forms of modular breakdowns to ease construction.

### **3.2.1 Obtaining Sample Head**

One of the problems faced by researchers who attempt to instrument a rat for many different sorts of measurements pertaining to the experience of a shockwave blast is the fur. It is easily deformable so that shape movement measurements taken during acceleration video analysis are often fraught with potential error. It provides very little as far as a stable surface to find landmarks and use them to record any movements a rodent may experience during blast winds. Another problem presented by the fur is its capacity for shedding. Shedding fur often gets in the way of instrumentation and can occasionally show up in videos. The nuisance of hair to making proper measurements, both physical and instrumental is dealt with the same way human measurements are dealt with in a surgical or non-invasive instrumentation setting. This method is shaving the site of interest and also clipping away any surrounding hair that may also interfere with the measurements.

When constructing a biofidelic model of a rat, there is a matter of feasibility and user friendliness that has to be taken into account. Though most of the rodents used in the testing of the effects of shockwave blasts are not the hairless variety, accounting for a fur layer in the most accurate way possible by micro-rooting wool by hand into a dermal layer would be extraneous. This is for several reasons. One is that it would take months of work to get the density of fur found

in the head of a rat. It is also because the different breeds and strains of rats used have a variation in the types of fur they present in hair thickness, length and density. Ultimately the work would have to be shaved off in patches of interest anyway. Because of these reasons, the entire layer of fur around the head was to be forgone in the design process.

The problem that was presented by the decision to not include a fur layer was obtaining accurate dimensions of a rat with a close and uniform shave. Electrical clippers are not the most precise when dealing with the small curves of a rodent head and depilatory products such as creams and waxes were likely to compromise the integrity of the measurements if they led to unintended consequences soft tissue decomposition or inflammation.

Rather than attempt to get a rough estimate of the dimensions with a patchy rat for reference, a non-physical reference was used in its place. The center for injury biomechanics, materials and methods (CIBM<sup>3</sup>) has used MRI and CT scans on rats to obtain imaging of real life rodent anatomy. These images were then separated into the layers of the outer skin, the skeleton and brain to be separate three dimensional models. The image slices of the rats were then converted into digital three-dimensional models using computer programs such as mimics as described in detail in the book "Brain Neurotrauma: Molecular, Neuropsychological and Rehabilitation Aspects." (Chandra and Sundaramurthy) . Figure 3.1 shows the rat's outer dermal layer in the form of a stereolithographic image as a result of the above process.

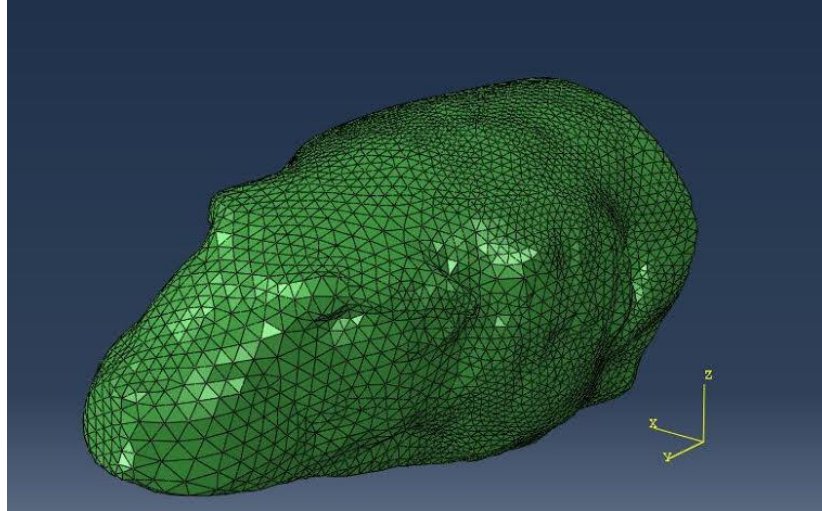


**Figure 3.1** Digital three dimensional model of the rodent skin outer layer obtained from an original MRI scan of the animal into the form of a stereolithographic image file as seen here.

These digital models were then converted into tangible physical models using a three dimensional printer to be worked with. The parts were printed in white acrylonitrile butadiene styrene (ABS) plastic to allow for easy marking during the measurement and design process with these being used as a reference. These physical models are shown in Figure 3.2 below.

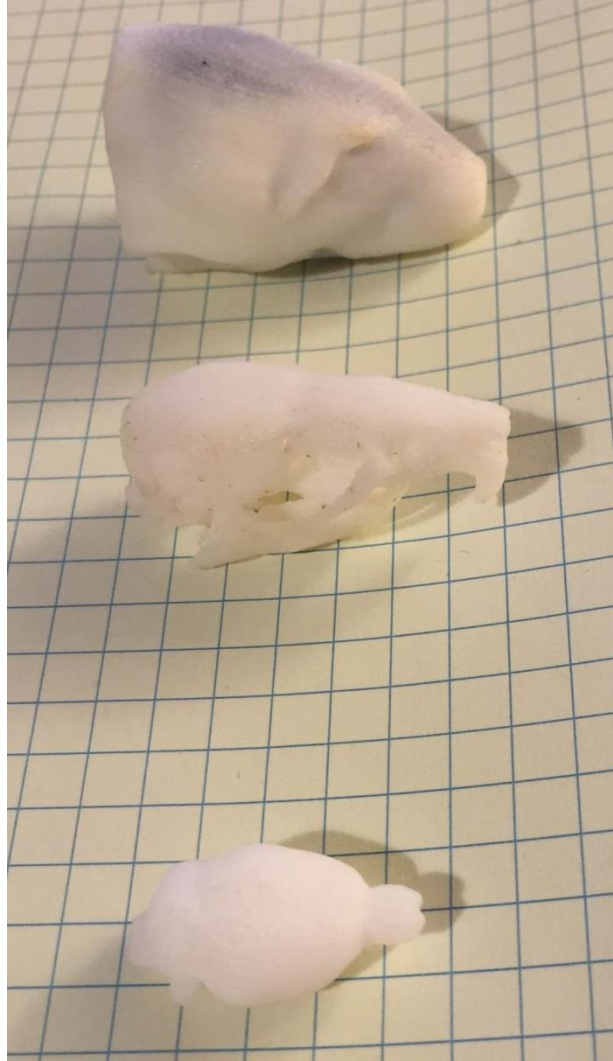


**Figure 3.2** Physical three dimensional models of three layers of a rat's head. From top to bottom they are the skin, the skull and the brain printed in white acrylonitrile butadiene styrene and used for physical measurements and size feasibility tests in the real world.

### **3.2.2 Deconstruction**

Once a physical model was obtained of a rat head without fur, the process of breaking the structure down into a simpler form that could still easily be manufactured began. This was done first by taking into consideration the landmarks of a rat's head. The chosen locations were the tip of the nose, the

stop (the proximal end of the animal's muzzle), the brow, the peak of the head, crown, and the edge of the skull. Measurements were taken at the length between these points. This data was collected into table 3.1 below.

**Table 3.1** The Lengths Between Points of Interest in the Head-form of the Rat

<b>Points</b>	<b>Locations</b>	<b>Length between (mm)</b>
1-2	Nose to stop	14.3
2-3	Stop to brow	10.2
3-4	Brow to peak	7.3
4-5	Peak to crown	10.3
5-6	Crown to edge	2.7

The widths and heights were then taken at these points in order to break the figure down into ellipsoid slices to simplify the geometry while still retaining much of the general angular shapes of the overall structure. These dimensions are listed in Table 3.2

**Table 3.2** Heights and Widths of the Head-form at Points of Interest

<b>Point</b>	<b>Location</b>	<b>Height (mm)</b>	<b>Width (mm)</b>
1	Nose	7.51	7.51
2	Stop	18.15	18.15
3	Brow	24.00	28.00
4	Peak	29.00	26.00
5	Crown	28.00	23.00
6	Edge	26.00	24.00

Using the program Creo Parametric 2.0, these ellipses were then input as individual sketches with the acquired distances between them set as the measured lengths. A continuous sweep from point to point then rendered the simplified head model as one solid piece. This piece is shown in Figure 3.3.



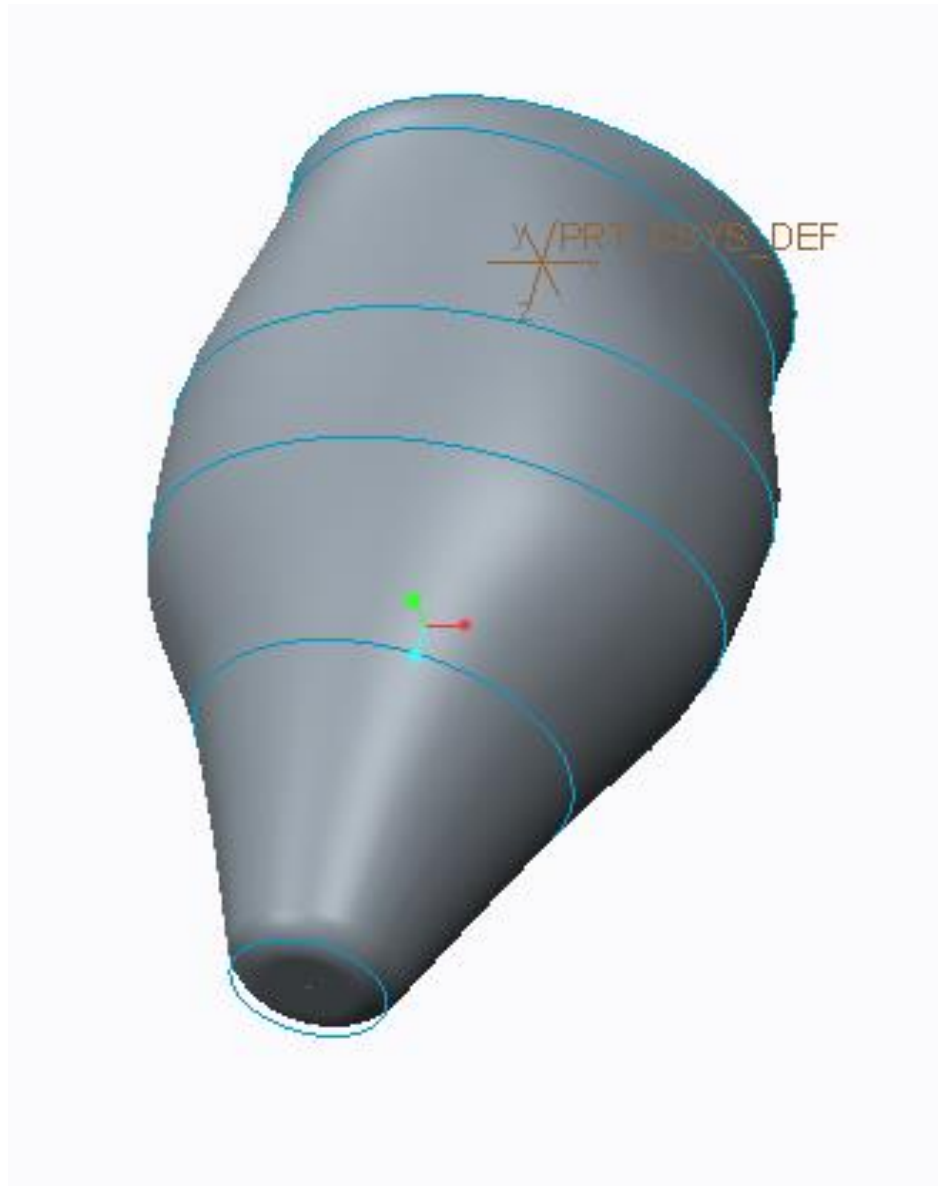


**Figure 3.3** Simplified solid model of rat head as a digital rendering made using the swept blend function through the ellipses drawn from the sample size at structurally significant parts of the head. The model was rendered in Creo Parametric 2.0 software.

### **3.2.3 Adaption for Instrumentation**

Once the bulk of the head was designed, consideration needed to be taken for how it would be instrumented. The process of choosing the sensors and the specific uses for each of the sensing elements will be discussed in depth in section 4.2 of this paper. This section is dedicated to the discussion of handling the practical design aspects of adapting the surrogate head model to accommodate these sensors.

At least two pressure sensors are needed for this device. The first will be at the very tip of the nose which will encounter the complete head on force of the blast. This is important to measure because whether the animal is positioned supine or prone, it is the first point of the rodent body to encounter a shockwave if it is placed head first. This is an indicator of not only how much pressure that particular point has but also, as it is the nose, it has a clear correlation to how much pressure could travel directly to the lungs of the animal through the open passageway of the nostrils. In order to instrument this part, a hole was made the same size as the sensor going from the end of the nose all the way through to where the neck would be in order to be able to run the cables through. Exposing the cables to the shock wave or subsequent blast winds could cause unnecessary noise in data collection.

Another hole was made to accommodate a second pressure sensor in the head. This hole however was not to be perfectly flat like the other but instead was to measure the pressure at the natural angle of the head at a specific location. The location chosen was the stop of the muzzle which is where the blast

wave would make contact closest to the brain first. In order to do this, the hole was made so that its circumference is tangential to the natural angle of the animal's muzzle. In doing this, a more precise angle of measurement can be used to determine whether or not the animal actually may have encountered a blast wave to that point in the head. This feature was also united with the cavity left for cable leads as to once again not expose the cables to the blast wave which could damage them or produce noise in the subsequent readings. The head including features to accommodate sensors is depicted in the Figure 3.4.

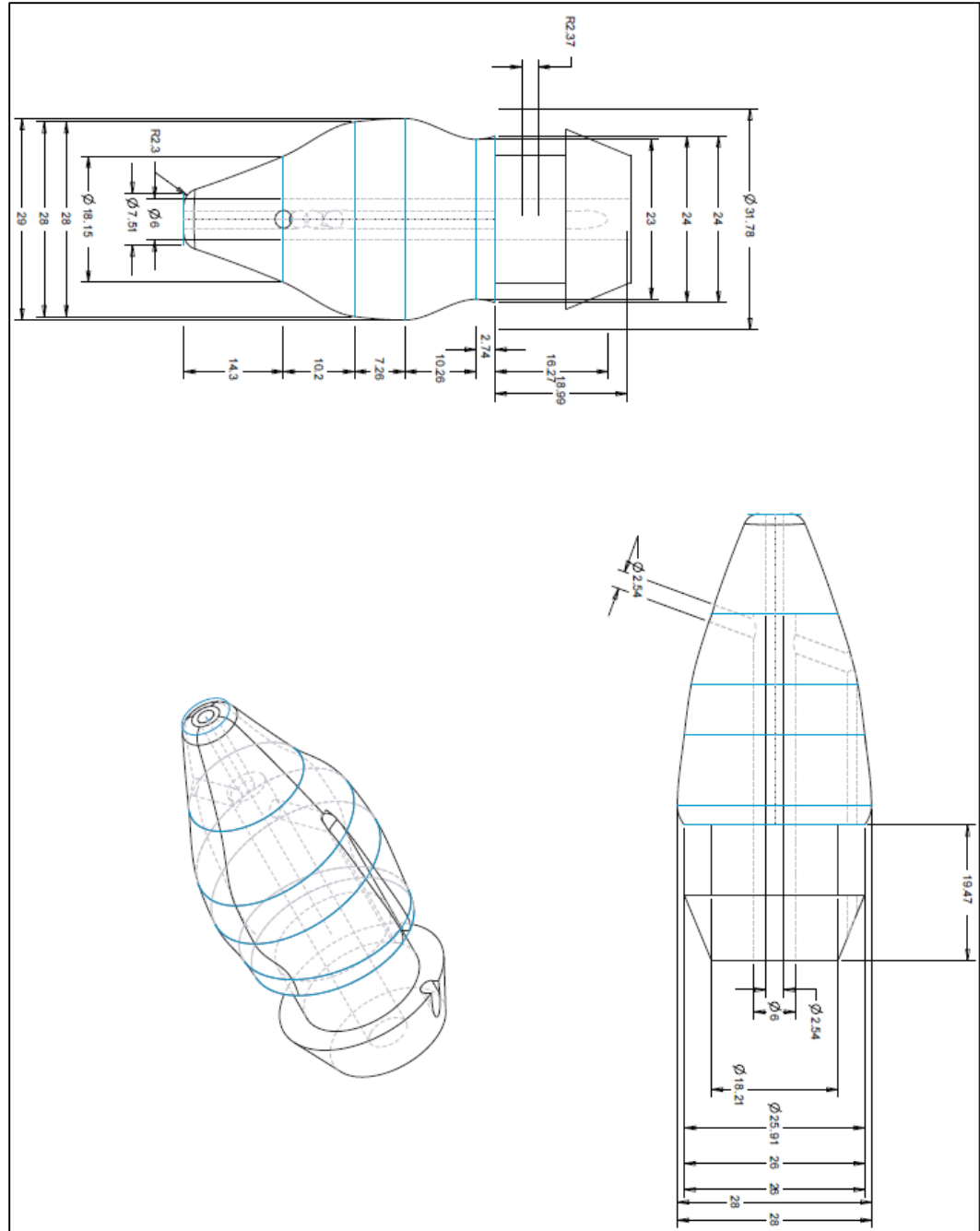


**Figure 3.4** Simplified rat head model with instrumentation features included depicted as a digital, three dimensional rendering. Front sensor hole is shown at the bottom left corner and the angled sensor cavity is shown above it. A section is cut away to view the hollow of the skull at the top where the cables will go through.

### 3.3 Body

Modeling the body of a rat apart from the head had its own specific challenges. Although deformable, because the exterior of the body is not intended to be heavily instrumented with sensors, the fur was allowed to be kept on the references during measurements. It was not necessary to resort to the digital shaving with MRI that was previously necessary in the head modeling.

There was however a problem with the general shape of the rats. Although they have close masses, the body shape of individual rats can vary based on where they carry most of their weight much like human beings. The first attempt at rendering a body model of a rat had some oversights and oversimplifications because of this.

In the first attempt a single Sprague-Dawley rat was taken and measured at every half inch along the seven inches of its body. No special attention was paid to any of the anatomical landmarks and as a result, despite the high sampling rate, it was not an accurate depiction of the body of a rat even in simplified form. Markers such as the shoulder and the pelvic structure were missed and by chance some heights such as those found in the legs and the widest point of the shoulders were still taken. As a result, the image was distorted as a swept blend because it was not sweeping between landmarks of the body but instead was just blending between random points. A drawing of this first version of the model can be seen in figure 3.5.

Anatomically a vertebrate body acquires the majority of its shape, aside from that provided by hair or feathers, from the stretching of the skin over protrusions made from bones, fat or muscle. Neglecting the highest points and

lowest points of value and instead leaving them for chance and high sampling leads to fewer of these points between these sweeps and as a result paints a very inaccurate looking picture of what was attempted to be modeled.

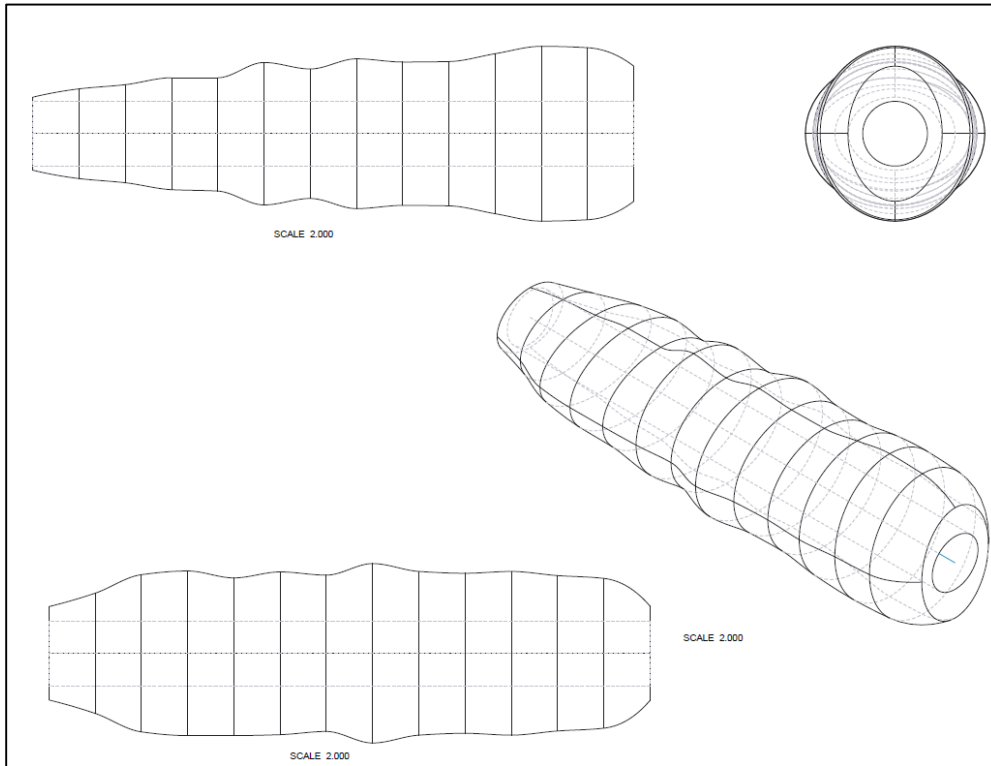


**Figure 3.5** Drawing of first draft of the RTD body.

Another issue with this version of the model was that this single rat may not have had a body that was necessarily representative of all Sprague-Dawley rats with the same amount of confidence. As a result, the plan for the body was completely overhauled to include the key details about anatomical landmarks as well as enough samples to ensure a confidence in the data.

### **3.3.1 Obtaining Body Geometry Samples**

In order to gather a massive amount of data on the geometry of Sprague-Dawley rats, a strategy had to be developed as well as several techniques of image analysis software and anatomical studies.

There were a total of twenty-four rats that were measured and they were all in varying states of life. Some of them were anesthetized, some were recently deceased and some were thawed out frozen rats. All of them were roughly the same age and of similar masses as will be discussed further in section 3.3. The reason why the forms of life the rats were in was not highly concerning was because they were not in a state of decay and the landmarks that were picked were based on skeletal structure more than that of musculature or fat pockets which may have been damaged or obscured by the freezing and unfreezing process, rigor mortis or even the stiffness/looseness characteristic of anaesthetized animals that may not be present in live ones. The animals were photographed from a side on angle as well as from a bird's-eye view.

In order to properly use image analysis software, in this case Pro-Analyst, the photographs required a physical reference of known size in each photograph. It was necessary to design a ruler that would be able to be seen from both points of view that the pictures were being taken. A device was designed in Creo 2.0 to accommodate this need and it was 3-D printed in ABS plastic to be physically used in the process. A drawing of the reference ruler device can be seen in Figure 3.6. A photo of the device in use with a live but anaesthetized animal can be seen in Figure 3.7 from a side on view.

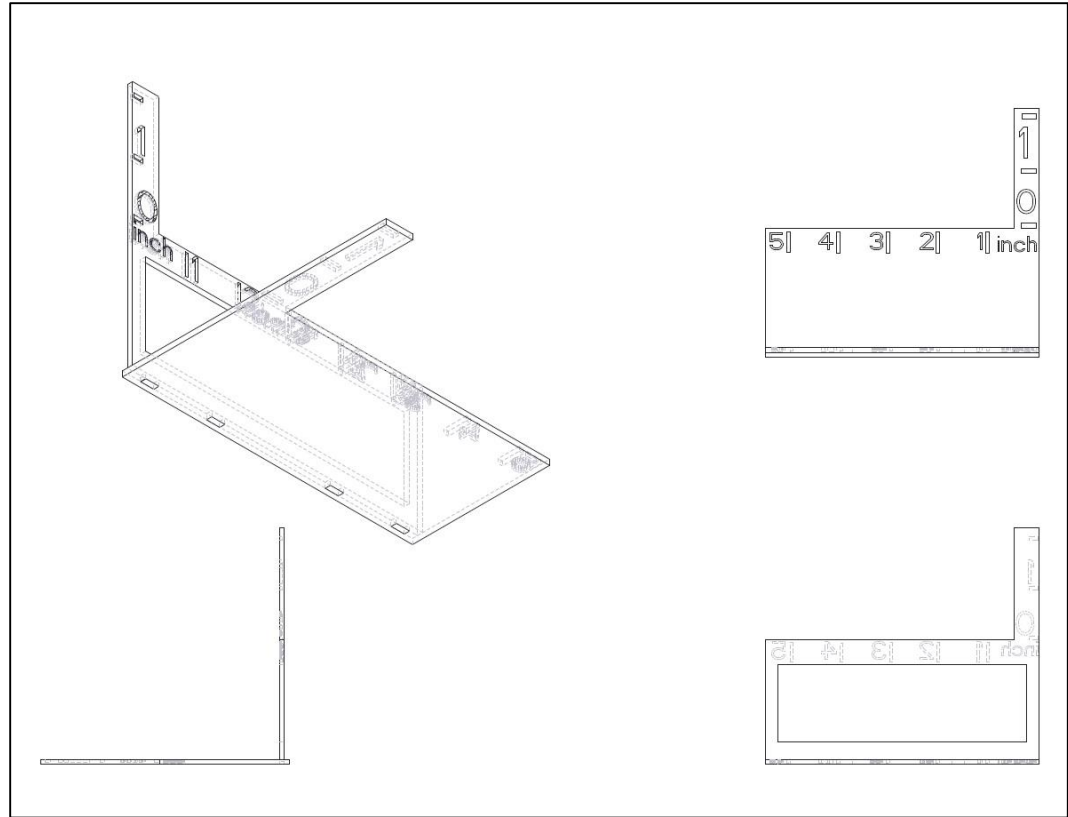


**Figure 3.6** Drawing of reference ruler device for assisting in image analysis of rats. It was necessary to consider the natural way the body would lay upon the surface or up against a wall and how that would distort the measurements. As a result the ruler was given a solid floor but a wall with a large window cut out so that any extra mass from the thighs would not be impeded or squished up by a wall. The ruler was made in a bright color to contrast with the white fur of the rat so that it would be easier to spot certain landmarks against the background of red. Views from top left going clockwise are isometric, top, back, left.



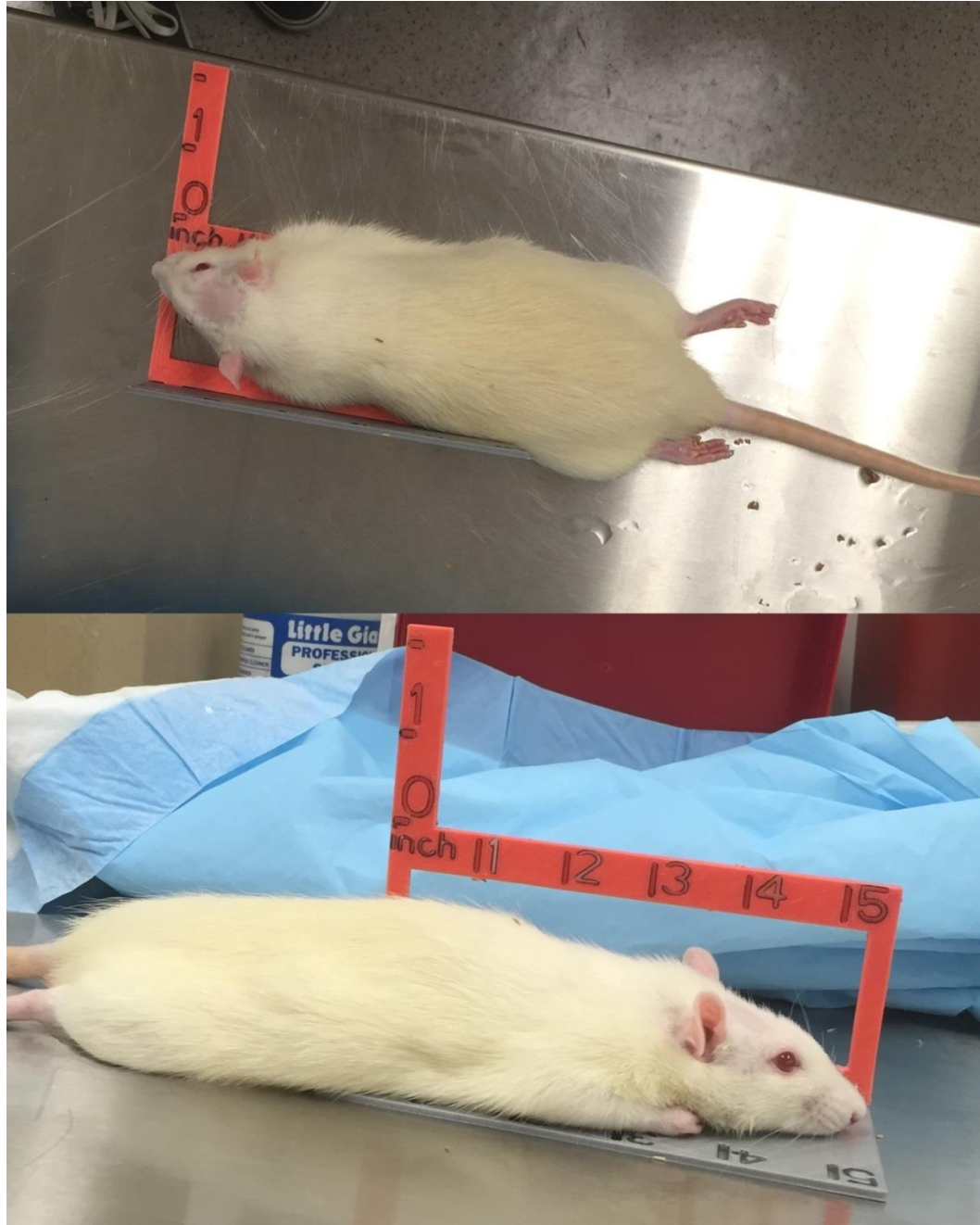


**Figure 3.7** Photos of a rat resting upon the ruler device. Above is the bird's eye view and below is a side on view. This rat was anaesthetized and all of its muscles are relaxed. Its head is shaved on the top for easy instrumentation for another experiment.

Two images were taken out of each of the twenty-four rats in this manner and uploaded into Pro-Analyst to analyze the geometric data. With the ruler as a reference point for an inch, the animals were each marked with seven reference points. These points were specific to the base of the neck, the end of the neck, the shoulder, the last rib, the pelvis, the thigh and the base of the tail. These points were chosen because they present the most recognizable skeletal features of the rat. The lengths between these points were noted and the heights and widths of these points per rat were taken down as well. Tables A.1, 8 and 16 in the appendix contain this data.

### **3.3.2 Establishing Normal Geometry**

In order to be satisfied with the data obtained, it must be established that the data follows a normal distribution. Several methods were employed in doing this regarding the physical dimensions of the rats.

The first method was to do a cursory check for asymmetry or tails in the data set using the skew function of excel. This gives a quick glance into whether a data set is asymmetrical to the upper or lower end of the data which would obscure it from being a normal distribution. This method was not strong as it did not give anything more than a very rough positive or negative value to describe the polarity of skewness but was unclear about the severity of how it was leaning.

The next method was to establish an estimate of whether or not the data followed a normal distribution. In order to do this, each data set was organized smallest to largest and the amount of data, twenty-four, was tallied, averaged, and the standard deviation was found. Once this was done, a set of cumulative

distribution factors (CDF) needed to be established that correlate to the place where the numbers would fall in the breakdown. These CDF were then put into a normal inverse function of Microsoft Excel along with the mean and standard deviation to output the expected theoretical values at that value. The theoretical and observed values at these points were then compared by graphing them with z-values as the x-axis. This provided a rough estimate of whether or not the samples obtained fell along a normal distribution if they overlapped with the expected values.

Once it was established that some of the data sets may have had outliers that were massively skewing the results, a methodology was established to sleuth out those data points. In order to do this, the following was needed to be calculated: the first quartile (Q1), the second quartile (Q2), the interquartile range (IQR; Q2-Q1) (D'Agostino, Sullivan and Beiser). The upper fence cutoff was determined to be:  $\text{mean} + 1.5 * \text{standard deviation}$ . The lower fence was determined to be:  $\text{mean} - 1.5 * \text{standard deviation}$ . After the upper and lower fences were established then the raw data of lengths, widths and heights were pared from the few outliers they contained and obtained a more normalized appearance when graphed again using the previous method. An example of this can be observed in Figure 3.8 below. This was repeated when outliers were present and skewing the data but was not necessary for all of the data sets. Tables A.2-7, 9-15, and 17-23 contain this updated data without outliers.

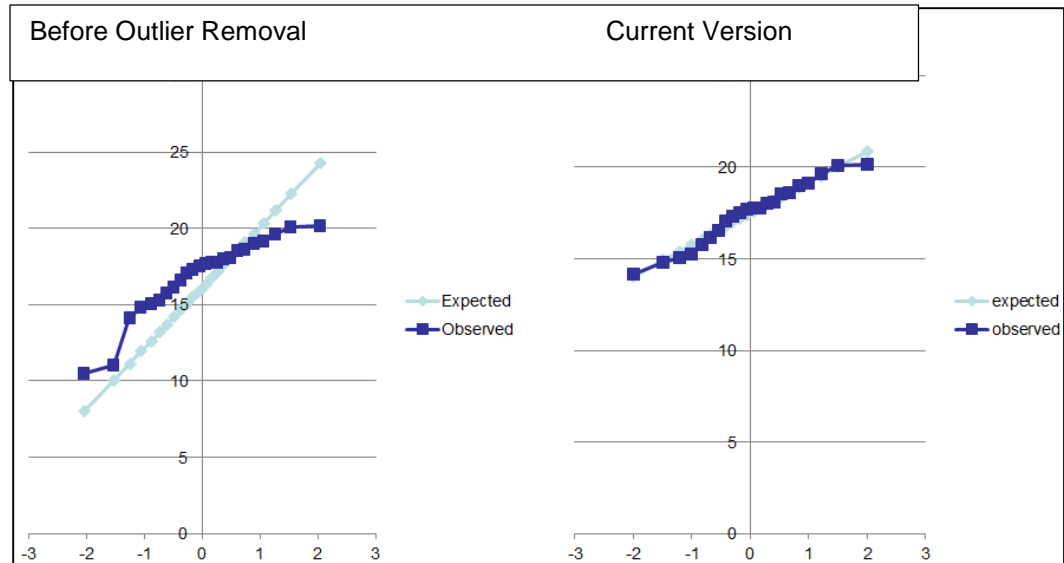


**Figure 3.8** Figures of observed and expected data before and after outlier removal. The x axis depicts the z-values and the y axis is millimeters of length between two points in the body. After the outliers were removed, the data points followed a normal distribution much better as it was very close to the expected outcome line.

Finally, once this process was finished the final method to clarify that the data fell along a normal distribution was to use the Ryan-Joiner method. This method is similar to the Shapiro-Wilk test which is a form of checking for proof that a data set does not follow a normal distribution (D'Agostino, Sullivan and Beiser). This was accomplished by using the program minitab and the P-value output by the program was compared with an established alpha value of 0.05. The result of the P-values being greater than alpha leads to the conclusion that it follows a normal distribution.

### 3.3.3 Designing 50<sup>th</sup> Percentile Body

Once it was established that the data at each point falls under a normal distribution, different sized models could be established to work for different size range rat bodies. The dimensions for the 50<sup>th</sup> percentile male body of a rat were

found by using the inverse normal cumulative distribution function of Excel. These numbers are listed in table 3.3.

**Table 3.3** The Lengths Between Points of Interest and the Heights and Widths at those Points of Interest in Millimeters for the 50<sup>th</sup> Percentile Male Sprague-Dawley Rat

Position	Length between (mm)	Height (mm)	Width (mm)
1	17.4365	41.1325	39.10445
2	11.38354	44.10393	43.82494
3	36.85298	47.55217	51.52368
4	44.66971	54.29552	60.61238
5	40.6654	55.96283	69.39611
6	26.01856	50.57267	54.28814
7		28.73789	23.61623

Once these dimensions were acquired, they were translated into seven ellipses with six lengths between them. A swept blend was created to go between these ellipses and the result was the model of the 50<sup>th</sup> percentile male body. It can be seen in Figure 3.9.

One observation that can be made about the general structure of the 50<sup>th</sup> percentile male is that the widest point of this rat is in the thighs. While the neck and ribs are much thinner than this which forms an overall conical shape with the point going towards the head.

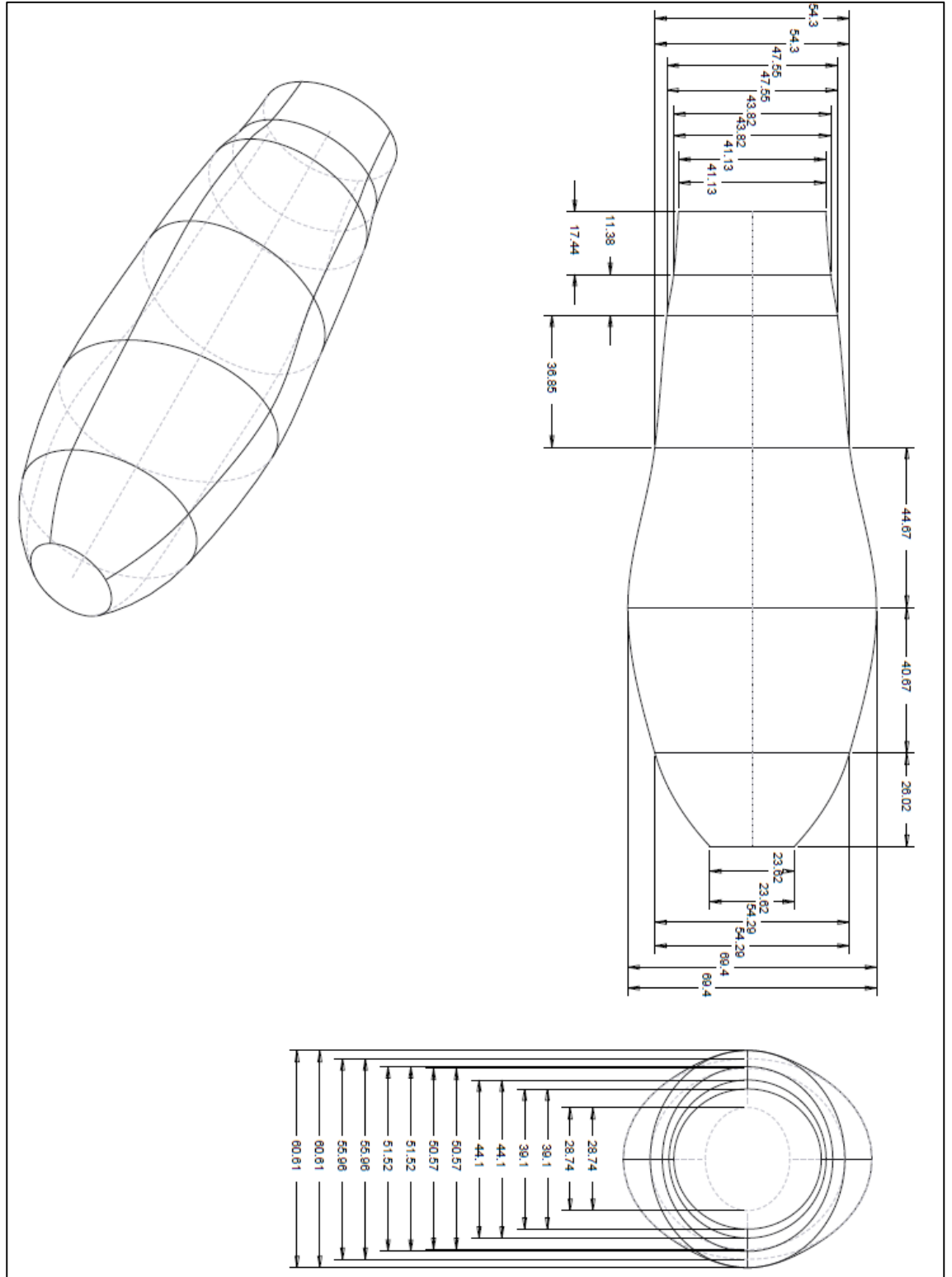


**Figure 3.9** 50<sup>th</sup> percentile Sprague-Dawley drawings with dimensions in millimeters. Views starting top right going clockwise are top, front and isometric.

### 3.3.4 Designing 90<sup>th</sup> Percentile Body

The dimensions for the 90<sup>th</sup> percentile male body of a rat were found by using the inverse normal cumulative distribution function of Excel but by requesting .9 instead of .5 in the input. These numbers are listed in table 3.4.

**Table 3.4** The Lengths Between Points of Interest and the Heights and Widths at those Points of Interest in Millimeters for the 90<sup>th</sup> Percentile Male Sprague-Dawley Rat

Position	Length between (mm)	Height (mm)	Width (mm)
1	19.65216	53.11392	41.96289
2	15.66593	56.5367	47.64056
3	40.66514	60.86347	65.85578
4	46.91071	57.47492	77.48961
5	48.94547	60.70458	75.97154
6	35.24141	56.00125	72.83595
7		36.12833	27.91288

These dimensions were also translated into ellipses and then using Creo 2.0, layered at the given length distances and a swept blend was featured between these ellipses to create the body shape of the 90<sup>th</sup> percentile rat model.

An observation that can be made about the body shape of this animal is that there is much more uniformity in the overall shape and the body itself resembles a flattened cylinder. It is not particularly wide on either end. This model can be viewed in Figure 3.10 with exact dimensions.

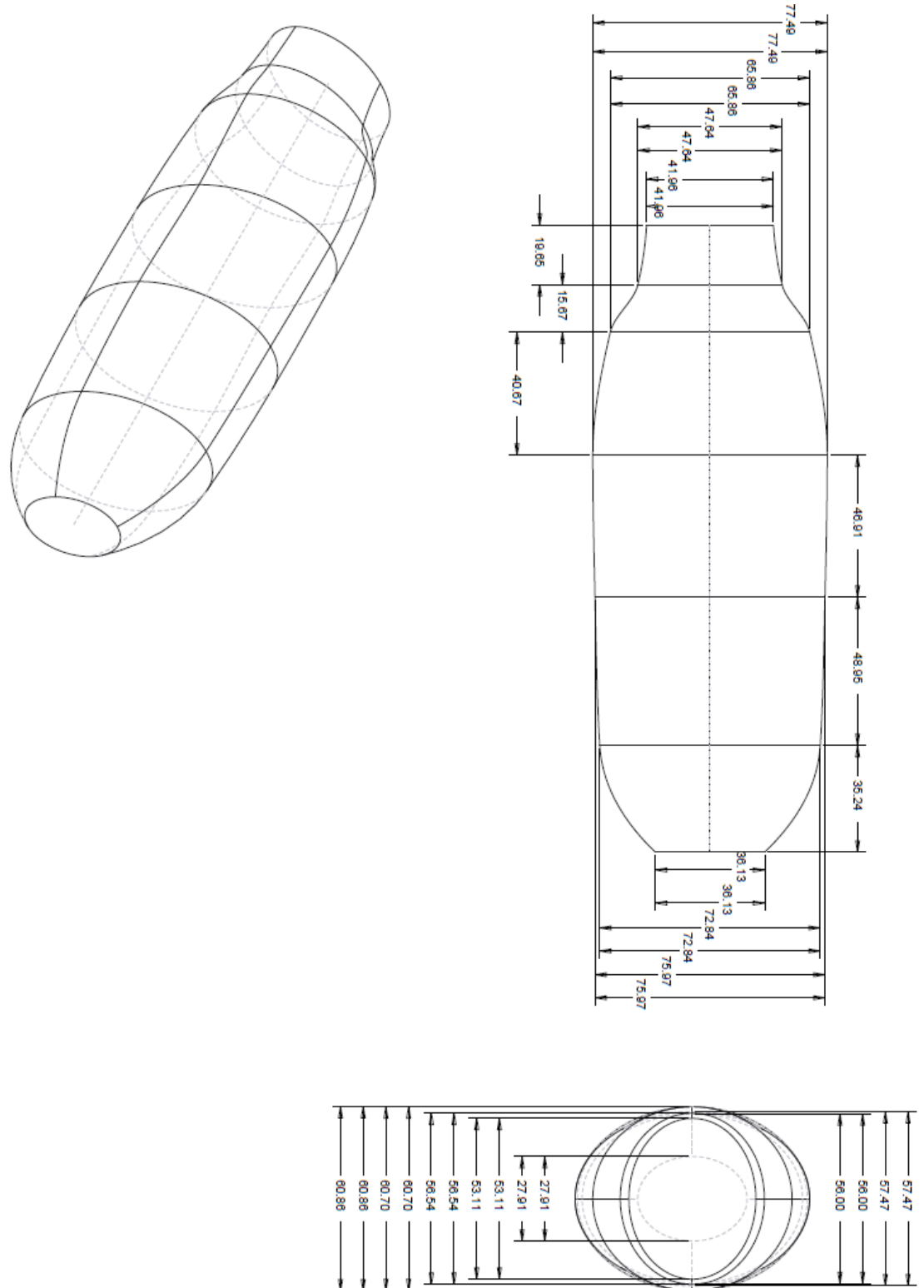


**Figure 3.10** 90<sup>th</sup> percentile Sprague-Dawley drawings with dimensions in millimeters. Views starting top right going clockwise are top, front and isometric.



### 3.3.5 Designing 95<sup>th</sup> Percentile Body

The dimensions for the 95<sup>th</sup> percentile male body of a rat were found by using the inverse normal cumulative distribution function of Excel but by requesting .95 instead of .5 in the input. These numbers are listed in table 3.5.

**Table 3.5** The Lengths Between Points of Interest and the Heights and Widths at those Points of Interest in Millimeters for the 95<sup>th</sup> Percentile Male Sprague-Dawley Rat

Position	Length between (mm)	Height (mm)	Width (mm)
1	20.27257	56.51049	42.77322
2	32.74957	60.06121	48.72224
3	41.74957	64.63704	69.91873
4	47.546	58.37624	82.27408
5	51.29276	62.04881	77.83559
6	37.85596	57.54018	78.094
7		38.22342	29.13092

These dimensions were also translated into ellipses and then using Creo 2.0, layered at the given length distances and a swept blend was featured between these ellipses to create the body shape of the 95<sup>th</sup> percentile rat model.

An observation that can be made about the body shape of this animal is that there is much more uniformity in the overall shape than that of the 50<sup>th</sup> percentile male. However though the body itself resembles a flattened cylinder like the 90<sup>th</sup> percentile, it does have a wide point at the ribcage which suggests that rats carry their extra weight in their torsos but when they are thinner most of their width is in their legs. This model can be viewed in Figure 3.11 with exact dimensions.

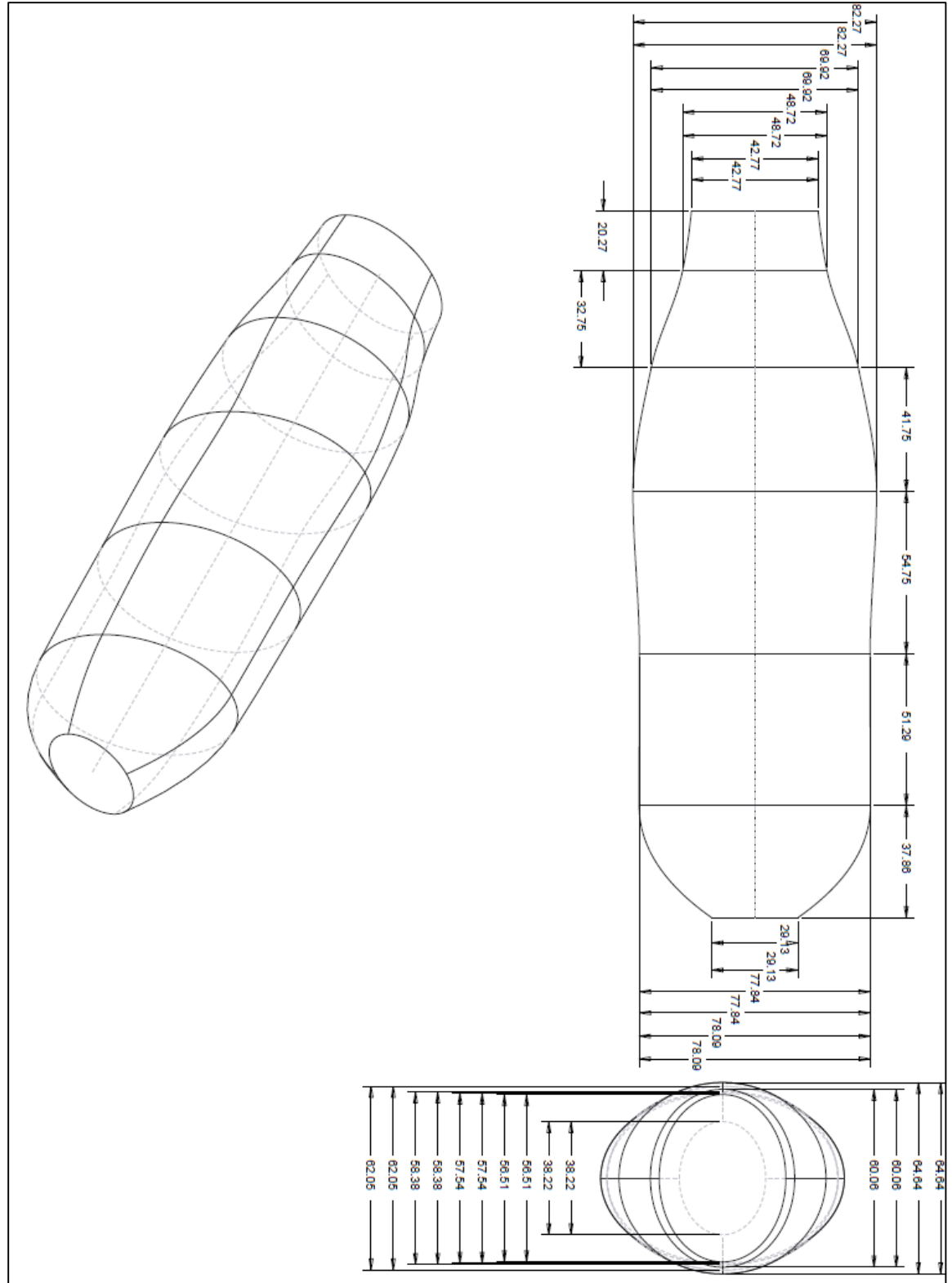


**Figure 3.11** 95<sup>th</sup> percentile Sprague-Dawley drawings with dimensions in millimeters. Views starting top right going clockwise are top, front and isometric.

### **3.4 Mass**

Just as important to the geometry of the animal, the mass of the animal naturally needs to have a degree of biofidelity. This is because when testing blast injury models, primary injury, injury due to the direct effects of pressure is not the only consideration when there is also secondary, effects of projectiles, and tertiary, effects due to wind (DePalma, Burriss MD and Champion). The effects due to wind are especially important to have the RTD experience. This is because just like how the precision of focusing the magnitude, duration and impulse of a blast wave is still a current topic of debate and research, the precise control of blast wind features are also not completely perfected or not proven to be completely repeatable in many labs. The mass of the rat surrogate needs to be similar to the rat so that it can behave similarly in a given blast wind so that because of the behavior it can be recognized as experiencing the difference between blast winds and a shockwave.

#### **3.4.1 Obtaining Mass Samples**

The center for injury biomechanics, materials and medicine has been conducting tests on rodent models for over a year and through it, there can be found a large record of certain biometric data on the animals that have been used for testing. Specifically records were kept on the masses of 90 of the rats that have been used for testing so far. The raw data can be found in Table B.1 in the appendix.

### **3.4.2 Establishing Normality of Mass Values**

Although there was a large sample size of masses, it was not guaranteed that the samples would follow a normal distribution pattern. Because the tests have been done over the course of a year, there may have been rats that were of a much larger or smaller size because of the nature of a specific test in the lab which was outside of the typical distribution that would be found. Once again there were several methods used to establish the level of normality in this data like those of the geometric data points.

The cursory check using the skew function of excel showed that there was a high likelihood that the data was going to have a tail on the upper end. As a result, it was understood that there were likely outliers to be found so after the Q1, Q3, IQR were calculated using the method from Section 3.3.2 upper fence was calculated as was the lower fence. Using these as cutoffs, the outliers were removed and a graph of the expected and observed versus the z-values was made once again using the same method as in 3.3.2 and it can be seen below in Figure 3.12.

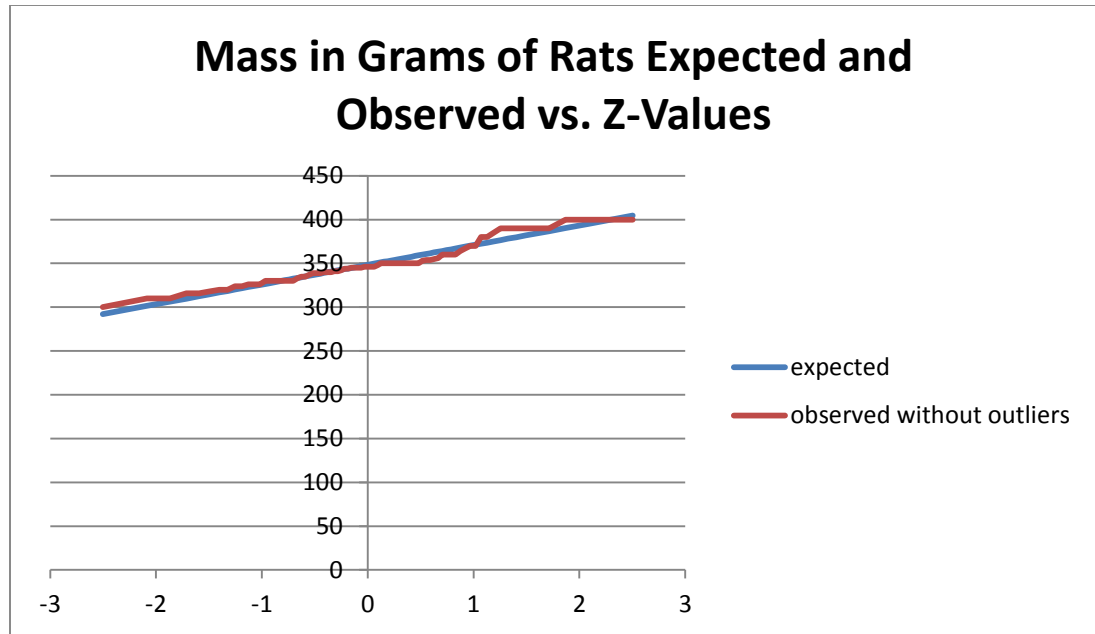


**Figure 3.12** Figure of observed and expected data versus z-values with outliers removed. The two figures are consistent with shape and values.

As a final check, the Ryan-Joiner method was employed to give a last clarification of if the data fell along a normal distribution curve. Using minitab, the output indicated a high likelihood of normality. The output can be seen in the appendix.

### 3.4.3 Finding 50<sup>th</sup>, 90<sup>th</sup>, 95<sup>th</sup> Percentile Masses

Once the data was satisfactorily proven to fall along a normal distribution, the different percentile masses could be calculated to observe how much mass the RTD at the different percentiles should have. The ones sought after were the 50<sup>th</sup>, 90<sup>th</sup>, and 95<sup>th</sup> percentile which were found by using the inverse normal cumulative function of excel corresponding to the CDF values, the average and the standard deviation of the data. These numbers are listed in the below table 3.6.

**Table 3.6** Calculated Masses of Different Percentile Rats Using the Normal Data

<b>Calculated Masses of different percentile rats</b>	
Percentile	Mass (grams)
50 <sup>th</sup>	348.33
90 <sup>th</sup>	377.15
95 <sup>th</sup>	385.32

### **3.4.4 Reconciling Difference in Mass**

When considering the masses at a given percentile such as those found in Table 3.6, it is important to consider how that would reconcile with the volume of a given percentile such as those found in section 3.3. Using the silicone material the reasoning for which is given in Section 4.1.1, the difference in density between the silicone and the flesh of a rat leads to a difference when using it to represent the body of a rat. Given the volumes of a given percentile and the density of the material of 1.34 g/cc (Smooth-On) the mass of the model made of the material can be calculated. The difference between the model mass and the mass of the actual rat can be found. This difference in mass can then be translated back into a volume of silicone that would need to be eliminated. Conveniently this negative amount of silicone would be used as the void space for instrumentation in the body design as a hollow chamber through the center. These values can be seen in Table 3.7 below. Given any variances in the constructed body mass from the theoretical body mass from imperfect blending or factually incorrect material specification sheets, more void space can be drilled out to remove excess mass.

**Table 3.7** Calculated Void Volumes of RTD Body

<b>Percentile</b>	<b>Volume (mm<sup>3</sup>)</b>	<b>Mass (g)</b>	<b>Volume of Silicone Given mass (mm<sup>3</sup>)</b>	<b>Difference in volume aka void volume (mm<sup>3</sup>)</b>
50 <sup>th</sup>	404012	348.33	259701	144419
90 <sup>th</sup>	632828	377.15	281479	351470
95 <sup>th</sup>	786892	385.32	287310	499582

## Chapter 4

### PROTOTYPE DEVELOPMENT

Without a physical prototype, the design process for a device does not offer much in the way of information or problem solving unless digital models are used to simulate the conditions that a physical model would experience. This is not an optimal choice in the development of a device meant to verify the existence of a shockwave in an actual shock tube. As a result, the construction of the prototype was put into process.

#### 4.1 Manufacturing

In order to properly manufacture the device, the process of translating a series of digital sketches into physical models began with selecting a medium. At first, a physical model was to be produced out of wood by producing the different diameters and a smooth transfer between the points on a lathe by a trained machinist. This turned out to not be as feasible as originally thought because the smooth rotational movements and curvatures produced by such a tool lend themselves to sweeps between circular diameters but do not accommodate elliptical shapes like the many that make up the layers of the body design.

The next choice was to use a three dimensional printer to flesh out a prototype that would serve as the RTD body. Normally this would not be an option because most 3D printers are much too small to handle printing out a device the size of a small rolling pin but the CIBM<sup>3</sup> laboratory uses an Ultimaker 2 Extended printer which has a very large build tank and allows for a prototype to



be printed out in a vertical position. An example of the build tank size can be seen below in Figure 4.1.

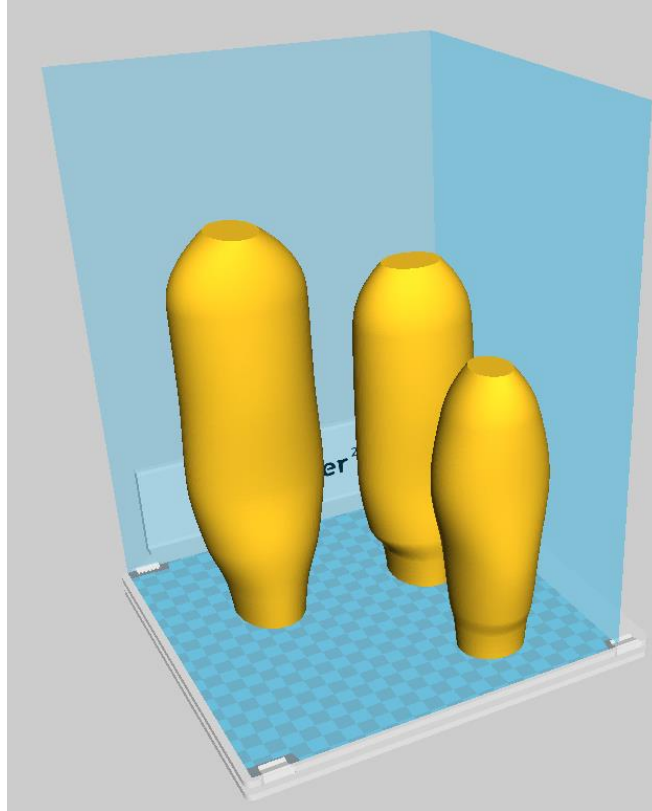


**Figure 4.1** A demonstration of the build tank size of the 3D printer in the program Cura 2.0 used to arrange parts intended for printing.

The available materials for 3D printing with the Ultimaker do not offer the sort of properties that are desirable for this particular function. This will be further discussed in Section 4.1.1. Instead it was decided that a mold needed to be made and cast to form the body of the RTD out of a material with more ideal properties.

#### **4.1.1 Material Selection**

The process of selecting a material came down to several criteria: specific gravity, modulus of elasticity, and durability. The materials considered under

these criteria were foam, ABS plastics such as those found in the 3D printer, ballistics gel and silicone.

Polyurethane (PU) foams have remarkable chemical properties such as insulation, and low heat conduction as well as good mechanical strength. (Witkiewicz and Zielinski). They present an impressive compressive modulus as well as shear and tensile strength in planes parallel and perpendicular to foam rise as seen in Table 4.1. The problem is that the nature of the material has two properties that are fundamentally detrimental to the nature of how the device would be used. One is that it is too lightweight. After accounting for the void space of the body cavity necessary for wires, the material would be much too light to act as a surrogate for the rat because it may be much more sensitive to the effects of blast winds on its acceleration if there are any. The other problem is that it is filled with air bubbles. These bubbles could behave similarly to microcracks which have been shown to be exploited by damaging energy presented by explosive blasts (Liu and Katsabanis). While experiencing a blast wave, compressible foam such as PU foam may either attenuate the magnitude of the pressure wave if there is a gap between it and the site of instrumentation or it could amplify it if it has no gap (Seitz and Skews).

**Table 4.1** Physical, Mechanical and Chemical Properties of Polyurethane Foams

Property	Test standard or specimens dimensions	Unit	Property at different foam density	
Apparent density	ISO 845	kg/m <sup>3</sup>	62	16
Compressive strength parallel to foam rise	ISO 844	MPa	0.64	0.033
Compressive stress perpendicular to foam rise			0.41	0.018
Compressive modulus parallel to foam rise			19.5	0.92
Compressive modulus perpendicular to foam rise			10.1	0.34
Tensile strength parallel to foam rise	ISO 1926		0.79	
Tensile strength perpendicular to foam rise			0.44	
Tensile modulus parallel to foam rise			26.7	
Tensile modulus perpendicular to foam rise			12.3	
Poisson's ratio $\nu_{12}$	75x50x50		0.72	
Poisson's ratio $\nu_{22}$			0.32	
Poisson's ratio $\nu_{21}$			0.30	
Shear strength in plane parallel to foam rise	ASTM C-273	MPa	0.34	
Shear strength in plane perpendicular to foam rise			0.36	
Shear modulus in plane parallel to foam rise			6.4	
Shear modulus in plane perpendicular to foam rise			6.2	
Reduction of buoyancy after 7 day immersion in water	150x150x150	pct.	0.62	8.05
Reduction of buoyancy after 30 day immersion in water			1.05	17.8
Maximum compressive stress no causing plastic deformation above 5% after 10,000 cycles, perpendicular to foam rise	ISO 844	MPa	1.24	
Average burning rate after exposure at 48 h for °C	ISO 9722	mm/min	45.80	
Average burning rate after exposure at 168 h for 70°C			54.90	

Source: Witkiewicz, Wit and Andrzej Zielinski. "Properties of the Polyurethane (PU) light foams." *Advances in Material Science* (2006): 35-51.

The problem with ABS plastics was that there was no stretch to the material. The main mechanism of assembly for the device relies on a certain amount of give for the body to stretch around the head and hold it in place. This material would require a complete redesign of the body that would need to be produced as two halves of a shell that lock together.

Ballistics gel would have been a great material for use due to it being a commonly used flesh model. It would have additionally been great because it is transparent which would have allowed for seeing if the embedded accelerometer shifted during testing. There is one main problem with the ballistics gel that put a hamper on using it and that is the melting point for being able to pour it. The polylactic acid that was to be used as the printed mold can warp at relatively low temperatures and anything that requires a hot plate to liquefy may pose a threat to the structural integrity of the mold.

Silicone was narrowed down to the best choice as a result of its flexibility and the close specific gravity to that of water of 1.34 g/cc (Smooth-On), which is the largest contributor to the mass of the real rat body. It also cures at room temperature so it does not pose a threat to the shape of the mold from heat warping.

#### **4.1.2 Mold Design**

There were two versions of mold making that were attempted in the process of developing this device's body. Each of them had strengths and weaknesses but ultimately only one was useful for this particular prototyping.

The first was to make the mold by using an old technique of pouring a container holding a facsimile with a molding material. The facsimile was a 3D printed version of the RTD body which was placed in a plastic container that was half filled with soft clay. The body was sprayed with a mold release and pressed halfway into the clay and plaster of Paris was poured into the remaining space. It

was allowed to set for an hour before it was overturned and the clay was taken out. The body and the half mold of plaster were sprayed once again with mold release, placed back into the container and then the remaining void space was filled with plaster of Paris. The container was set upon a shaking table to release any bubbles that would interfere with the quality of the mold.

The second method devised to form a mold was to render one and 3D print it as a piece that could be poured into. This was accomplished by creating an assembly in Creo featuring a simple rectangular block slightly larger than the RTD body. Then the RTD body was used as a cut feature to carve out its exact shape. The piece was then bisected and given positive notches on one side and negative on another with a small tolerance so they may be easily joined together as a locking mechanism for the mold set up. Because it is radially symmetrical, the same half piece could be printed twice and lock together to be poured into. This can be seen in Figure 4.2. The two halves were printed in poly-lactic acid (PLA) plastic for finer shape.

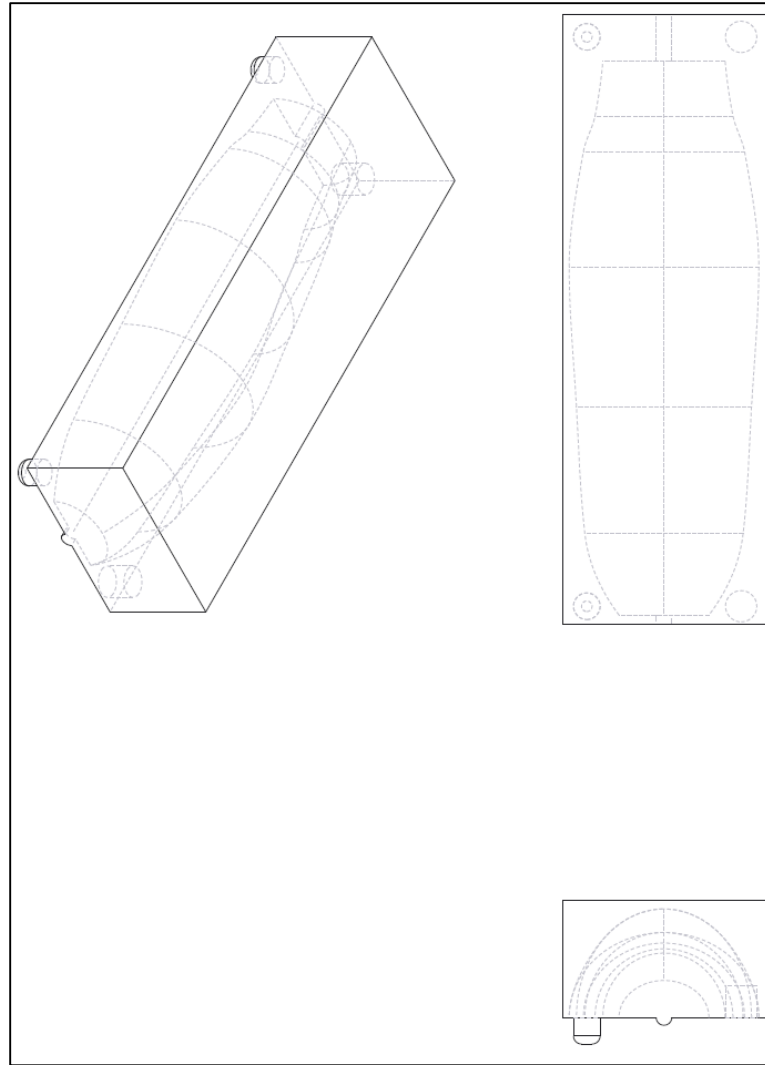


**Figure 4.2** Drawing of half of the mold with views from top left: isometric, bottom, left.

### 4.1.3 Casting

The two halves of printed mold were assembled and sealed with hot glue along the edges. Liquid tin-cure silicone rubber was then mixed in a separate container. Special care was taken to reduce all possible bubbles. The first way this was accomplished was to pour the liquid in from a very high position. In pouring liquid silicone from a high position, the flow of material is reduced to a narrow stream

and when the stream is extremely narrow, bubbles are likely to surface and are no longer in the bulk of the liquid thus present no hazard to the quality of the cast. The second measure that was taken was to rest the curing mold on a chemical shaking table to agitate the bubbles out with mechanical motion. Once these were done, a vacuum tank was applied to really make sure that the bubbles were reduced so that the device would be as durable as possible with the upcoming blast tests.

#### **4.1.4 Compiling Parts**

The parts were assembled by fitting the design elements together in their male to female leads. The head plugs into the void space of the body and the assembly is sealed into place with a little extra silicone to prevent slipping out of place but still allowing it to remain able to move like a real rat neck would.

### **4.2 Instrumentation**

In the most initial phase of testing, the head of the rat will be equipped with two kulite pressure sensors of model number XCL-072 and XCL-152-17BARA as shown in Figure 4.3 and Figure 4.4 below (Kulite). The XCL-152 will be at the nose to measure the stagnation pressure and the XCL-072 will be at an angle tangent to that of the muzzle stop to measure the pressure that would hit the brow of the animal and lead to the brain.

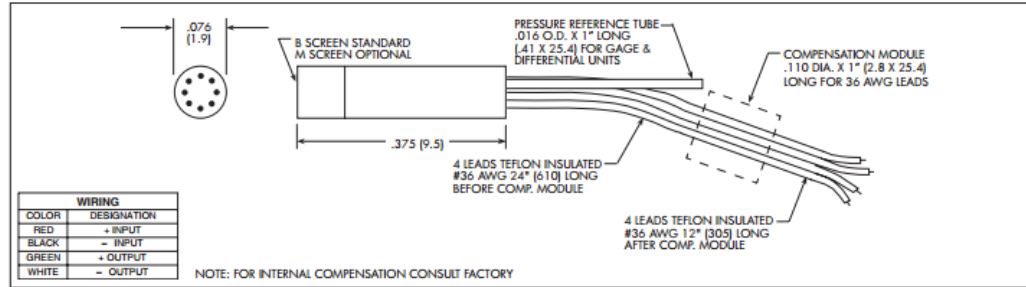


**Figure 4.3** Schematic of a Kulite XCL-072 Pressure Sensor.

Source: Kulite. "Miniature Leadless Pressure Transducer XCL-072 series." n.d.  
[http://www.kulitesensors.com.cn/pdf\\_Data\\_Sheets/XCL-072.pdf](http://www.kulitesensors.com.cn/pdf_Data_Sheets/XCL-072.pdf). 10 11 2015.

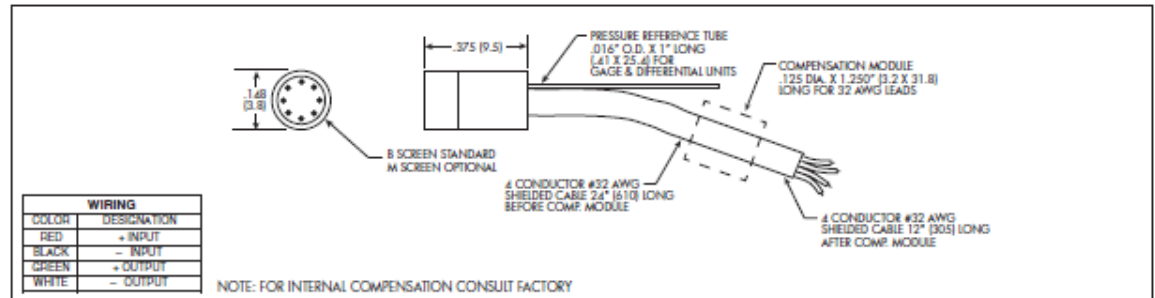


**Figure 4.4** Schematic of a Kulite XCL-152 Pressure Sensor.

Source: Kulite "Short Length Pressure Transducer XCL-152 Series." 2015.  
<http://www.kulite.com/docs/products/XCL-152.pdf>. 11 10 2015.

In order to understand the acceleration effects on the models, the device was designed to accommodate an accelerometer sensor. Specifically the endevco 7264C accelerometer which has a small size and is graded for crash and shock testing will be the sensor used in these tests. A schematic of the sensor is featured below in Figure 4.5.



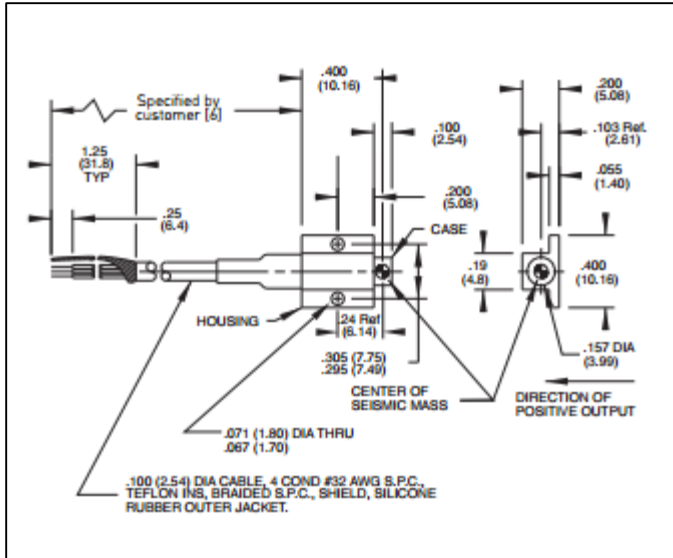


**Figure 4.5** Endevco 7264C piezoresistive accelerometer schematic.

Source: Endevco. "Model 7264C Piezoresistive accelerometer." n.d.  
<https://www.endevco.com/product/prodpdf/7264C.pdf>. 2015.

In the RTD model, the instrumentation process was simple because all the sensors were considered in the design process. The two pressure sensors easily fit into their respective places in the head and the accelerometer was put into the cavity of the void space within the body. All the cables were fed through the body of the device so that they would be protected from the blasts.

In the rat cadaver model, it was not nearly as convenient. While the nose sensor was easily glued to beneath the nose of the animal, the head sensor located at the brow required surgical intervention to make the sensor sit flush with the head of the animal. The head was shaved and a small hole was drilled through the skull to allow the sensor to be placed through and the sensor was secured in place with epoxy and silicone gel.

The accelerometer also required surgery to be properly placed. The torso of the rat was cut so that there was a small pouch formed between the muscle and the skin of the rat just below the ribcage. The accelerometer was encased in silicone and placed into this new cavity. The area was stapled shut.

All cables and wires were then secured to the underbelly of the rat which would be the spot with the most protection for them as it lay in the prone position on the testing bed.

## CHAPTER 5 TESTING

Experiments are to be conducted using the CIBM<sup>3</sup> 9" diameter shock tube. The test models were to be both the instrumented RTD and a cadaveric rat. Both of these were to be placed on the bed of the harness device pictured in Figure 5.1 for each of the tests and placed either inside or outside the tube in a given test.

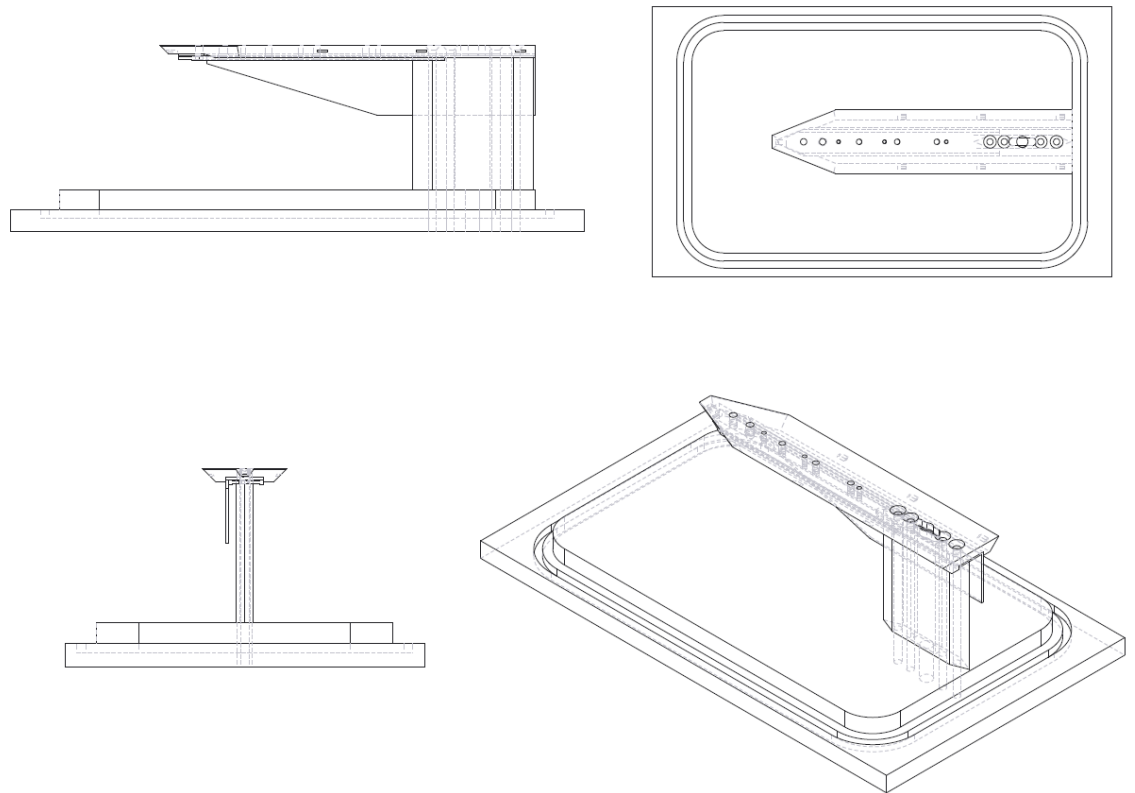


**Figure 5.1** The harness clockwise from top left: right, top, isometric and front.

The first scenario was to test the RTD inside the tube as it withstood a blast using two 0.9mm Mylar membranes between the driving section and the driven section. The RTD was secured into place using a cloth strap that is part of the assembly of the harness structure. A pressure sensor was also located at the

surface of the shock tube to record incident pressure of the wave as well. This test was repeated three times. The RTD in this set up is featured below in Figure 5.2. This testing scenario was repeated three times with the rat cadaver model as well.



**Figure 5.2** RTD inside the shock tube with a harness.

The next testing scenario was similar to the previous in that it was also secured with the strap and it took place inside the shock tube only it used four Mylar membranes rather than two. This was also repeated on the rat cadaver. Each model experienced three tests.

The third scenario is similar to the first where it has only two membranes and takes place inside the shock tube except the model is not strapped down and allowed to move freely if it is forced to by the blast wave or subsequent

winds. Three tests of this were planned for each of the models. The rat cadaver model is depicted below in Figure 5.3 in this set up.



**Figure 5.3** Rat cadaver inside shock tube without harness

The model and harness bed were then moved outside the shock tube where the model was placed so that the nose sensor was exactly four inches from the end of the barrel with two membranes. The test was repeated three times strapped and three times not strapped down on both the RTD and the rat cadaver model. The unstrapped RTD outside of the shock tube is pictured in Figure 5.4. A pressure sensor probe was also placed four inches outside of the shock tube from the height of the top of the shock tube to record the incident pressure.



**Figure 5.4** RTD unstrapped outside shock tube barrel.

## **CHAPTER 6**

### **Results, Summary and Future**

#### **6.1 Results**

The data that was gathered from the instrumentation was divided into four points of interest. Peak overpressures describe how much pressures the models experience at each sensor location and angle as well as the peak pressure experienced at the incident pressure sensor along the tube to be a control checking for consistency of the shots. Impulse values are signifier of several features of a shockwave such as the peak overpressure and duration because they are the area formed under the peak of a pressure versus time graph. This will be discussed in greater detail in Section 6.1.2. The accelerations were measured by the Endevco sensor and give an output of how many g the model experienced in the positive or negative direction in alignment with the tube. Finally the velocities were calculated to verify shock occurred.

##### **6.1.1 Peak Overpressures**

The first set of overpressures to look over is the peak overpressures found by the sensor located at the nose. These values are depicted in Figure 6.1.

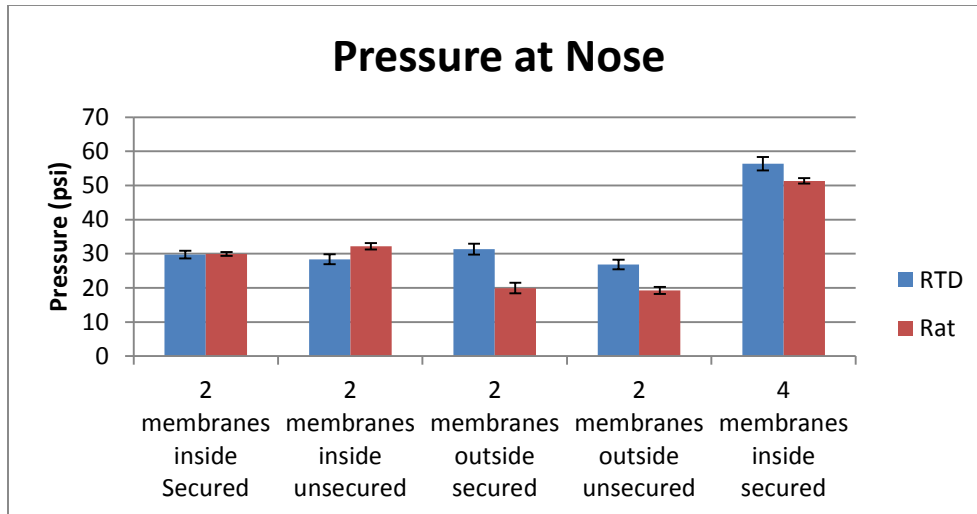


**Figure 6.1** Overpressures at nose sensor.

Given the small sample size of shots, the majority of these values between the RTD and the rat for a given scenario were very similar. There was some difference however in the overpressures found in the tests that took place outside of the shock tube.

The next set of overpressures was measured on the brow ridge at the top of the head which sat flush with the head. These values are depicted in Figure 6.2.



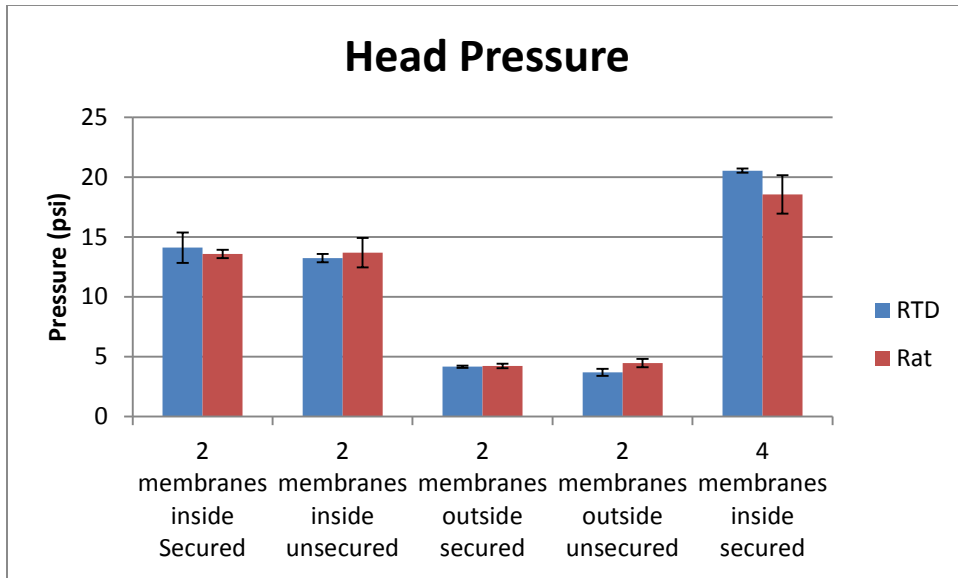


**Figure 6.2** Overpressures at head sensor.

The overpressures found in this location were consistent except for a slight disparity in the higher membrane tests. This is to be expected in such a test because greater pressures often have greater variances from test to test. This can be noticed by the large standard deviation in the value of the peak overpressures for the rat at four membranes.

The last set of peak overpressures examined is the incident pressures which are depicted in Figure 6.3. These are meant to indicate the consistency of the pressures from shot to shot in a sensor that has nothing to do with the RTD or rat cadaver model. The differences between the overpressures for each given scenario may have several contributing factors. One being that the RTD and rat models were tested on different days so environmental factors such as humidity and temperature may have affected the overpressure.

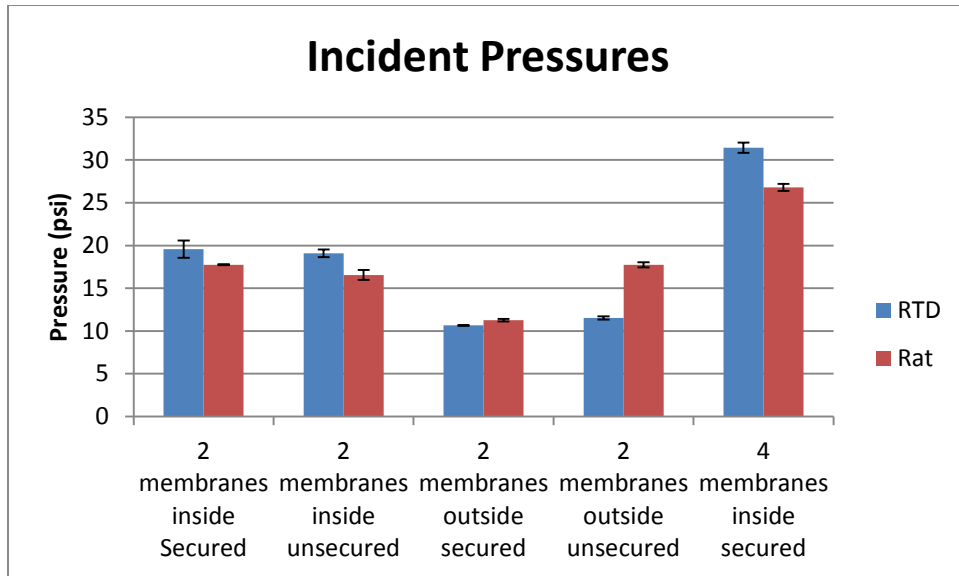


**Figure 6.3** Incident pressures.

### 6.1.2 Impulses

The impulse values are key to understanding the shape of the wave that is encountered. Because the effects of a blast wave are not limited to simply the pressures presented by the peak overpressure but rather by all of the pressures that occur on the body including the subsequent blast winds as the overpressure degrades, it is an important value to evaluate the effectiveness of a surrogate for a test model. This evaluation is mainly based on reporting the consistency of the impulses in a given scenario between the RTD and the rat models.

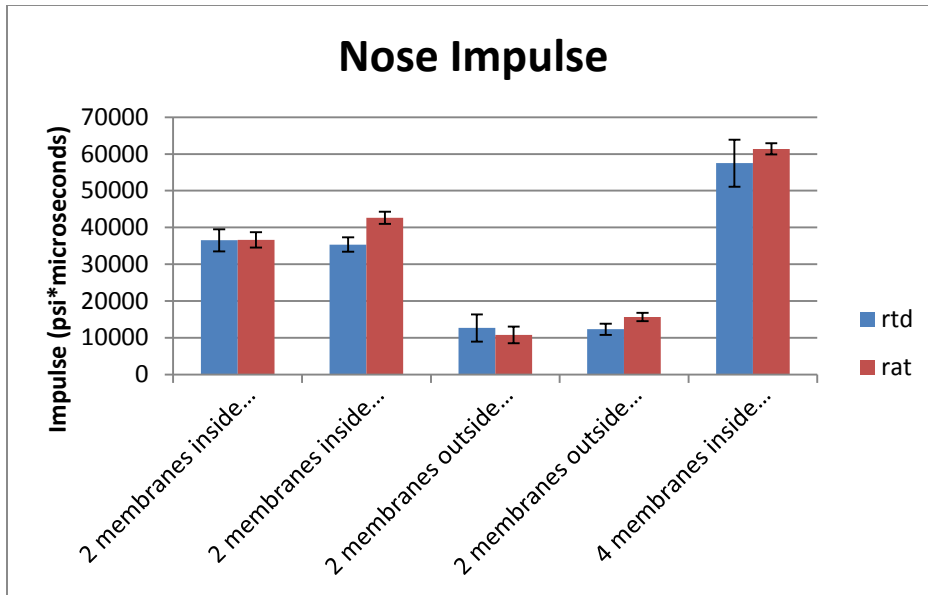


**Figure 6.4** Nose Impulse.

In Figure 6.4, the impulse values can be seen as having a consistent similarity for all of the given scenarios. As to be expected, there was a large standard deviation in the tests using four membranes instead of two. This is because the higher pressures tend to have a noisier signal and are less predictable than the lower pressure tests.

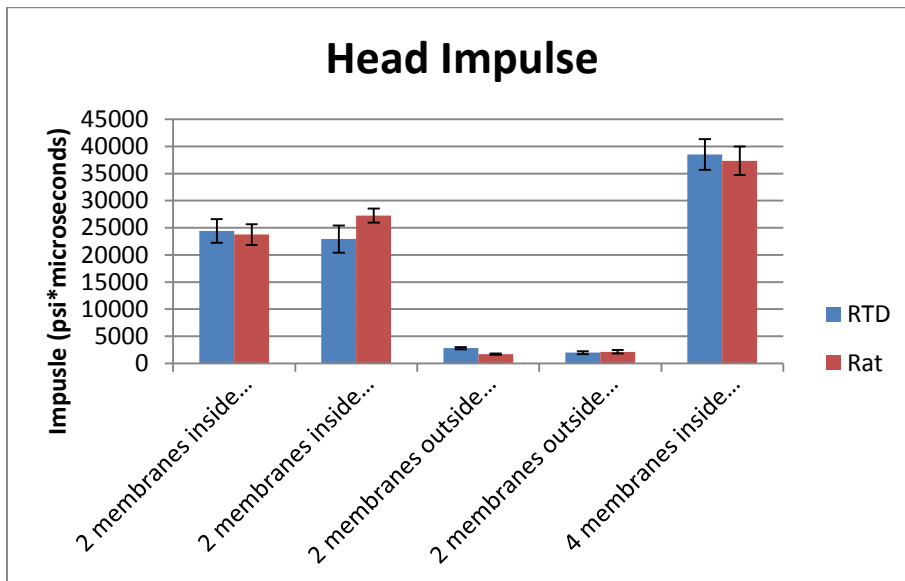


**Figure 6.5** Head Impulse.

The impulse values for the head sensors are even more consistent than those of the nose. This implies that the geometry used for the placement of the sensor as well as the shape of the RTD head was especially accurate to the geometry of a rat because the sensor encountered the wave in a very similar manner between the two different models.

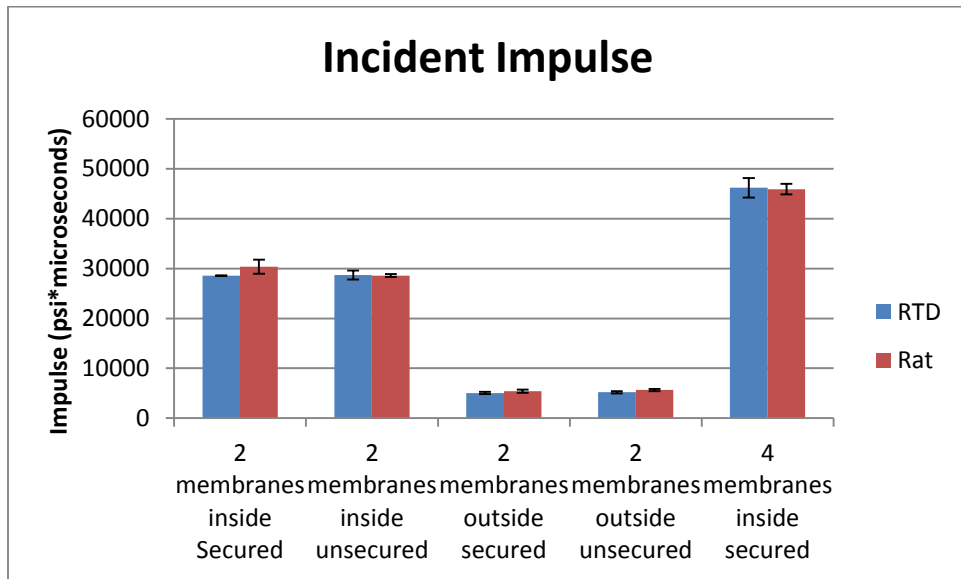


**Figure 6.6** Incident Impulse.

The closeness of impulse values between the different shots during each impulse verify that the waves were consistent and show that there were not any anomalous types of wave shapes during this series of tests.

### 6.1.3 Accelerations

The acceleration values are important in shockwave testing because there are secondary and tertiary causes for injury that can be predicted with acceleration values such as whiplash and falls. The following figures correspond to the acceleration sensed by the accelerometer. The positive values sense when the sensor was forced forward toward the membrane and the negative sensor

indicates when the sensor was experiencing a force moving away from the membrane. The first peak encountered was the negative value which is to be expected as the models would first be pushed back and then either fall or move back towards their original position by the compression resistant properties of their materials, flesh or silicone.

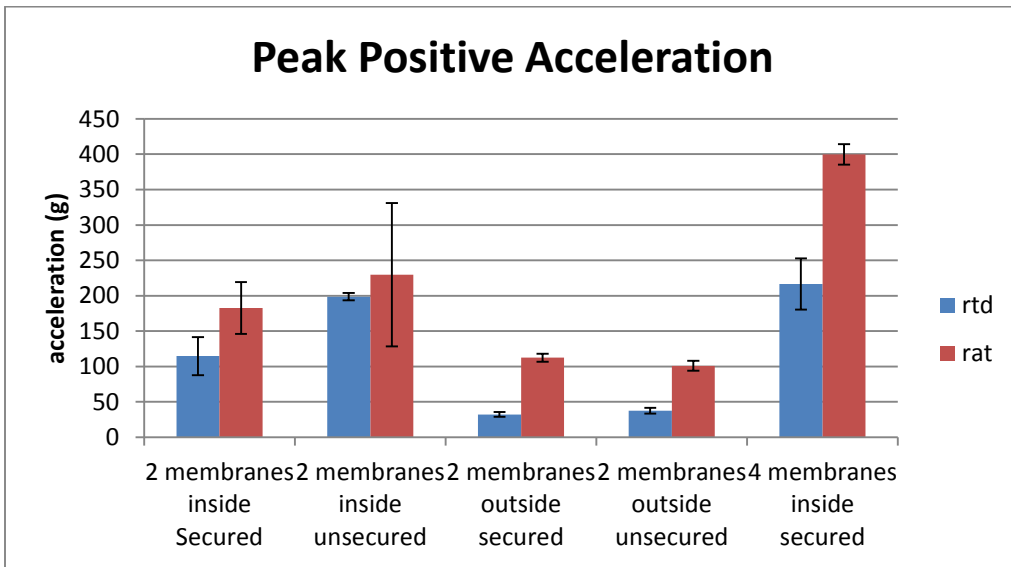


**Figure 6.7** Peak positive acceleration.

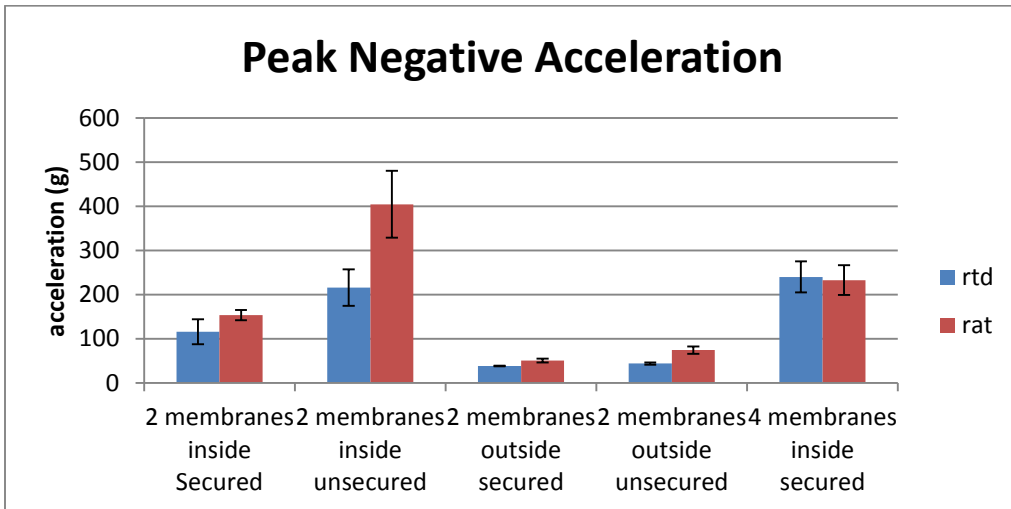


**Figure 6.8** Peak negative acceleration.

Looking at the negative peak, the only disparity that is very clear are the tests that were inside the tube and not strapped down. This makes sense because the rat was lighter than the RTD and the fur on the rat's underbelly made a lower friction contact with the bed of the harness than the silicone of the RTD body.

### 6.1.4 Velocities

The velocities were found by finding the differences in distances from each sensor location and dividing them by the difference in arrival times between each sensor. These were then found for each of the spaces between the sensors along the shock tube as well as the sensors in the head of the models. For the shots outside of the tube there was an added value for the incident pressure sensor's velocity.

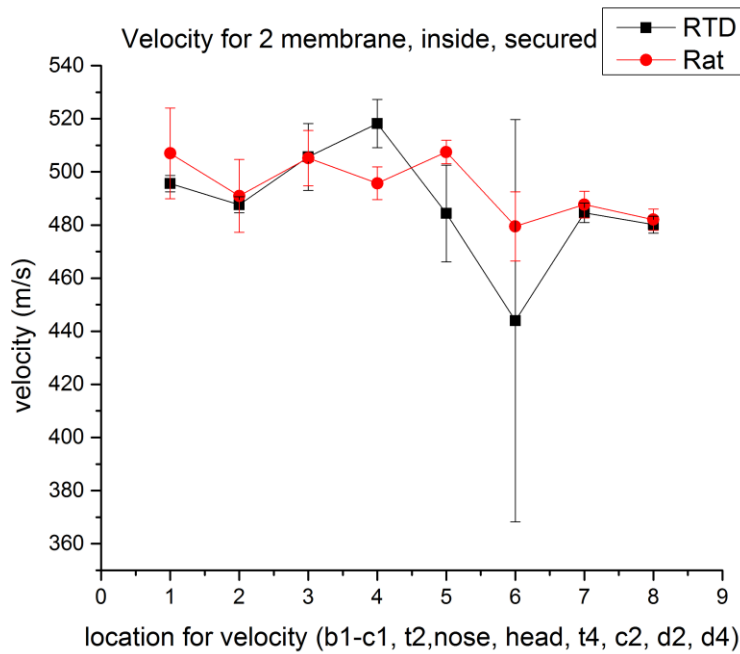


**Figure 6.9** Velocities for 2 membranes, inside shock tube, secured by strap.

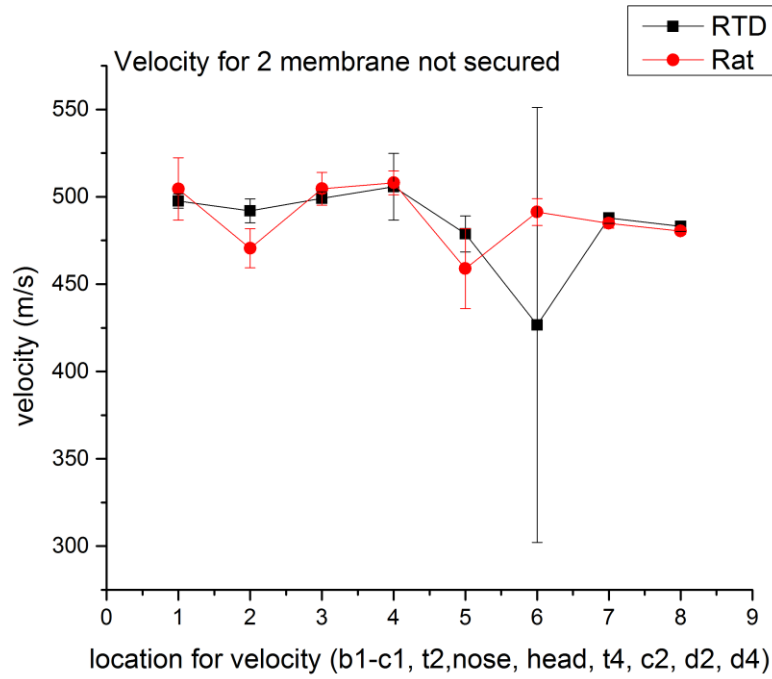


**Figure 6.10** Velocities for 2 membrane, inside shock tube, not secured by strap.

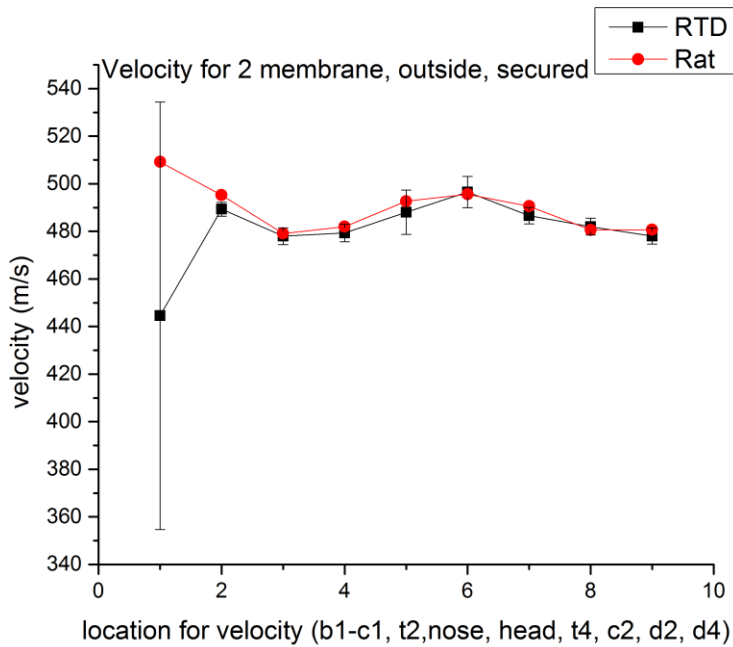


**Figure 6.11** Velocities for 2 membrane, outside shock tube, secured by a strap.

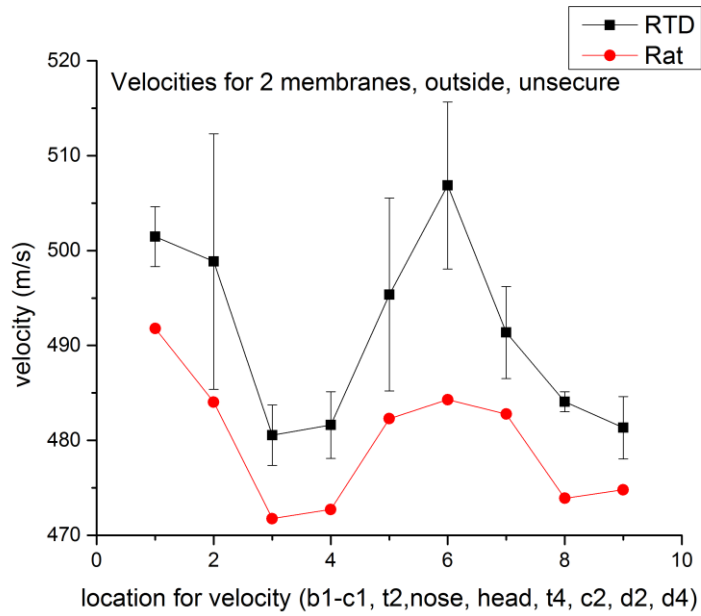


**Figure 6.12** Velocities for 2 membrane, outside shock tube, not secured by strap.

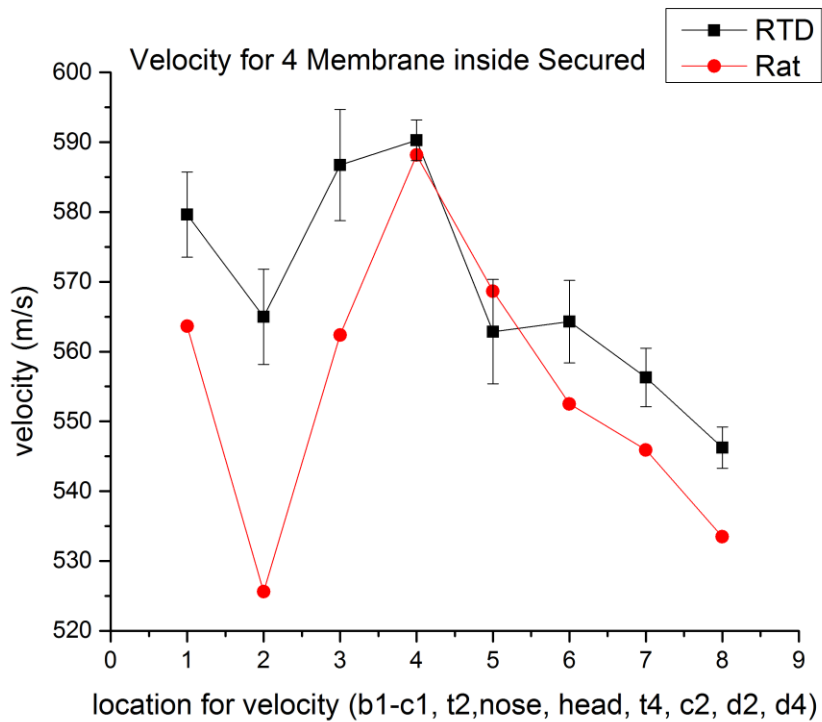


**Figure 6.13** Velocities for 4 membrane, inside shock tube, not secured by strap.



The values across the board for the sensors of interest in the head between the RTD and the rat models were consistent with each other. This indicates that they experienced the same velocity of shock front in these locations. Furthermore because all of the velocities in both the incident pressure sensors and the head sensors were well above the acoustic velocity of air in standard temperature and pressure, 340.4m/s (Kinney and Graham) , it can be verified that the models did indeed experience shock waves in each scenario.

## **6.2 Summary**

When comparing the RTD to a rat cadaver, several conclusions can be made given the test results discussed in this paper. The RTD senses the same incident pressures as the rat model with close outputs in each pressure sensor located in the head. This allows it to verify the peak overpressures that the rat would experience in a given scenario. Also from these pressure sensors, the RTD allows the user to calculate the impulse values closely to those experienced by the rat cadaver. Because of this, not only can the peak overpressure be found but the shape of the wave that the rat would encounter can be found as well. This is significant in discussing the mechanisms of injury for a rat in a given blast wave based injury. This shows that the geometry of the head and body were accurate to that of a real rat.

Also important in evaluating the mechanism of an injury is the accelerometer tests. Most of these tests were accurate in both the positive and negative peaks except for those tests where the rat was not harnessed. The differences between them can be accounted for by considering the mass

difference of almost 200 grams between the RTD and the rat cadaver. Also the rat has less friction with the bed of the harness due to fur as opposed to silicone. In future iterations, a larger void space will be made within the RTD body to make up for the extra weight of the sealing silicone and the instrumentation. Also it will have a lower friction surface on the underbelly.

### **6.3 Future**

There are a few ways that this project could be taken further. One way has been discussed before with alterations to the total mass of the RTD as well as reducing the friction of the outer shell. The RTD could also be instrumented with a gamut of sensors. These include external strain gauges to test the biofidelity of the outer layer to that of the skin of a rodent. Also the potential pressure of the inner cavity compared to those found in the lungs of the rat.

Another way that the project could go is based on the modular nature of the design. The head could be redesigned such that it would be able to change the angles of the neck to adapt to the different positions the rat may be placed in within other experimental set ups. Also all of these experiments could be done with different percentile sized rats or even repeated with mice and other rodents that are used for testing. The project can be taken in many directions.

## Appendix A

### Raw Geometric Data of the Rodent Body

Tables that display the length, width and height of the rat at varying points in the body of anatomical significance: base of neck, end of neck, shoulder, last rib, pelvis, thigh, tail base.

**Table A.1** Length in millimeters between points raw data

Rat	1 to 2	2 to 3	3 to 4	4 to 5	5 to 6	6 to 7
1	18.52	7.00	25.81	43.82	18.52	7.00
2	17.50	9.37	33.78	43.61	17.50	9.37
3	18.07	11.43	36.42	43.21	18.07	11.43
4	16.18	10.04	33.76	42.95	16.18	10.04
5	19.61	10.09	34.04	45.80	19.61	10.09
6	17.80	6.63	27.31	40.89	17.80	6.63
7	16.58	7.40	37.49	43.59	16.58	7.40
8	10.47	6.63	28.42	44.37	10.47	6.63
9	17.30	14.10	39.90	43.76	17.30	14.10
10	15.27	11.38	38.10	43.38	15.27	11.38
11	18.02	11.82	39.32	44.22	18.02	11.82
12	18.62	11.50	34.47	44.04	18.62	11.50
13	17.08	11.14	27.28	46.15	17.08	11.14
14	11.07	10.61	35.56	46.96	11.07	10.61
15	20.07	10.68	39.19	45.95	20.07	10.68
16	20.16	12.64	39.50	45.95	20.16	12.64
17	14.82	11.65	37.90	36.63	14.82	11.65
18	17.79	14.14	38.53	34.95	17.79	14.14
19	18.97	13.72	36.96	53.16	18.97	13.72
20	15.75	10.28	38.15	44.86	15.75	10.28
21	14.16	16.42	35.74	47.80	14.16	16.42
22	15.07	13.97	42.72	47.90	15.07	13.97
23	17.72	14.09	37.34	50.55	17.72	14.09
24	19.15	17.29	36.63	44.17	19.15	17.29
average	18.52	7.00	25.81	43.82	18.52	7.00
StdDev	17.50	9.37	33.78	43.61	17.50	9.37
Q 1	18.07	11.43	36.42	43.21	18.07	11.43
Q 3	16.18	10.04	33.76	42.95	16.18	10.04
IQR	19.61	10.09	34.04	45.80	19.61	10.09
U fence	17.80	6.63	27.31	40.89	17.80	6.63
L fence	16.58	7.40	37.49	43.59	16.58	7.40

**Table A.2** Length in millimeters between base of neck and end of neck with outliers removed

Length 1-2 in millimeters with outliers removed				
Rat	Measured length	CDF	Expected length	z-value
1	14.2	0.0	14.0	-2.0
2	14.8	0.1	14.9	-1.5
3	15.1	0.1	15.4	-1.2
4	15.3	0.2	15.8	-1.0
5	15.7	0.2	16.1	-0.8
6	16.2	0.3	16.3	-0.7
7	16.6	0.3	16.5	-0.5
8	17.1	0.3	16.8	-0.4
9	17.3	0.4	17.0	-0.3
10	17.5	0.4	17.2	-0.2
11	17.7	0.5	17.4	-0.1
12	17.8	0.5	17.6	0.1
13	17.8	0.6	17.8	0.2
14	18.0	0.6	18.0	0.3
15	18.1	0.7	18.2	0.4
16	18.5	0.7	18.4	0.5
17	18.6	0.8	18.6	0.7
18	19.0	0.8	18.9	0.8
19	19.2	0.8	19.2	1.0
20	19.6	0.9	19.5	1.2
21	20.1	0.9	20.0	1.5
22	20.2	1.0	20.9	2.0

**Table A.3** Length in millimeters between end of neck and shoulder outliers removed

Length 2-3 in millimeters with outliers removed				
Rat	Measured length	CDF	Expected length	z-value
1	6.63	0.02	4.58	-2.04
2	6.63	0.06	6.26	-1.53
3	7.00	0.10	7.18	-1.26
4	7.40	0.15	7.86	-1.05
5	9.37	0.19	8.42	-0.89
6	10.04	0.23	8.91	-0.74
7	10.09	0.27	9.34	-0.61
8	10.28	0.31	9.75	-0.49
9	10.61	0.35	10.13	-0.37
10	10.68	0.40	10.50	-0.26
11	11.14	0.44	10.86	-0.16
12	11.38	0.48	11.21	-0.05
13	11.43	0.52	11.56	0.05
14	11.50	0.56	11.91	0.16
15	11.65	0.60	12.27	0.26
16	11.82	0.65	12.63	0.37
17	12.64	0.69	13.02	0.49
18	13.72	0.73	13.42	0.61
19	13.97	0.77	13.86	0.74
20	14.09	0.81	14.35	0.89
21	14.10	0.85	14.91	1.05
22	14.14	0.90	15.59	1.26
23	6.63	0.02	4.58	-2.04
24	6.63	0.06	6.26	-1.53

**Table A.4** Length between shoulder and last rib in millimeters outliers removed

Length 3-4 in millimeters with outliers removed				
Rat	Measured length	CDF	Expected length	z-value
1	28.42	0.15	26.46	-1.05
2	33.76	0.19	27.77	-0.89
3	33.78	0.23	28.92	-0.74
4	34.04	0.27	29.95	-0.61
5	34.47	0.31	30.91	-0.49
6	35.56	0.35	31.81	-0.37
7	35.74	0.40	32.67	-0.26
8	36.42	0.44	33.51	-0.16
9	36.63	0.48	34.34	-0.05
10	36.96	0.52	35.16	0.05
11	37.34	0.56	35.99	0.16
12	37.49	0.60	36.83	0.26
13	37.90	0.65	37.69	0.37
14	38.10	0.69	38.59	0.49
15	38.15	0.73	39.55	0.61
16	38.53	0.77	40.58	0.74
17	39.19	0.81	41.73	0.89
18	39.32	0.85	43.04	1.05
19	39.50	0.90	44.64	1.26
20	39.90	0.94	46.82	1.53
21	42.72	0.98	50.77	2.04

**Table A.5** Length in millimeters between last rib and pelvis outliers removed

Length 4-5 in millimeters with outliers removed				
Rat	Measured length	CDF	Expected length	z-value
1	40.9	0.1	30.8	-1.3
2	43.0	0.1	32.8	-1.1
3	43.2	0.2	34.4	-0.9
4	43.4	0.2	35.8	-0.7
5	43.6	0.3	37.0	-0.6
6	43.6	0.3	38.2	-0.5
7	43.8	0.4	39.3	-0.4
8	43.8	0.4	40.4	-0.3
9	44.0	0.4	41.4	-0.2
10	44.2	0.5	42.4	-0.1
11	44.2	0.5	43.4	0.1
12	44.4	0.6	44.4	0.2
13	44.9	0.6	45.4	0.3
14	45.8	0.6	46.5	0.4
15	45.9	0.7	47.6	0.5
16	45.9	0.7	48.7	0.6
17	46.2	0.8	50.0	0.7
18	47.0	0.8	51.4	0.9
19	47.8	0.9	53.0	1.1
20	47.9	0.9	54.9	1.3

**Table A.6** Length in millimeters between pelvis and thigh outliers removed

Length 5-6 in millimeters with outliers removed				
Rat	Measured length	CDF	Expected length	z-value
1	30.0	0.1	24.7	-1.5
2	31.1	0.1	27.2	-1.3
3	31.2	0.1	29.1	-1.1
4	32.3	0.2	30.7	-0.9
5	34.9	0.2	32.0	-0.7
6	38.1	0.3	33.2	-0.6
7	38.2	0.3	34.4	-0.5
8	38.3	0.4	35.4	-0.4
9	38.3	0.4	36.4	-0.3
10	38.5	0.4	37.4	-0.2
11	40.3	0.5	38.4	-0.1
12	40.3	0.5	39.4	0.1
13	40.4	0.6	40.3	0.2
14	40.6	0.6	41.3	0.3
15	42.3	0.6	42.3	0.4
16	42.6	0.7	43.4	0.5
17	45.1	0.7	44.5	0.6
18	45.5	0.8	45.7	0.7
19	45.6	0.8	47.1	0.9
20	46.3	0.9	48.6	1.1
21	49.1	0.9	50.5	1.3
22	51.9	0.9	53.1	1.5
23	54.4	1.0	57.7	2.0



**Table A.7** Length in millimeters between thigh and tail base, outliers removed

Length 6-7 in millimeters with outliers removed				
Rat	Measured length	CDF	Expected length	z-value
1	15.9	0.0	11.4	-2.0
2	19.1	0.1	15.0	-1.5
3	20.4	0.1	17.0	-1.3
4	20.4	0.1	18.4	-1.1
5	20.5	0.2	19.6	-0.9
6	21.9	0.2	20.7	-0.7
7	22.8	0.3	21.6	-0.6
8	23.7	0.3	22.5	-0.5
9	24.7	0.4	23.3	-0.4
10	26.0	0.4	24.1	-0.3
11	26.4	0.4	24.9	-0.2
12	27.6	0.5	25.6	-0.1
13	27.7	0.5	26.4	0.1
14	28.8	0.6	27.2	0.2
15	28.8	0.6	27.9	0.3
16	29.1	0.6	28.7	0.4
17	29.7	0.7	29.5	0.5
18	30.4	0.7	30.4	0.6
19	31.3	0.8	31.4	0.7
20	35.0	0.8	32.4	0.9
21	35.4	0.9	33.6	1.1
22	36.9	0.9	35.1	1.3
23	40.2	0.9	37.1	1.5
24	41.3	1.0	40.7	2.0

**Table A.8** Height at varying points in the body raw data

Height in millimeters Raw Data							
Rat	1	2	3	4	5	6	7
1	35.3	35.8	46.0	54.1	55.4	54.7	32.1
2	33.5	35.7	45.8	54.6	57.9	53.5	38.1
3	39.4	39.5	50.8	67.5	59.5	37.6	25.9
4	39.6	43.2	48.5	60.5	63.6	60.3	37.2
5	35.8	41.4	47.2	55.8	56.8	51.7	29.9
6	41.9	43.1	48.9	52.3	53.3	50.5	39.7
7	36.0	36.2	46.5	53.6	57.1	52.0	36.4
8	40.4	46.3	51.3	49.8	51.3	50.9	27.2
9	53.7	51.8	53.7	54.3	57.1	50.7	27.7
10	46.3	50.1	54.9	56.5	58.3	47.6	20.6
11	45.8	46.9	53.4	54.8	54.8	54.8	31.2
12	43.8	47.6	51.0	58.0	60.8	52.9	28.5
13	41.3	42.8	45.5	52.3	48.5	49.4	29.0
14	49.7	49.6	48.8	53.7	56.2	48.8	29.1
15	45.3	50.8	51.0	53.9	55.7	52.1	30.0
16	40.7	46.4	48.7	52.3	51.0	50.7	26.4
17	40.5	44.0	48.3	54.9	55.8	50.4	29.4
18	36.3	39.0	45.1	56.8	61.2	51.2	33.4
19	49.9	55.2	56.9	73.1	85.4	70.9	43.3
20	44.9	46.8	47.9	53.7	56.2	43.6	22.3
21	48.2	47.1	48.2	51.2	50.9	32.1	18.2
22	36.8	41.8	46.1	51.1	48.5	38.5	20.2
23	40.4	47.1	52.0	56.2	60.6	44.9	23.3
24	40.4	46.2	48.3	62.5	56.7	40.7	25.0
mean	41.9	44.8	49.4	56.0	57.2	49.6	29.3
Std Dev	5.2	5.1	3.2	5.3	7.2	7.8	6.4
Q 1	38.8	41.7	47.0	53.3	54.5	46.9	25.7
Q 3	45.4	47.3	51.1	56.6	58.6	52.3	32.5
IQR	6.6	5.6	4.1	3.3	4.1	5.3	6.8
Upper fence	55.3	55.6	57.2	61.5	64.8	60.3	42.6
Lower fence	28.8	33.3	40.8	48.4	48.2	38.9	15.5

**Table A.9** Height at base of neck in millimeters with outliers removed

Height 1 in millimeters with outliers removed				
Rat	Measured height	CDF	Expected height	z-value
1	33.5	0.0	22.1	-2.0
2	35.3	0.1	26.8	-1.5
3	35.8	0.1	29.4	-1.3
4	36.0	0.1	31.3	-1.1
5	36.3	0.2	32.8	-0.9
6	36.8	0.2	34.2	-0.7
7	39.4	0.3	35.4	-0.6
8	39.6	0.3	36.6	-0.5
9	40.4	0.4	37.6	-0.4
10	40.4	0.4	38.7	-0.3
11	40.4	0.4	39.7	-0.2
12	40.5	0.5	40.6	-0.1
13	40.7	0.5	41.6	0.1
14	41.3	0.6	42.6	0.2
15	41.9	0.6	43.6	0.3
16	43.8	0.6	44.6	0.4
17	44.9	0.7	45.7	0.5
18	45.3	0.7	46.8	0.6
19	45.8	0.8	48.1	0.7
20	46.3	0.8	49.4	0.9
21	48.2	0.9	51.0	1.1
22	49.7	0.9	52.9	1.3
23	49.9	0.9	55.5	1.5
24	53.7	1.0	60.2	2.0

**Table A.10** Height at end of neck in millimeters with outliers removed

Height 2 in millimeters with outliers removed				
Rat	Measured height	CDF	Expected height	z-value
1	35.7	0.0	24.3	-2.0
2	35.8	0.1	29.2	-1.5
3	36.2	0.1	31.9	-1.3
4	39.0	0.1	33.9	-1.1
5	39.5	0.2	35.5	-0.9
6	41.4	0.2	36.9	-0.7
7	41.8	0.3	38.2	-0.6
8	42.8	0.3	39.4	-0.5
9	43.1	0.4	40.5	-0.4
10	43.2	0.4	41.5	-0.3
11	44.0	0.4	42.6	-0.2
12	46.2	0.5	43.6	-0.1
13	46.3	0.5	44.6	0.1
14	46.4	0.6	45.6	0.2
15	46.8	0.6	46.7	0.3
16	46.9	0.6	47.7	0.4
17	47.1	0.7	48.8	0.5
18	47.1	0.7	50.0	0.6
19	47.6	0.8	51.3	0.7
20	49.6	0.8	52.7	0.9
21	50.1	0.9	54.3	1.1
22	50.8	0.9	56.3	1.3
23	51.8	0.9	59.0	1.5
24	55.2	1.0	63.9	2.0

**Table A.11** Height at shoulder in millimeters with outliers removed

Height 3 in millimeters with outliers removed				
Rat	Measured height	CDF	Expected height	z-value
1	45.1	0.0	26.4	-2.0
2	45.5	0.1	31.6	-1.5
3	45.8	0.1	34.5	-1.3
4	46.0	0.1	36.6	-1.1
5	46.1	0.2	38.3	-0.9
6	46.5	0.2	39.8	-0.7
7	47.2	0.3	41.2	-0.6
8	47.9	0.3	42.5	-0.5
9	48.2	0.4	43.7	-0.4
10	48.3	0.4	44.8	-0.3
11	48.3	0.4	45.9	-0.2
12	48.5	0.5	47.0	-0.1
13	48.7	0.5	48.1	0.1
14	48.8	0.6	49.2	0.2
15	48.9	0.6	50.3	0.3
16	50.8	0.6	51.4	0.4
17	51.0	0.7	52.6	0.5
18	51.0	0.7	53.9	0.6
19	51.3	0.8	55.3	0.7
20	52.0	0.8	56.8	0.9
21	53.4	0.9	58.5	1.1
22	53.7	0.9	60.6	1.3
23	54.9	0.9	63.5	1.5
24	56.9	1.0	68.7	2.0

**Table A.12** Height at last rib in millimeters with outliers removed

Height 4 in millimeters with outliers removed				
Rat	Measured height	CDF	Expected height	z-value
1	49.8	0.0	49.4	-2.0
2	51.1	0.1	50.7	-1.5
3	51.2	0.1	51.4	-1.2
4	52.3	0.2	51.9	-1.0
5	52.3	0.2	52.3	-0.8
6	52.3	0.3	52.7	-0.6
7	53.6	0.3	53.1	-0.5
8	53.7	0.4	53.4	-0.4
9	53.7	0.4	53.7	-0.2
10	53.9	0.5	54.0	-0.1
11	54.1	0.5	54.3	0.0
12	54.3	0.5	54.6	0.1
13	54.6	0.6	54.9	0.2
14	54.8	0.6	55.2	0.4
15	54.9	0.7	55.5	0.5
16	55.8	0.7	55.9	0.6
17	56.2	0.8	56.3	0.8
18	56.5	0.8	56.7	1.0
19	56.8	0.9	57.2	1.2
20	58.0	0.9	57.9	1.5
21	60.5	1.0	59.2	2.0

**Table A.13** Height at pelvis in millimeters with outliers removed

Height 5 in millimeters with outliers removed				
Rat	Measured height	CDF	Expected height	z-value
1	48.5	0.0	48.4	-2.0
2	48.5	0.1	50.3	-1.5
3	50.9	0.1	51.3	-1.3
4	51.0	0.1	52.1	-1.1
5	51.3	0.2	52.7	-0.9
6	53.3	0.2	53.2	-0.7
7	54.8	0.3	53.7	-0.6
8	55.4	0.3	54.2	-0.5
9	55.7	0.4	54.6	-0.4
10	55.8	0.4	55.0	-0.3
11	56.2	0.4	55.4	-0.2
12	56.2	0.5	55.8	-0.1
13	56.7	0.5	56.2	0.1
14	56.8	0.6	56.5	0.2
15	57.1	0.6	56.9	0.3
16	57.1	0.6	57.3	0.4
17	57.9	0.7	57.8	0.5
18	58.3	0.7	58.2	0.6
19	59.5	0.8	58.7	0.7
20	60.6	0.8	59.2	0.9
21	60.8	0.9	59.9	1.1
22	61.2	0.9	60.6	1.3
23	63.6	0.9	61.6	1.5

**Table A.14** Height at thigh in millimeters with outliers removed

Height 6 in millimeters with outliers removed				
Rat	Measured height	CDF	Expected height	z-value
1	40.7	0.1	35.3	-1.1
2	43.6	0.2	37.2	-0.9
3	44.9	0.2	38.9	-0.7
4	47.6	0.3	40.4	-0.6
5	48.8	0.3	41.8	-0.5
6	49.4	0.4	43.1	-0.4
7	50.4	0.4	44.3	-0.3
8	50.5	0.4	45.6	-0.2
9	50.7	0.5	46.8	-0.1
10	50.7	0.5	48.0	0.1
11	50.9	0.6	49.2	0.2
12	51.2	0.6	50.4	0.3
13	51.7	0.6	51.6	0.4
14	52.0	0.7	52.9	0.5
15	52.1	0.7	54.3	0.6
16	52.9	0.8	55.8	0.7
17	53.5	0.8	57.5	0.9
18	54.7	0.9	59.4	1.1
19	54.8	0.9	61.7	1.3
20	60.3	0.9	64.8	1.5



**Table A.15** Height at base of tail in millimeters with outliers removed

Height 7 in millimeters with outliers removed				
Rat	Measured height	CDF	Expected height	z-value
1	18.2	0.0	12.0	-2.0
2	20.2	0.1	15.8	-1.5
3	20.6	0.1	17.9	-1.3
4	22.3	0.1	19.5	-1.1
5	23.3	0.2	20.8	-0.9
6	25.0	0.2	21.9	-0.7
7	25.9	0.3	22.9	-0.6
8	26.4	0.3	23.8	-0.5
9	27.2	0.4	24.7	-0.4
10	27.7	0.4	25.5	-0.3
11	28.5	0.4	26.4	-0.2
12	29.0	0.5	27.2	-0.1
13	29.1	0.5	28.0	0.1
14	29.4	0.6	28.8	0.2
15	29.9	0.6	29.6	0.3
16	30.0	0.6	30.4	0.4
17	31.2	0.7	31.3	0.5
18	32.1	0.7	32.3	0.6
19	33.4	0.8	33.3	0.7
20	36.4	0.8	34.4	0.9
21	18.2	0.0	12.0	-2.0
22	20.2	0.1	15.8	-1.5
23	20.6	0.1	17.9	-1.3

**Table A.16** Width raw data at varying points in millimeters

Width in millimeters Raw Data							
Rat	1	2	3	4	5	6	7
1	38.7	38.8	46.1	53.0	68.0	77.4	44.3
2	30.7	37.1	58.6	60.4	66.9	73.2	45.6
3	35.9	41.9	57.0	65.7	75.8	69.6	25.9
4	38.0	44.9	58.2	64.5	69.3	59.3	28.8
5	36.8	43.5	58.2	61.5	68.6	65.5	28.5
6	39.4	41.7	48.9	64.6	70.0	61.5	24.4
7	40.4	43.0	53.5	67.5	68.8	59.2	27.0
8	45.0	47.9	61.1	54.9	55.4	47.8	21.0
9	38.1	45.6	52.1	63.8	65.5	47.8	19.9
10	44.3	52.7	58.5	60.4	61.1	58.8	26.8
11	38.4	44.3	58.9	65.5	73.9	71.7	19.5
12	40.7	44.8	55.0	61.4	64.6	70.2	25.8
13	41.8	49.5	56.5	58.3	78.6	75.8	26.0
14	38.5	44.5	50.1	60.1	65.9	45.1	25.4
15	39.6	44.2	48.6	60.5	68.5	55.3	23.8
16	37.8	40.8	51.2	67.0	70.8	63.0	21.4
17	38.6	43.4	50.9	65.9	77.2	57.9	27.2
18	36.5	40.9	51.7	66.0	72.1	63.0	24.6
19	36.3	47.7	58.0	67.6	67.0	48.8	20.3
20	38.3	44.3	52.9	64.8	71.5	53.0	18.4
21	42.3	45.7	55.2	61.5	72.6	34.5	22.2
22	42.6	47.2	53.9	73.4	76.5	65.8	22.8
23	36.7	40.7	50.8	63.5	65.6	43.4	22.9
24	40.4	45.8	49.4	57.7	57.3	35.8	16.9
average	39.0	44.2	54.0	62.9	68.8	58.5	25.4
StdDev	3.0	3.4	4.0	4.5	5.8	12.0	6.8
Q 1	37.5	41.8	50.9	60.4	65.8	48.5	21.3
Q 3	40.5	45.7	58.0	65.8	72.3	66.7	26.9
IQR	2.9	3.9	7.1	5.4	6.4	18.2	5.6
Upper fence	44.9	51.5	68.7	73.9	81.9	94.0	35.2
Lower fence	33.2	36.0	40.2	52.3	56.2	21.2	13.0

**Table A.17** Width in millimeters at the base of the neck with outliers removed

Width 1 in millimeters with outliers removed				
Rat	Measured width	CDF	Expected width	z-value
1	35.9	0.1	25.4	-1.5
2	36.3	0.1	27.7	-1.3
3	36.5	0.1	29.3	-1.1
4	36.7	0.2	30.7	-0.9
5	36.8	0.2	31.9	-0.7
6	37.8	0.3	33.0	-0.6
7	38.0	0.3	33.9	-0.5
8	38.1	0.4	34.9	-0.4
9	38.3	0.4	35.8	-0.3
10	38.4	0.4	36.7	-0.2
11	38.5	0.5	37.5	-0.1
12	38.6	0.5	38.4	0.1
13	38.7	0.6	39.2	0.2
14	39.4	0.6	40.1	0.3
15	39.6	0.6	41.0	0.4
16	40.4	0.7	41.9	0.5
17	40.4	0.7	42.9	0.6
18	40.7	0.8	44.0	0.7
19	41.8	0.8	45.2	0.9
20	42.3	0.9	46.6	1.1
21	42.6	0.9	48.2	1.3
22	44.3	0.9	50.5	1.5

**Table A.18** Width in millimeters at the end of the neck with outliers removed

Width 2 in millimeters with outliers removed				
Rat	Measured width	CDF	Expected width	z-value
1	37.1	0.0	24.0	-2.0
2	38.8	0.1	28.7	-1.5
3	40.7	0.1	31.3	-1.3
4	40.8	0.1	33.2	-1.1
5	40.9	0.2	34.7	-0.9
6	41.7	0.2	36.1	-0.7
7	41.9	0.3	37.3	-0.6
8	43.0	0.3	38.4	-0.5
9	43.4	0.4	39.5	-0.4
10	43.5	0.4	40.5	-0.3
11	44.2	0.4	41.5	-0.2
12	44.3	0.5	42.5	-0.1
13	44.3	0.5	43.5	0.1
14	44.5	0.6	44.4	0.2
15	44.8	0.6	45.4	0.3
16	44.9	0.6	46.5	0.4
17	45.6	0.7	47.5	0.5
18	45.7	0.7	48.7	0.6
19	45.8	0.8	49.9	0.7
20	47.2	0.8	51.2	0.9
21	47.7	0.9	52.8	1.1
22	47.9	0.9	54.7	1.3
23	49.5	0.9	57.2	1.5

**Table A.19** Width in millimeters at the shoulder with outliers removed

Width 3 in millimeters with outliers removed				
Rat	Measured width	CDF	Expected width	z-value
1	46.1	0.0	28.7	-2.0
2	48.6	0.1	34.4	-1.5
3	48.9	0.1	37.5	-1.3
4	49.4	0.1	39.7	-1.1
5	50.1	0.2	41.6	-0.9
6	50.8	0.2	43.2	-0.7
7	50.9	0.3	44.7	-0.6
8	51.2	0.3	46.1	-0.5
9	51.7	0.4	47.3	-0.4
10	52.1	0.4	48.6	-0.3
11	52.9	0.4	49.8	-0.2
12	53.5	0.5	50.9	-0.1
13	53.9	0.5	52.1	0.1
14	55.0	0.6	53.3	0.2
15	55.2	0.6	54.5	0.3
16	56.5	0.6	55.7	0.4
17	57.0	0.7	57.0	0.5
18	58.0	0.7	58.3	0.6
19	58.2	0.8	59.8	0.7
20	58.2	0.8	61.4	0.9
21	58.5	0.9	63.3	1.1
22	58.6	0.9	65.6	1.3
23	58.9	0.9	68.7	1.5
24	46.1	0.0	28.7	-2.0

**Table A.20** Width in millimeters at the last rib with outliers removed

Width 4 in millimeters with outliers removed				
Rat	Measured width	CDF	Expected width	z-value
1	53.0	0.0	33.8	-2.0
2	54.9	0.1	40.4	-1.5
3	57.7	0.1	44.0	-1.3
4	58.3	0.1	46.7	-1.1
5	60.1	0.2	48.9	-0.9
6	60.4	0.2	50.8	-0.7
7	60.4	0.3	52.6	-0.6
8	60.5	0.3	54.2	-0.5
9	61.4	0.4	55.7	-0.4
10	61.5	0.4	57.1	-0.3
11	61.5	0.4	58.5	-0.2
12	63.5	0.5	59.9	-0.1
13	63.8	0.5	61.3	0.1
14	64.5	0.6	62.7	0.2
15	64.6	0.6	64.1	0.3
16	64.8	0.6	65.5	0.4
17	65.5	0.7	67.0	0.5
18	65.7	0.7	68.6	0.6
19	65.9	0.8	70.4	0.7
20	66.0	0.8	72.3	0.9
21	67.0	0.9	74.5	1.1
22	67.5	0.9	77.2	1.3
23	67.6	0.9	80.8	1.5
24	73.4	1.0	87.4	2.0

**Table A.21** Width in millimeters at the pelvis with outliers removed

Width 5 in millimeters with outliers removed				
Rat	Measured width	CDF	Expected width	z-value
1	57.3	0.1	43.3	-1.5
2	61.1	0.1	47.4	-1.3
3	64.6	0.1	50.3	-1.1
4	65.5	0.2	52.8	-0.9
5	65.6	0.2	54.9	-0.7
6	65.9	0.3	56.8	-0.6
7	66.9	0.3	58.6	-0.5
8	67.0	0.4	60.3	-0.4
9	68.0	0.4	61.9	-0.3
10	68.5	0.4	63.4	-0.2
11	68.6	0.5	65.0	-0.1
12	68.8	0.5	66.5	0.1
13	69.3	0.6	68.0	0.2
14	70.0	0.6	69.6	0.3
15	70.8	0.6	71.2	0.4
16	71.5	0.7	72.9	0.5
17	72.1	0.7	74.6	0.6
18	72.6	0.8	76.6	0.7
19	73.9	0.8	78.7	0.9
20	75.8	0.9	81.1	1.1
21	76.5	0.9	84.1	1.3
22	77.2	0.9	88.1	1.5
23	78.6	1.0	95.5	2.0

**Table A.22** Width in millimeters at the thigh with outliers removed

Width 6 in millimeters with outliers removed				
Rat	Measured width	CDF	Expected width	z-value
1	34.5	0.0	24.8	-2.0
2	35.8	0.1	32.1	-1.5
3	43.4	0.1	36.1	-1.3
4	45.1	0.1	39.0	-1.1
5	47.8	0.2	41.4	-0.9
6	47.8	0.2	43.6	-0.7
7	48.8	0.3	45.5	-0.6
8	53.0	0.3	47.2	-0.5
9	55.3	0.4	48.9	-0.4
10	57.9	0.4	50.5	-0.3
11	58.8	0.4	52.0	-0.2
12	59.2	0.5	53.5	-0.1
13	59.3	0.5	55.0	0.1
14	61.5	0.6	56.6	0.2
15	63.0	0.6	58.1	0.3
16	63.0	0.6	59.7	0.4
17	65.5	0.7	61.4	0.5
18	65.8	0.7	63.1	0.6
19	69.6	0.8	65.0	0.7
20	70.2	0.8	67.1	0.9
21	71.7	0.9	69.5	1.1
22	73.2	0.9	72.5	1.3
23	75.8	0.9	76.5	1.5
24	34.5	0.0	24.8	-2.0



**Table A.23** Width in millimeters at the base of the tail with outliers removed

Width 7 in millimeters with outliers removed				
Rat	Measured width	CDF	Expected width	z-value
1	16.9	0.0	16.9	-2.0
2	18.4	0.1	18.6	-1.5
3	19.5	0.1	19.6	-1.2
4	19.9	0.2	20.3	-1.0
5	20.3	0.2	20.8	-0.8
6	21.0	0.3	21.4	-0.7
7	21.4	0.3	21.8	-0.5
8	22.2	0.3	22.2	-0.4
9	22.8	0.4	22.6	-0.3
10	22.9	0.4	23.0	-0.2
11	23.8	0.5	23.4	-0.1
12	24.4	0.5	23.8	0.1
13	24.6	0.6	24.2	0.2
14	25.4	0.6	24.6	0.3
15	25.8	0.7	25.0	0.4
16	25.9	0.7	25.4	0.5
17	26.0	0.8	25.9	0.7
18	26.8	0.8	26.4	0.8
19	27.0	0.8	27.0	1.0
20	27.2	0.9	27.7	1.2
21	28.5	0.9	28.6	1.5
22	28.8	1.0	30.3	2.0

## Appendix B

### Collected and sorted rodent mass data

The following data in table B.1 is the masses in grams of 90 rats collected and sorted.

**Table B.1** Masses of rats both raw data and outliers removed in grams

rat	mass with outliers (g)	Mass with outliers removed (g)	CDF	Expected mass (g)	z-values
1	290.0	300.0	0.0	292.1	-2.5
2	300.0	310.0	0.0	301.4	-2.1
3	310.0	310.0	0.0	306.3	-1.9
4	310.0	316.0	0.0	309.8	-1.7
5	316.0	316.0	0.1	312.5	-1.6
6	316.0	318.0	0.1	314.8	-1.5
7	318.0	320.0	0.1	316.8	-1.4
8	320.0	320.0	0.1	318.5	-1.3
9	320.0	324.0	0.1	320.1	-1.3
10	324.0	324.0	0.1	321.6	-1.2
11	324.0	326.0	0.1	323.0	-1.1
12	326.0	326.0	0.1	324.2	-1.1
13	326.0	326.0	0.2	325.4	-1.0
14	326.0	330.0	0.2	326.6	-1.0
15	330.0	330.0	0.2	327.7	-0.9
16	330.0	330.0	0.2	328.7	-0.9
17	330.0	330.0	0.2	329.7	-0.8
18	330.0	330.0	0.2	330.7	-0.8
19	330.0	330.0	0.2	331.6	-0.7
20	330.0	330.0	0.2	332.5	-0.7
21	330.0	333.0	0.3	333.4	-0.7
22	333.0	335.0	0.3	334.2	-0.6
23	335.0	335.0	0.3	335.1	-0.6
24	335.0	337.0	0.3	335.9	-0.6
25	337.0	339.0	0.3	336.7	-0.5
26	339.0	339.0	0.3	337.5	-0.5
27	339.0	339.0	0.3	338.3	-0.4
28	339.0	340.0	0.3	339.0	-0.4
29	340.0	340.0	0.4	339.8	-0.4
30	340.0	340.0	0.4	340.5	-0.3
31	340.0	341.0	0.4	341.3	-0.3
32	341.0	341.0	0.4	342.0	-0.3
33	341.0	342.0	0.4	342.7	-0.3
34	342.0	344.0	0.4	343.4	-0.2
35	344.0	344.0	0.4	344.1	-0.2
36	344.0	345.0	0.4	344.8	-0.2
37	345.0	345.0	0.5	345.5	-0.1
38	345.0	345.0	0.5	346.2	-0.1
39	345.0	345.0	0.5	346.9	-0.1
40	345.0	346.0	0.5	347.6	0.0
41	346.0	346.0	0.5	348.3	0.0

Masses of rats both raw data and outliers removed in grams					
42	346.0	346.0	0.5	349.0	0.0
43	346.0	346.0	0.5	349.7	0.1
44	346.0	348.0	0.5	350.4	0.1
45	348.0	350.0	0.5	351.1	0.1
46	350.0	350.0	0.6	351.8	0.2
47	350.0	350.0	0.6	352.5	0.2
48	350.0	350.0	0.6	353.2	0.2
49	350.0	350.0	0.6	354.0	0.3
50	350.0	350.0	0.6	354.7	0.3
51	350.0	350.0	0.6	355.4	0.3
52	350.0	350.0	0.6	356.1	0.3
53	350.0	350.0	0.6	356.9	0.4
54	350.0	350.0	0.7	357.6	0.4
55	350.0	350.0	0.7	358.4	0.4
56	350.0	350.0	0.7	359.2	0.5
57	350.0	353.0	0.7	360.0	0.5
58	353.0	354.0	0.7	360.8	0.6
59	354.0	354.0	0.7	361.6	0.6
60	354.0	355.0	0.7	362.4	0.6
61	355.0	356.0	0.7	363.3	0.7
62	356.0	360.0	0.8	364.2	0.7
63	360.0	360.0	0.8	365.1	0.7
64	360.0	360.0	0.8	366.0	0.8
65	360.0	360.0	0.8	367.0	0.8
66	360.0	364.0	0.8	368.0	0.9
67	364.0	367.0	0.8	369.0	0.9
68	367.0	370.0	0.8	370.1	1.0
69	370.0	370.0	0.8	371.2	1.0
70	370.0	380.0	0.9	372.4	1.1
71	380.0	380.0	0.9	373.7	1.1
72	380.0	385.0	0.9	375.1	1.2
73	385.0	390.0	0.9	376.5	1.3
74	390.0	390.0	0.9	378.1	1.3
75	390.0	390.0	0.9	379.9	1.4
76	390.0	390.0	0.9	381.9	1.5
77	390.0	390.0	0.9	384.2	1.6
78	390.0	390.0	1.0	386.9	1.7
79	390.0	400.0	1.0	390.3	1.9
80	400.0	400.0	1.0	395.2	2.1
81	400.0	400.0	1.0	404.6	2.5
82	400.0	300.0	0.0	292.1	-2.5
83	410	-----	-----	-----	-----
84	410	-----	-----	-----	-----
85	420	-----	-----	-----	-----
86	420	-----	-----	-----	-----
87	435	-----	-----	-----	-----
88	440	-----	-----	-----	-----
89	440	-----	-----	-----	-----
Mean	354.7	348.3			
StdDev	31.9	22.5			
Q 1	335				
Q 2	364				

## Appendix C

### Normality Data

The following data represented by the figures in this section is the output of the Ryan-Joiner test in Minitab. Listed along with the graph is the P value which can be compared to a predetermined alpha value of .05, meaning that a P-value greater than 0.05 is a sign of normality.

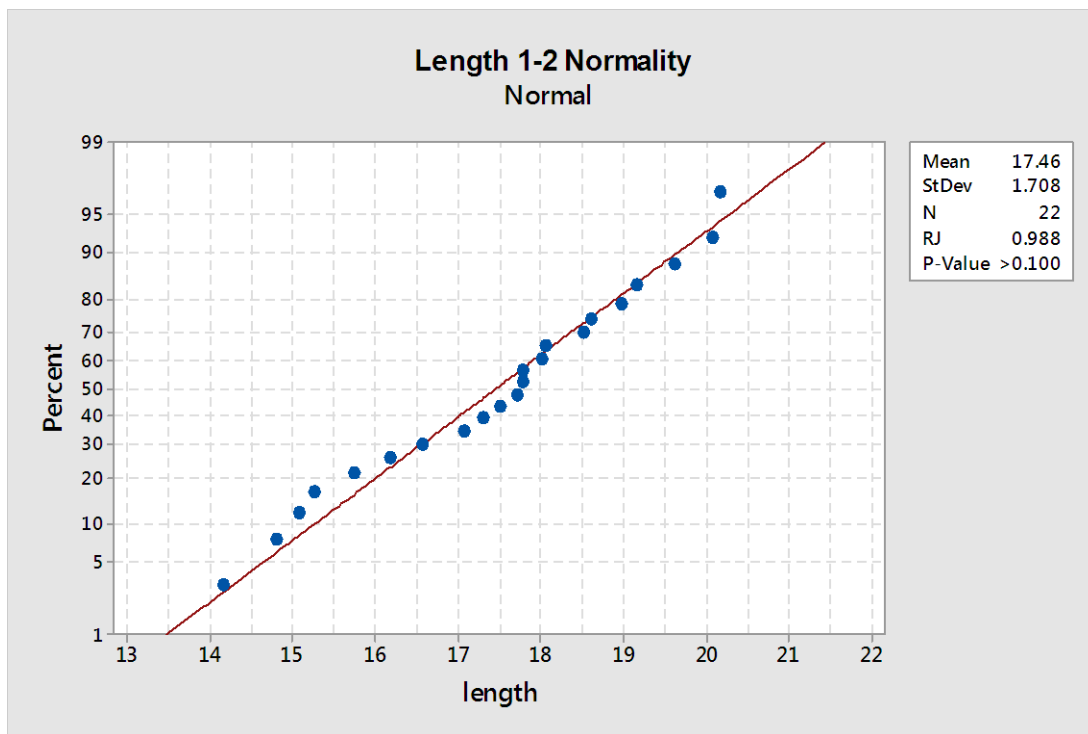


**Figure C.1** Normality of data for percentile versus neck length in mm.

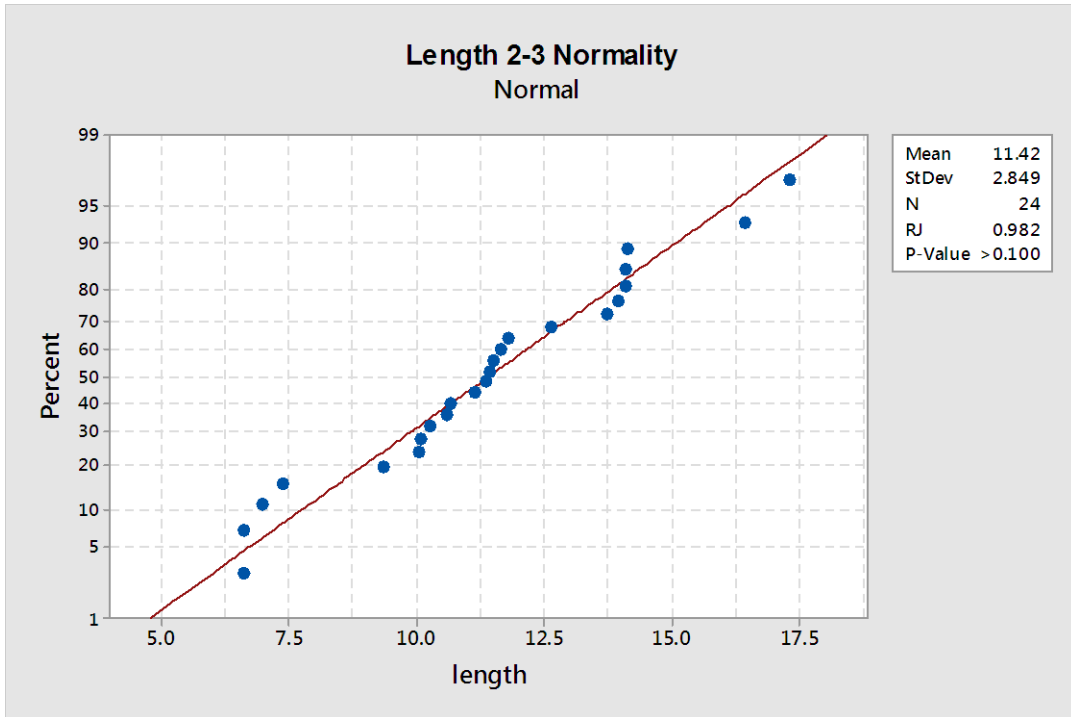


**Figure C.2** Normality of data for percentile versus neck to shoulder length in mm.

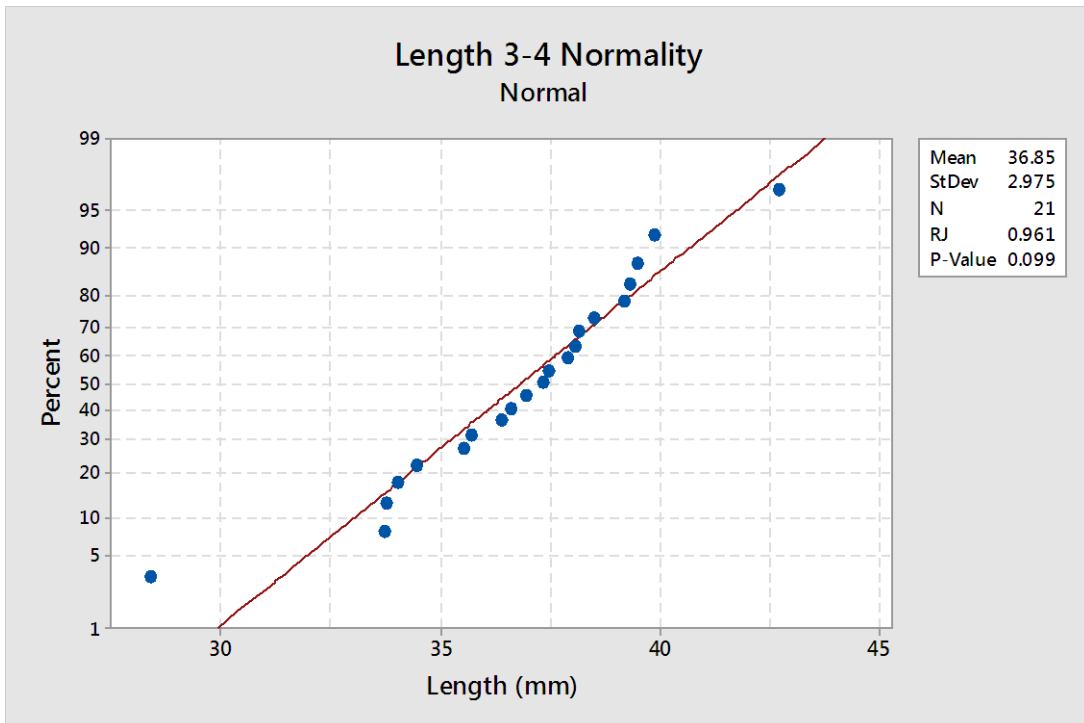


**Figure C.3** Normality of data for percentile versus shoulder to rib length in millimeters.

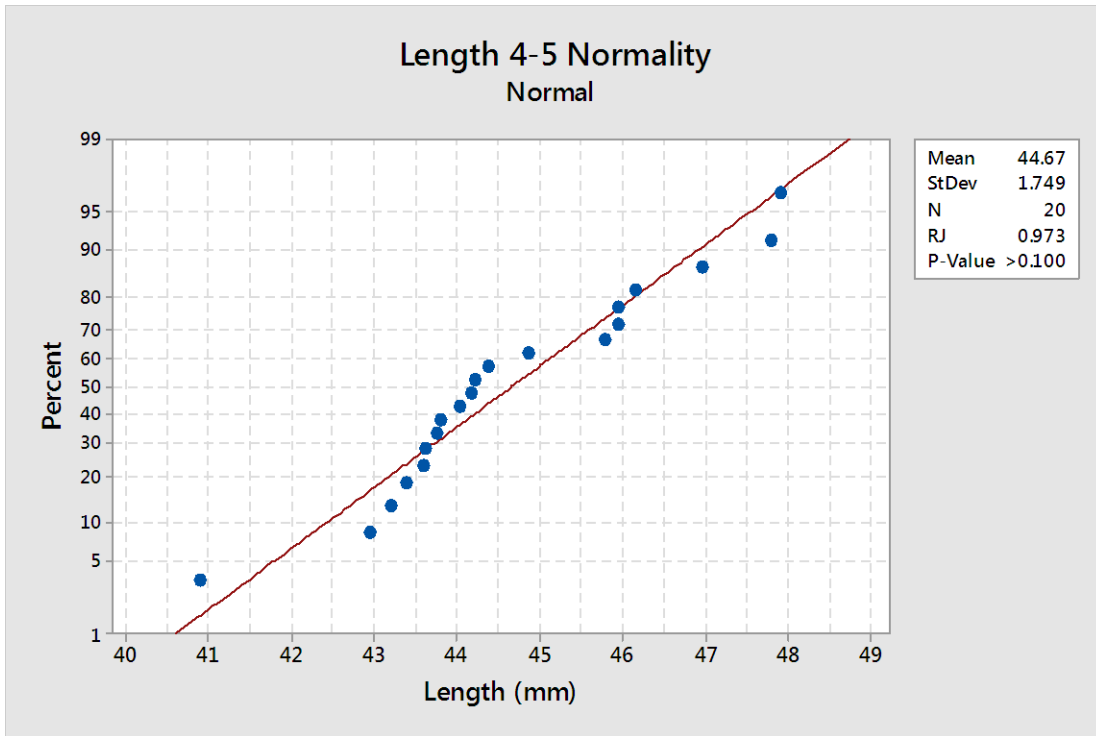


**Figure C.4** Normality of data for percentile versus rib to pelvis length in mm.

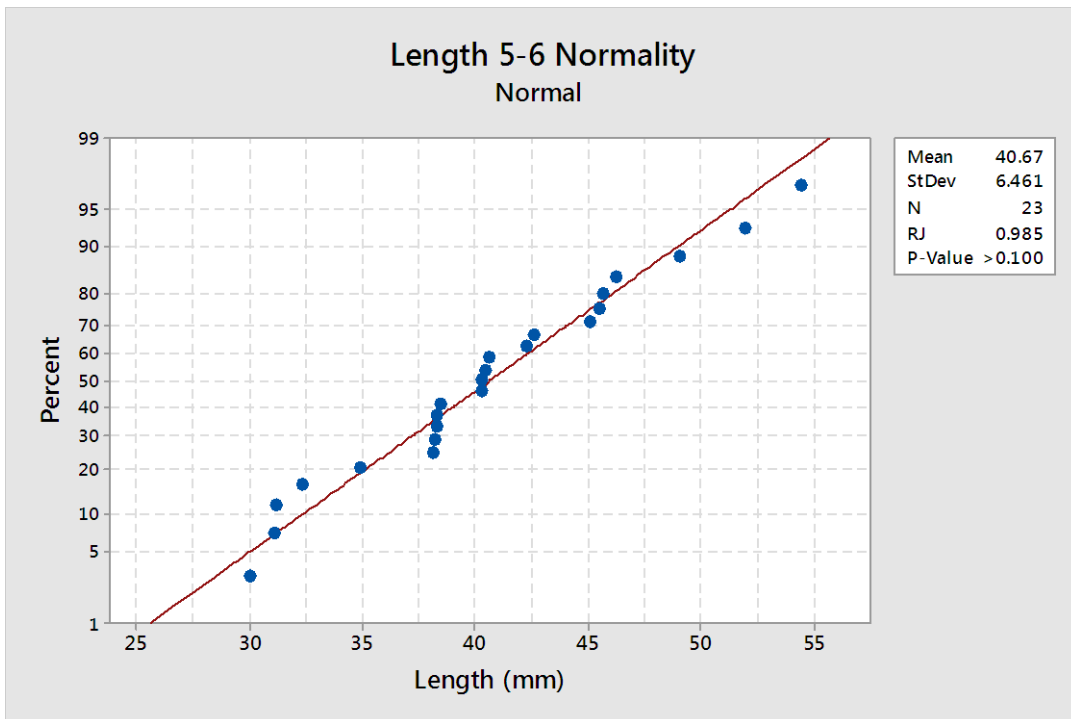


**Figure C.5** Normality of data for percentile versus pelvis to thigh length in millimeters.

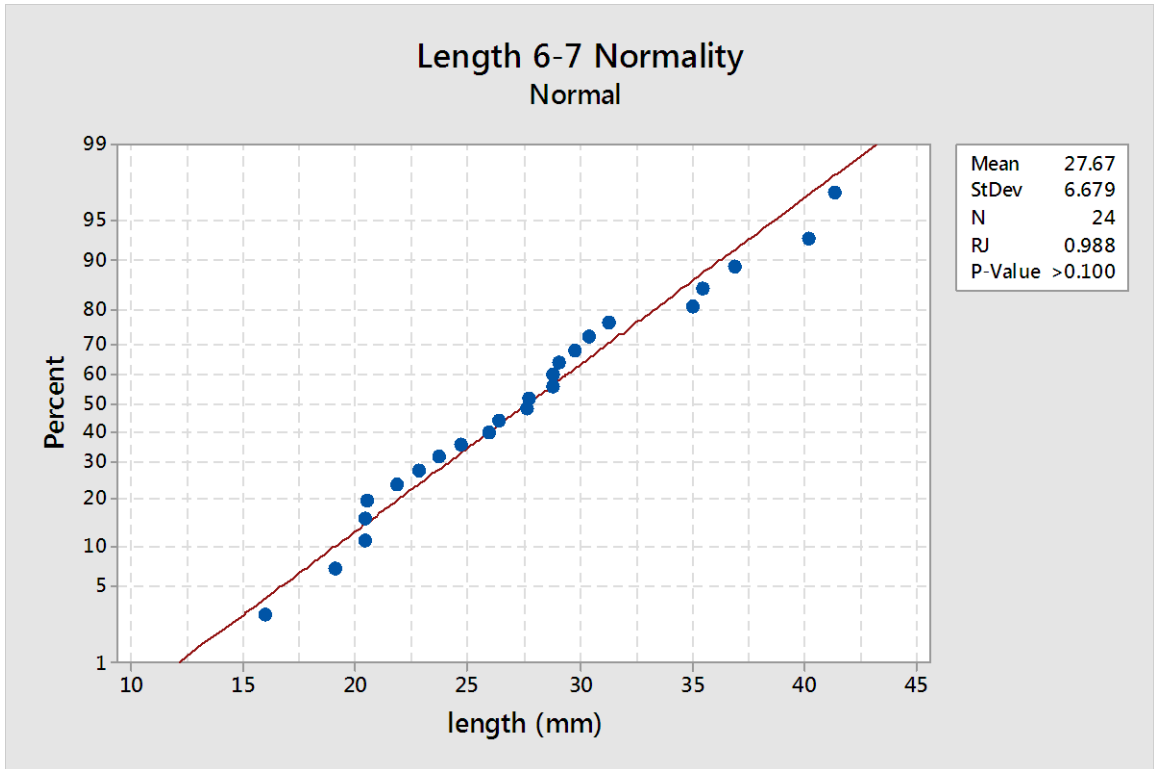


**Figure C.6** Normality of data for percentile versus thigh to tail base length.

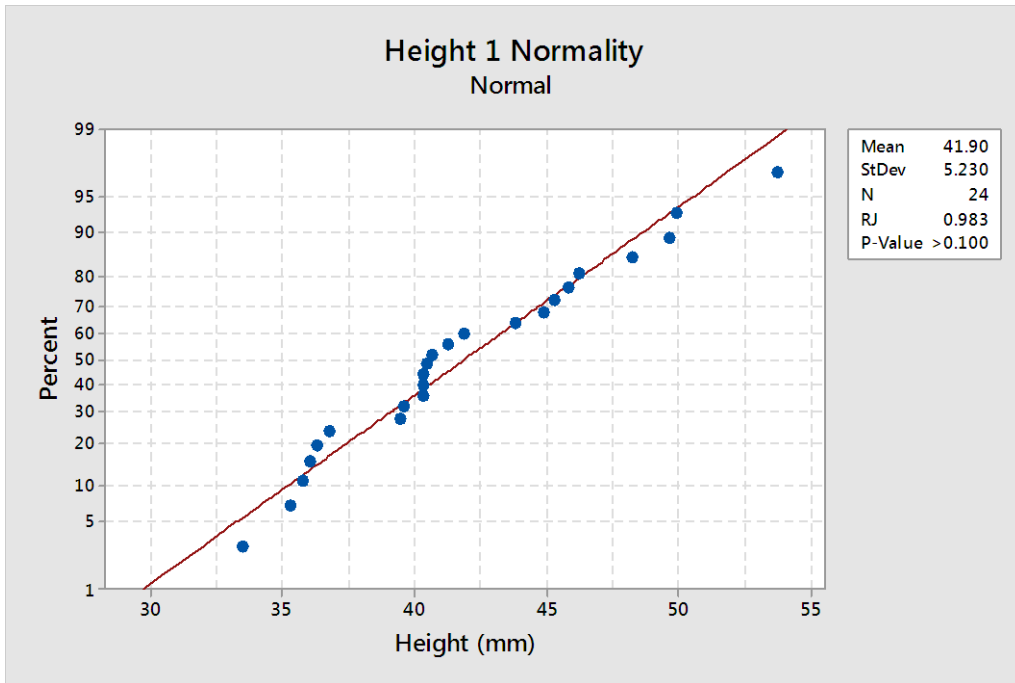


**Figure C.7** Normality of data for percentile base of neck height in millimeters.

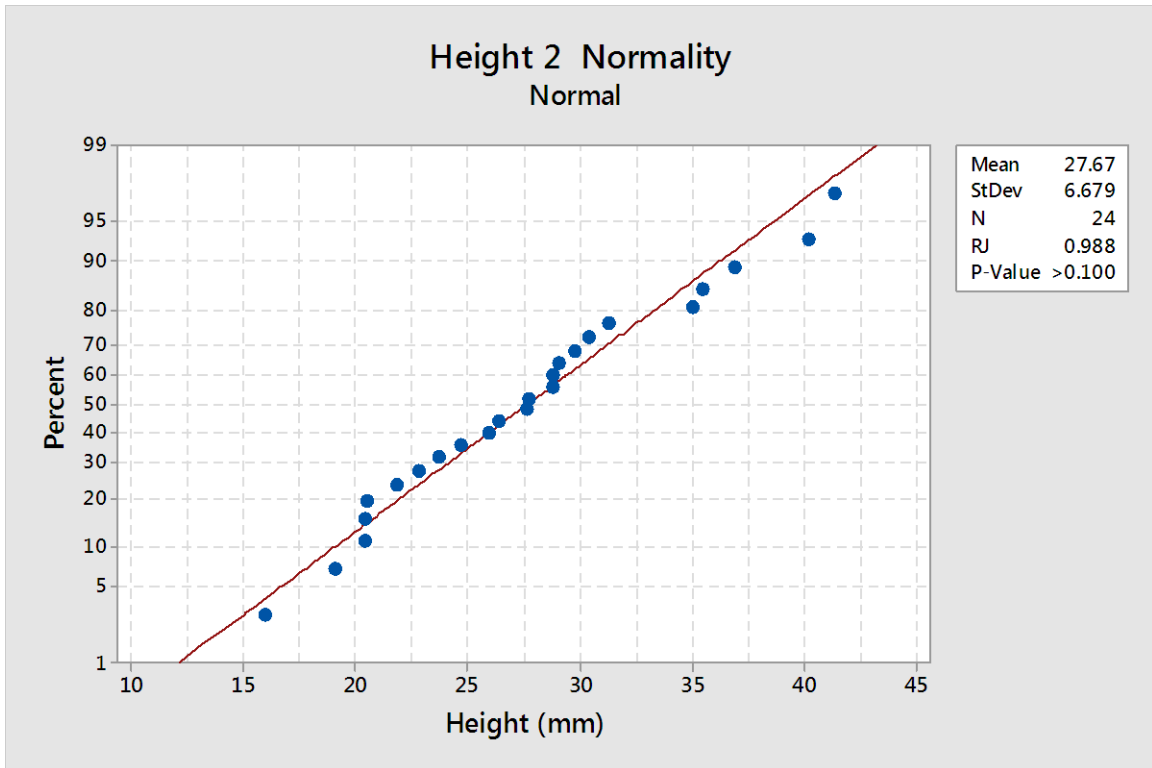


**Figure C.8** Normality of data for percentile end of neck height in mm.

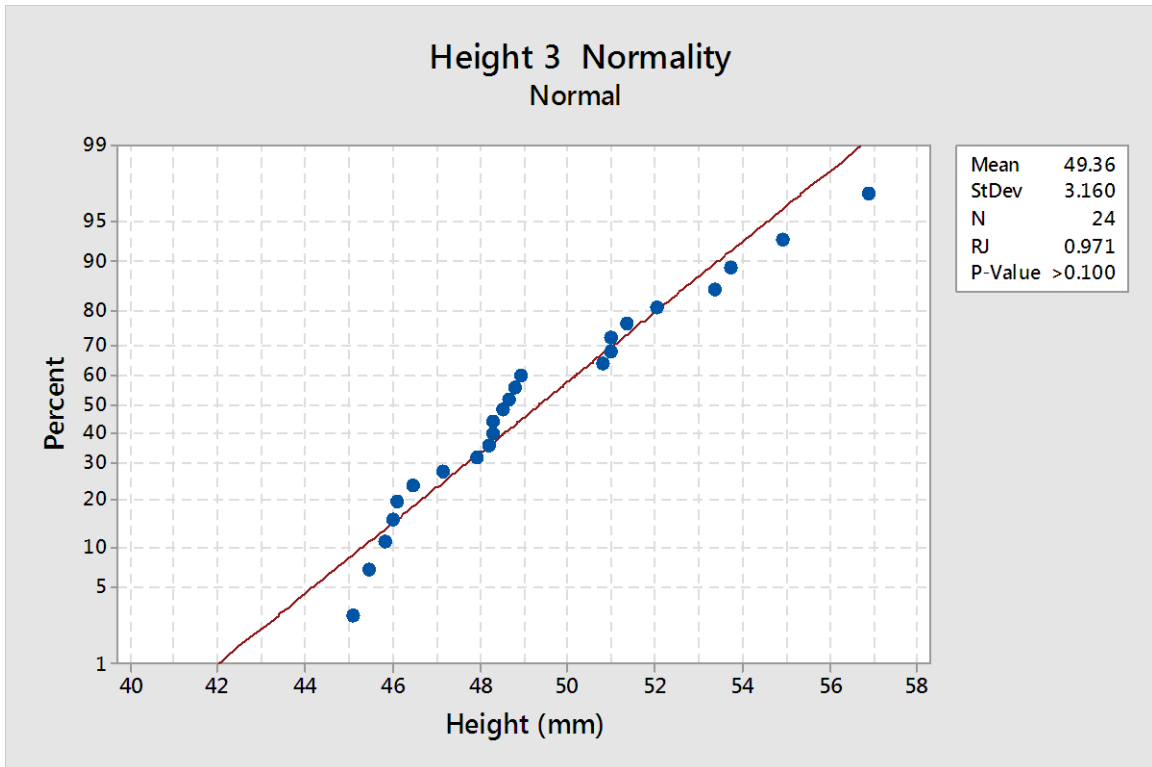


**Figure C.9** Normality of data for percentile shoulder height in millimeters.



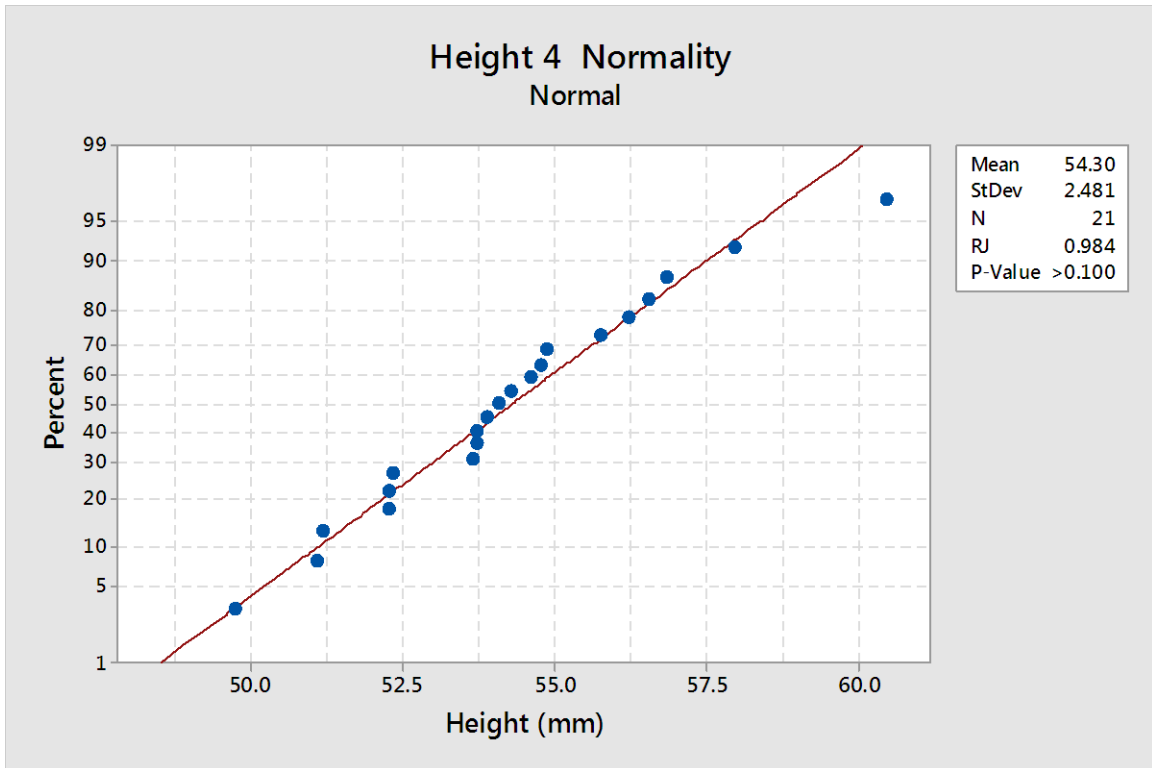


**Figure C.10** Normality of data for percentile rib height in millimeters.

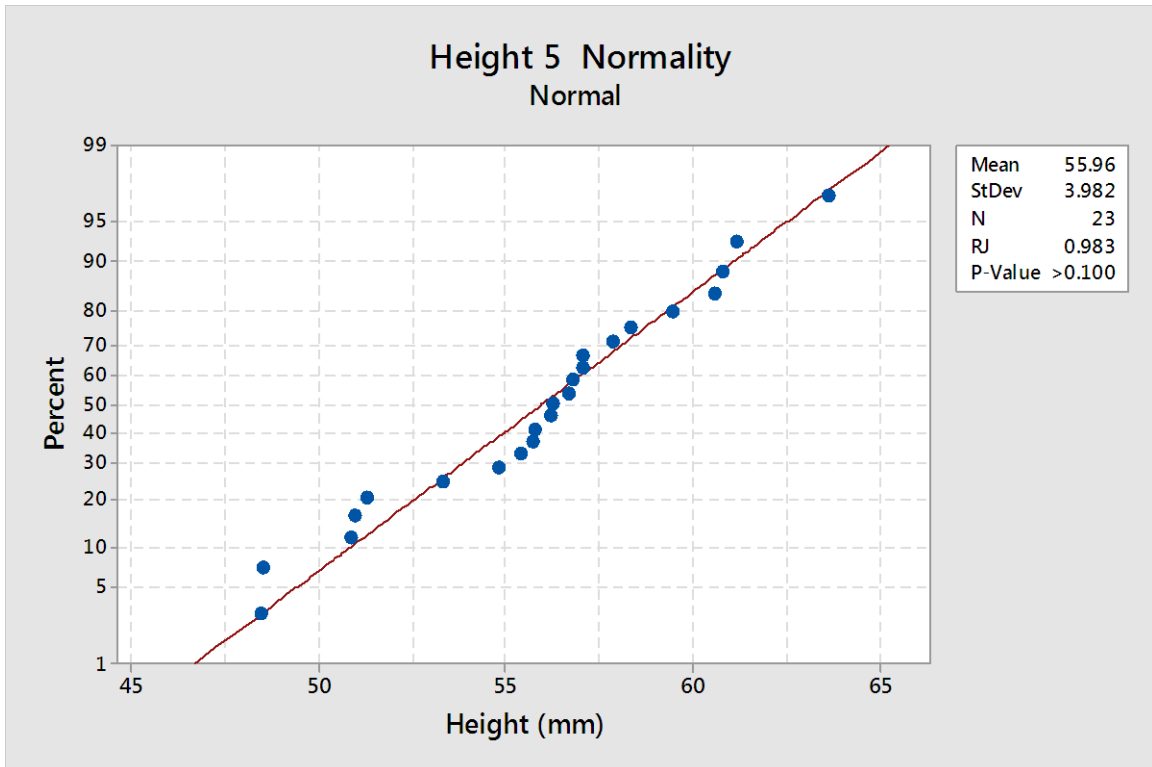


**Figure C.11** Normality of data for percentile pelvis height in millimeters.

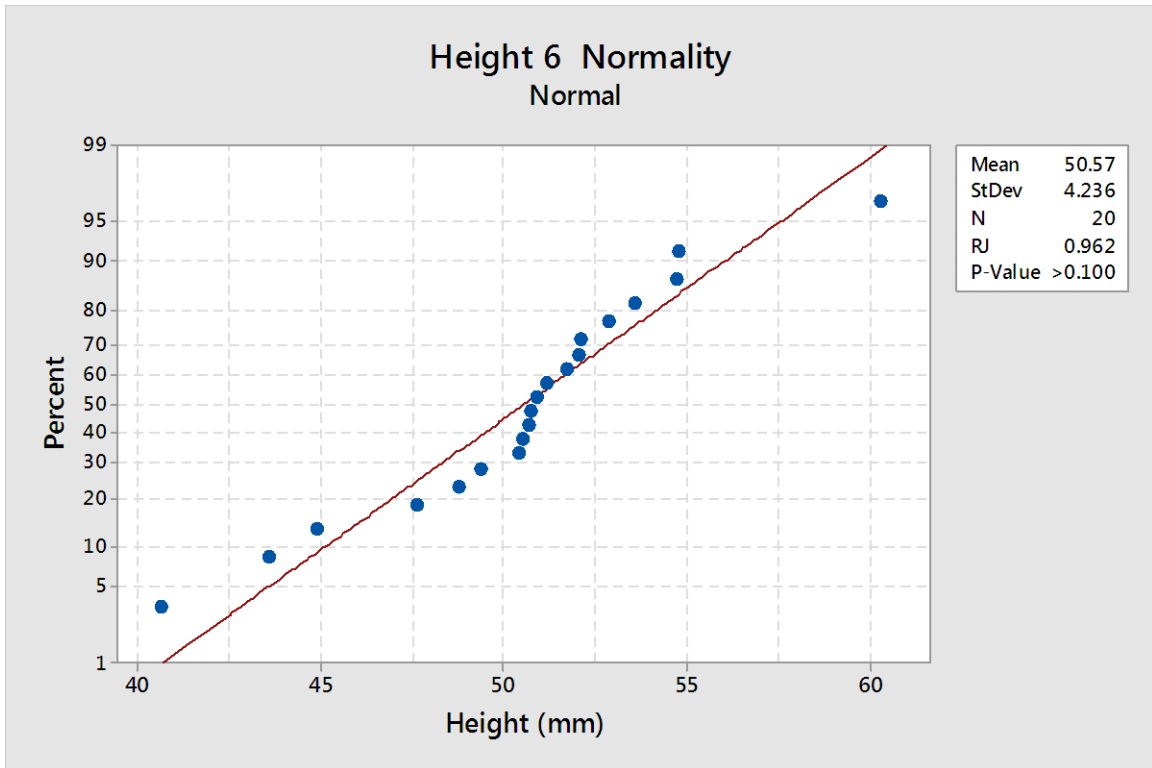


**Figure C.12** Normality of data for percentile thigh height in millimeters.

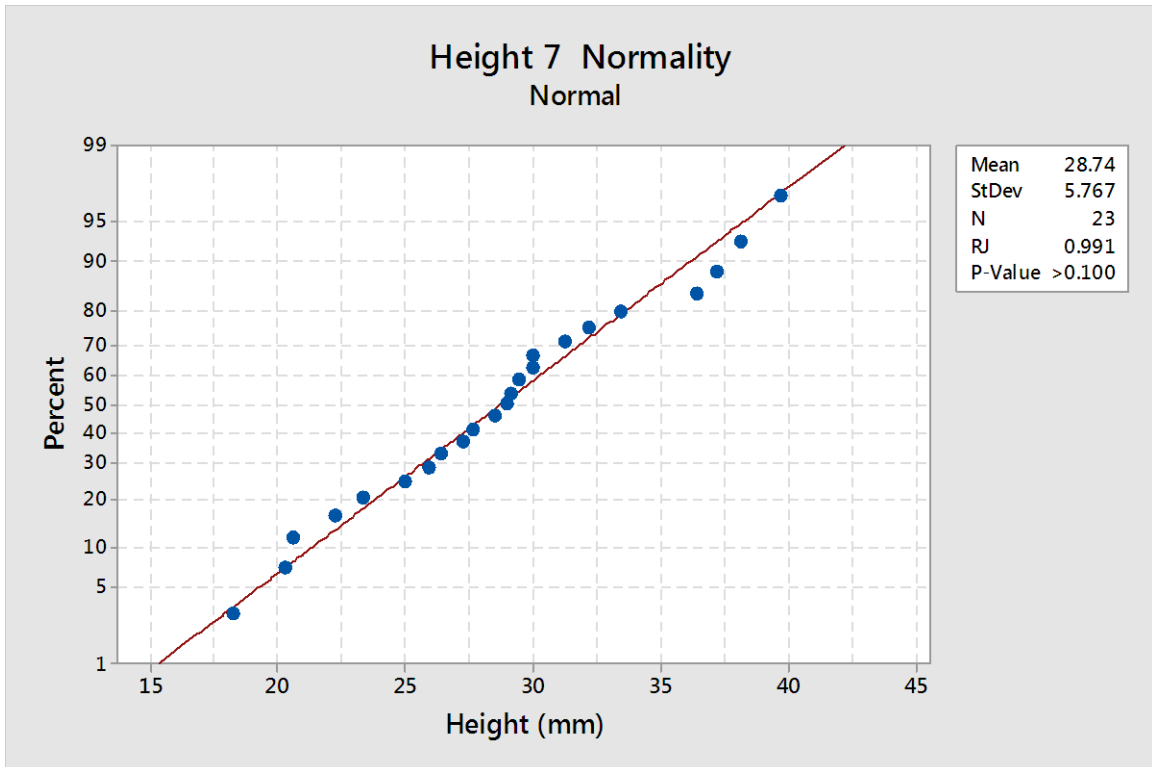


**Figure C.13** Normality of data for percentile tail base height in millimeters.

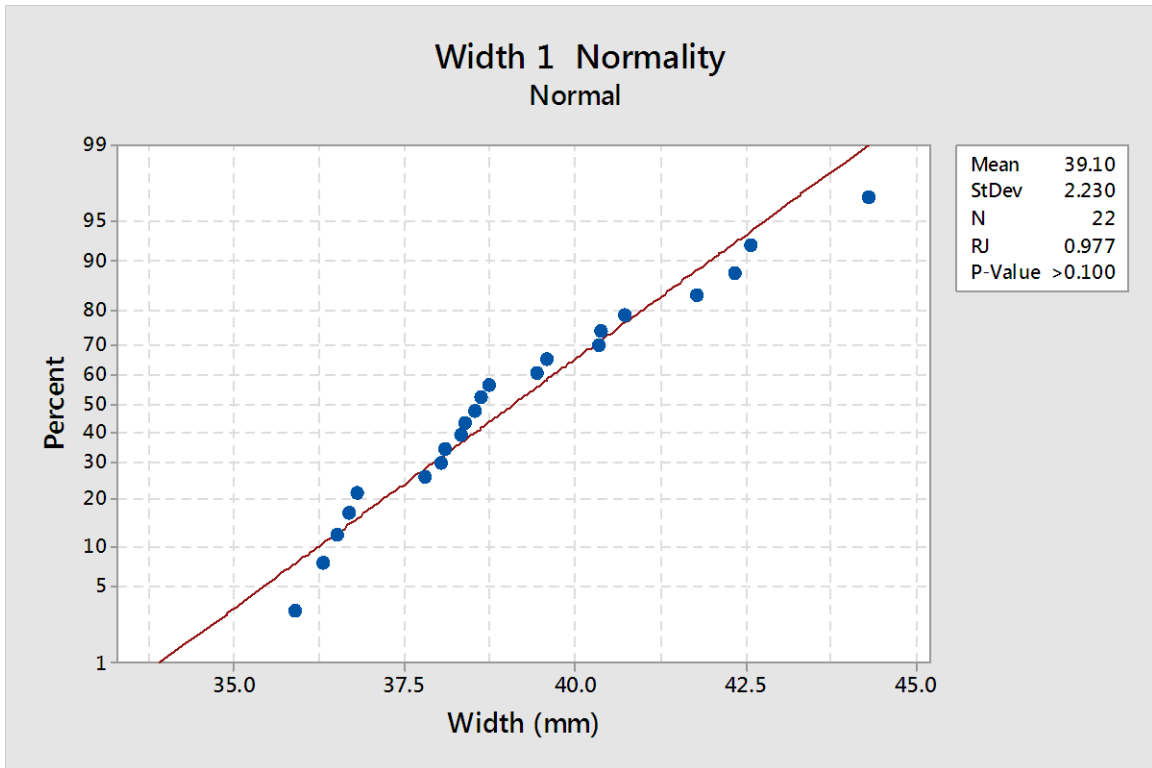


**Figure C.14** Normality of data for percentile base of neck width in millimeters

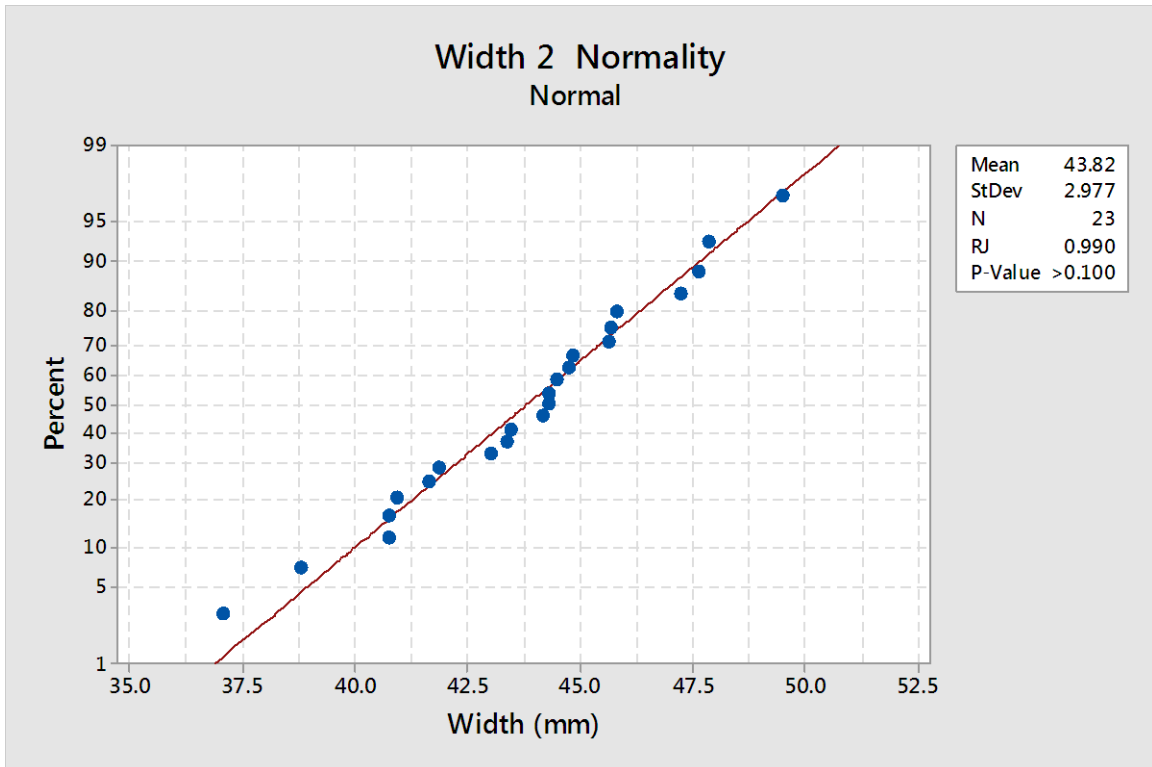


**Figure C.15** Normality of data for percentile end of neck width in millimeters

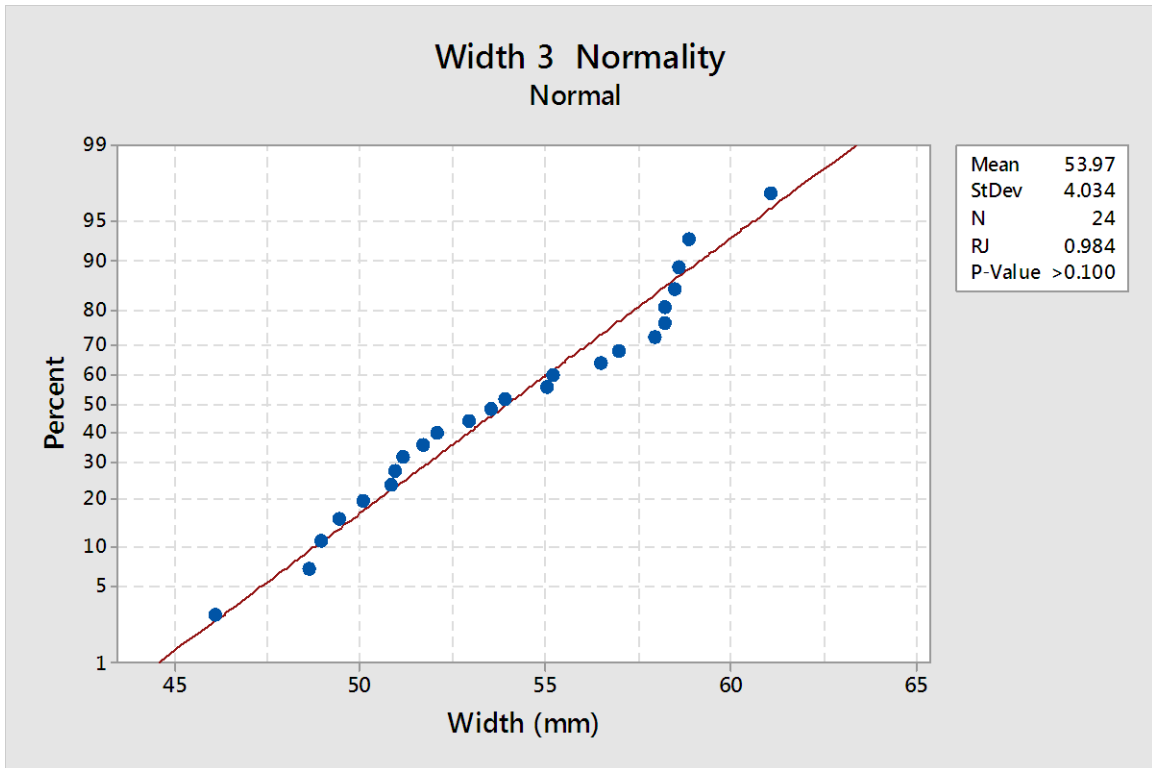


**Figure C.16** Normality of data for percentile shoulder width in millimeters.

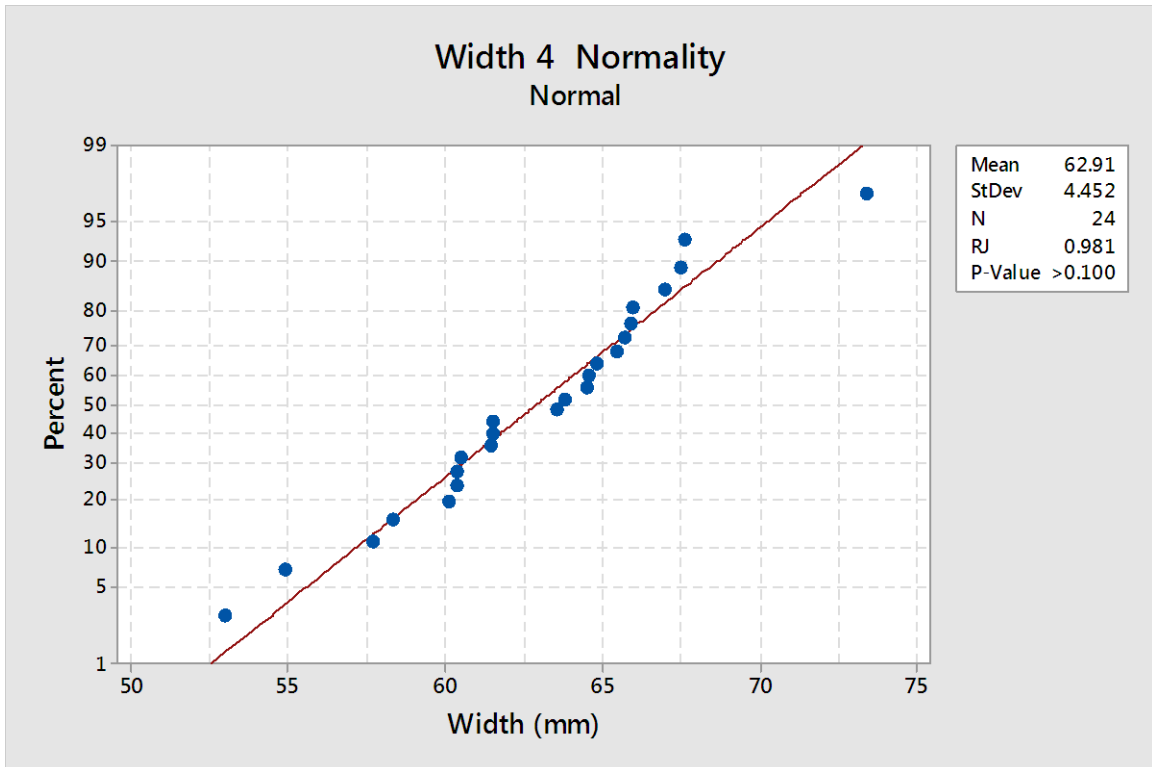


**Figure C.17** Normality of data for percentile rib width in millimeters.



**Figure C.18** Normality of data for percentile pelvis width in millimeters

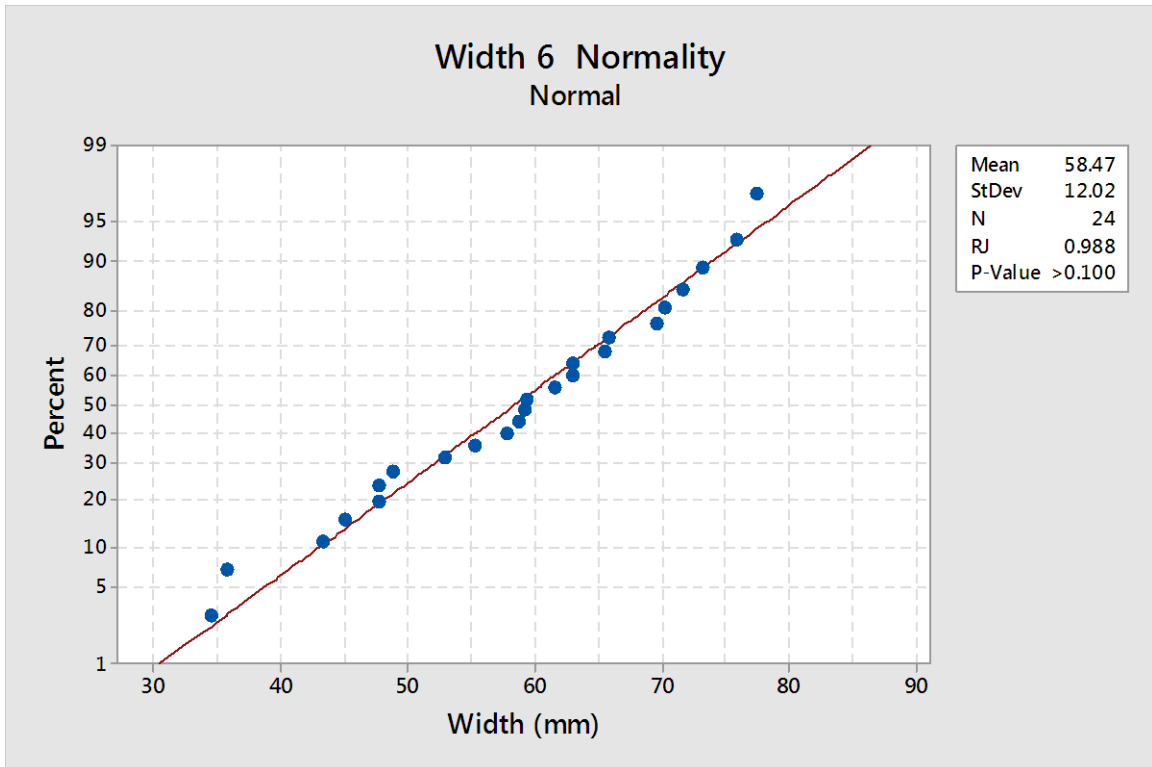


**Figure C.19** Normality of data for percentile thigh width in millimeters

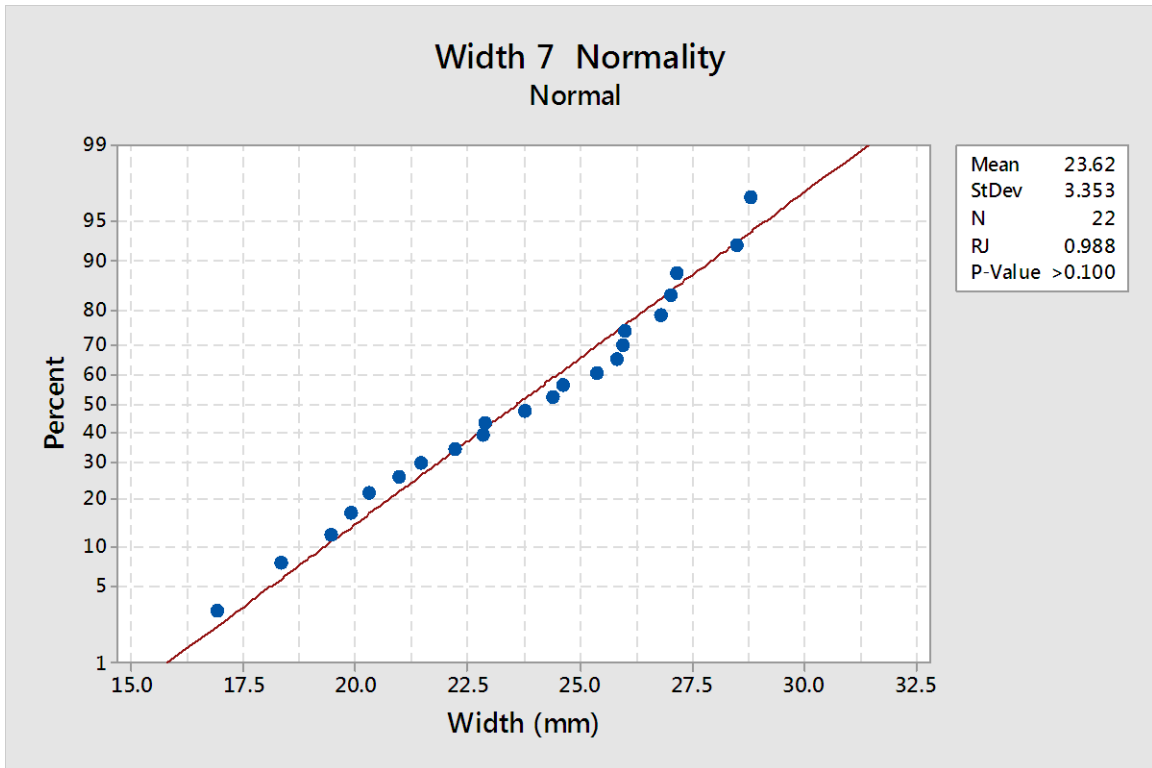


**Figure C.20** Normality of data for percentile tail base width in millimeters.

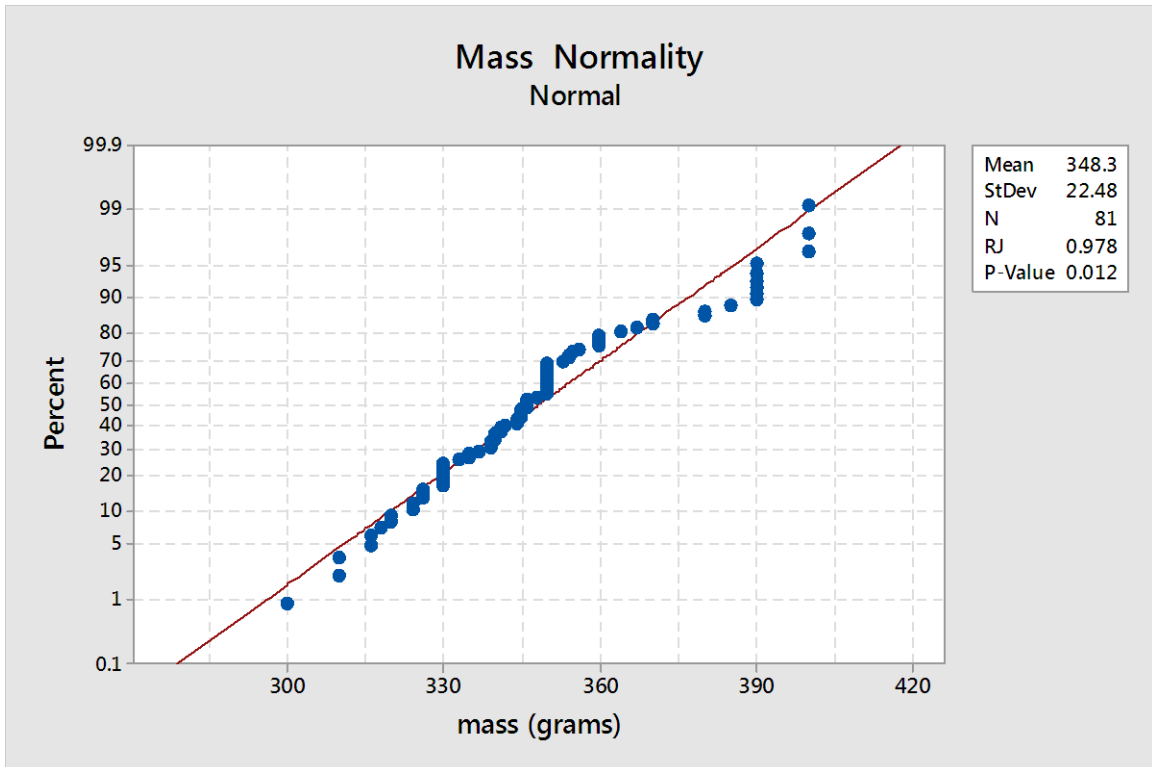


**Figure C.21** Mass normality

## APPENDIX D

### PRESSURE AND TIME GRAPHS

The following are the raw results of tests in the form of pressure and acceleration versus time graphs. The table, Table D.1 is the outline of the parameters of each test.

**Table D.1** Outline of Test Parameters

Shot Number	Number of Membranes	Location	Model	Secured with Strap
1535	2	Inside	RTD	Yes
1536	2	Inside	RTD	Yes
1537	2	Inside	RTD	Yes
1538	4	Inside	RTD	Yes
1539	4	Inside	RTD	Yes
1540	4	Inside	RTD	Yes
1541	2	Inside	RTD	No
1542	2	Inside	RTD	No
1543	2	Inside	RTD	No
1544	2	Outside	RTD	No
1545	2	Outside	RTD	No
1546	2	Outside	RTD	No
1547	2	Outside	RTD	Yes
1548	2	Outside	RTD	Yes
1549	2	Outside	RTD	Yes
1550	2	Outside	Rat	Yes
1551	2	Outside	Rat	Yes
1552	2	Outside	Rat	Yes
1553	2	Outside	Rat	No
1554	2	Outside	Rat	No
1555	2	Outside	Rat	No
1556	2	Inside	Rat	Yes
1557	2	Inside	Rat	Yes
1558	2	Inside	Rat	Yes
1559	4	Inside	Rat	Yes
1560	4	Inside	Rat	Yes
1561	4	Inside	Rat	Yes
1562	4	Inside	Rat	Yes
1563	2	Inside	Rat	No
1564	2	Inside	Rat	No
1565	2	Inside	Rat	No

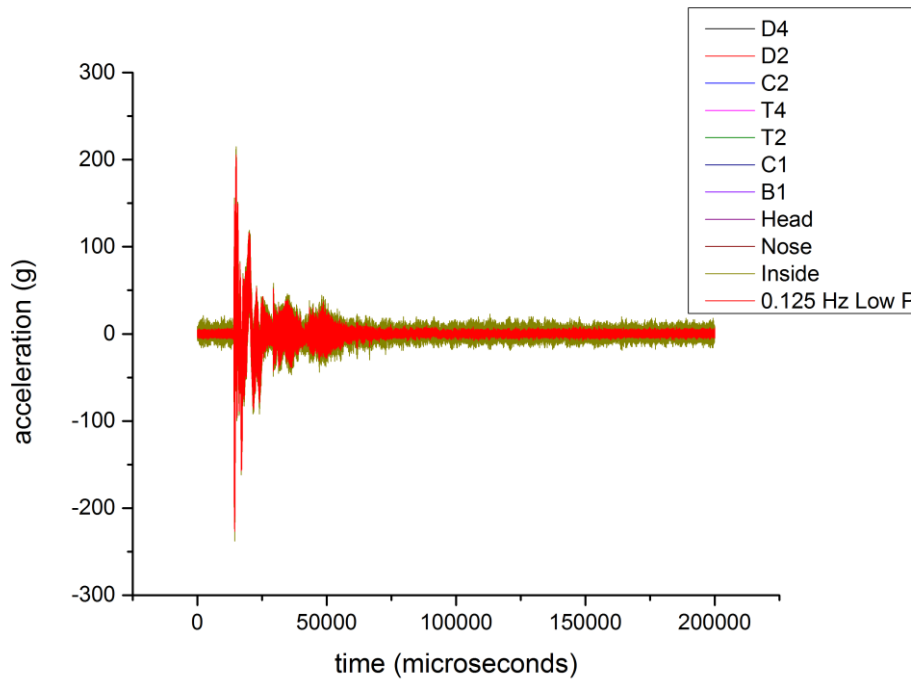


**Figure D.1** 1535 pcceleration versus time of shot.

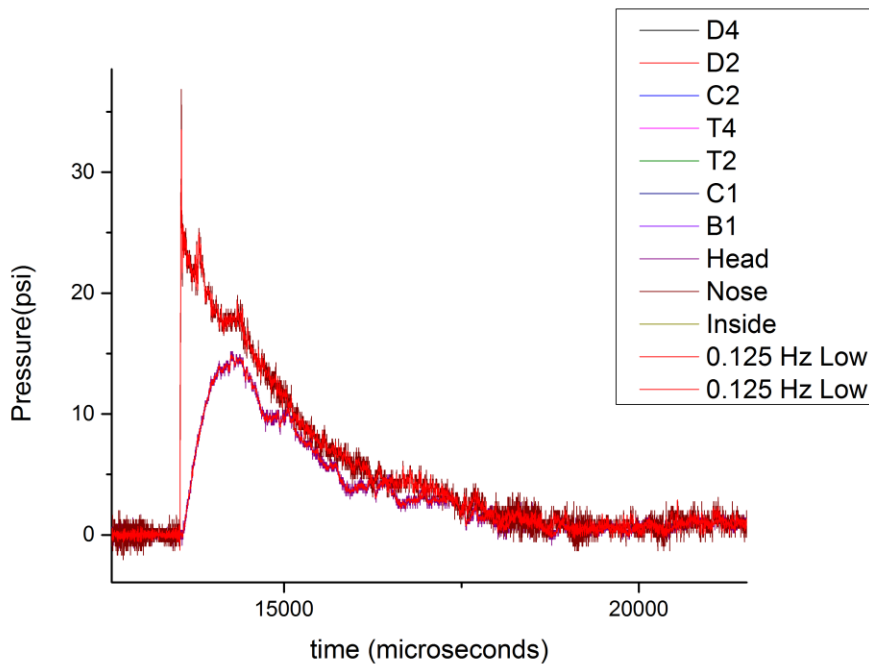


**Figure D.2** 1535 pressure versus time of nose, head and incident sensors.



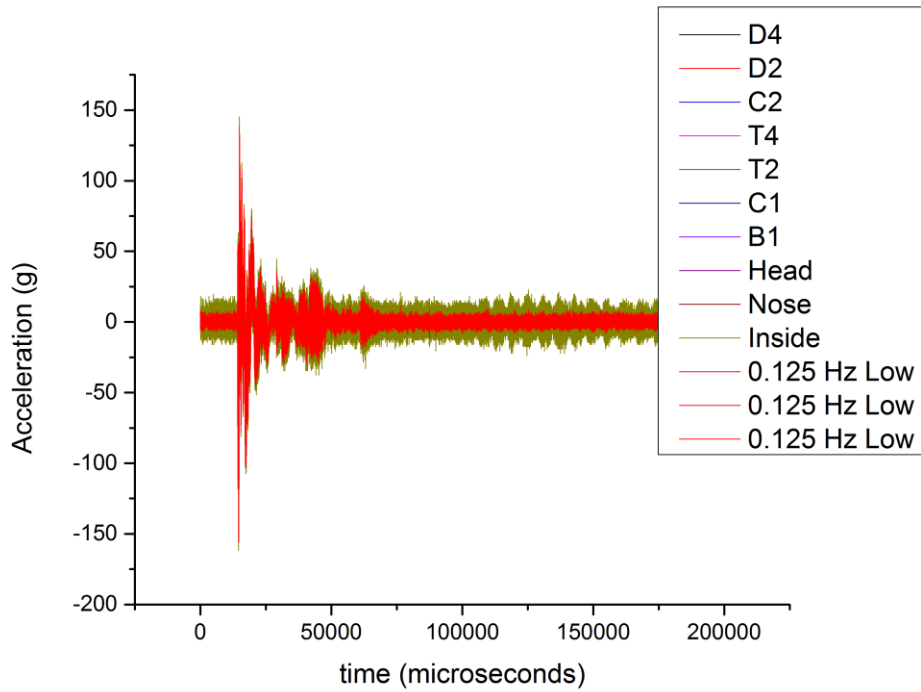


**Figure D.3** 1536 acceleration versus time of shot.

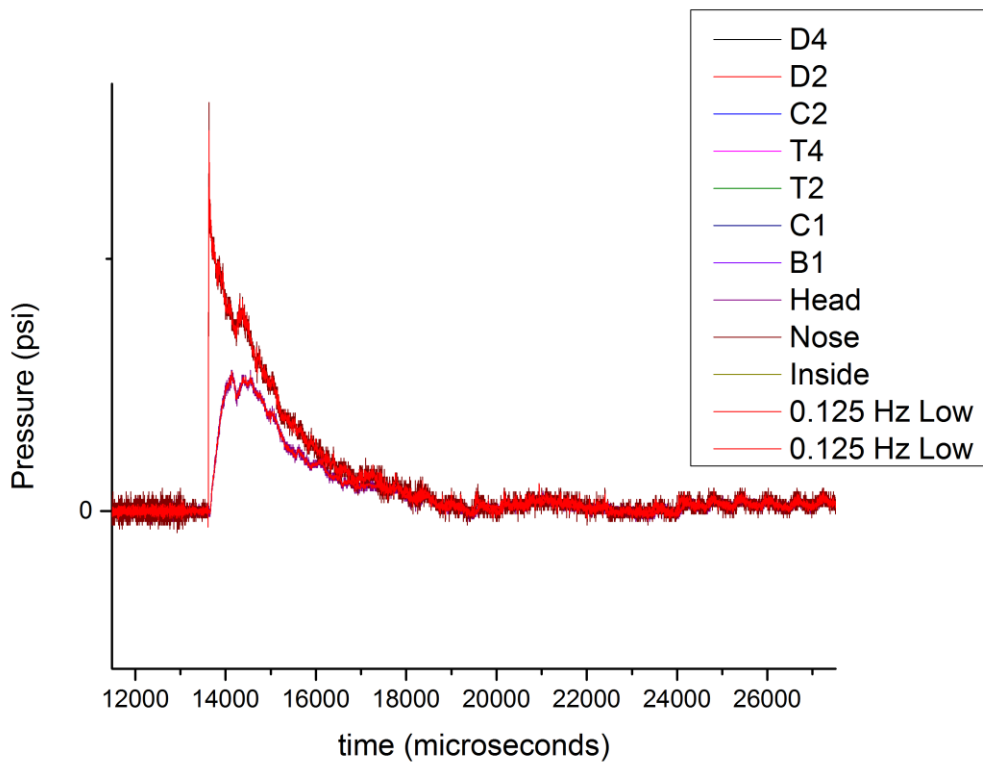


**Figure D.4** 1536 Pressure Versus Time of Nose, Head and Incident Sensors.

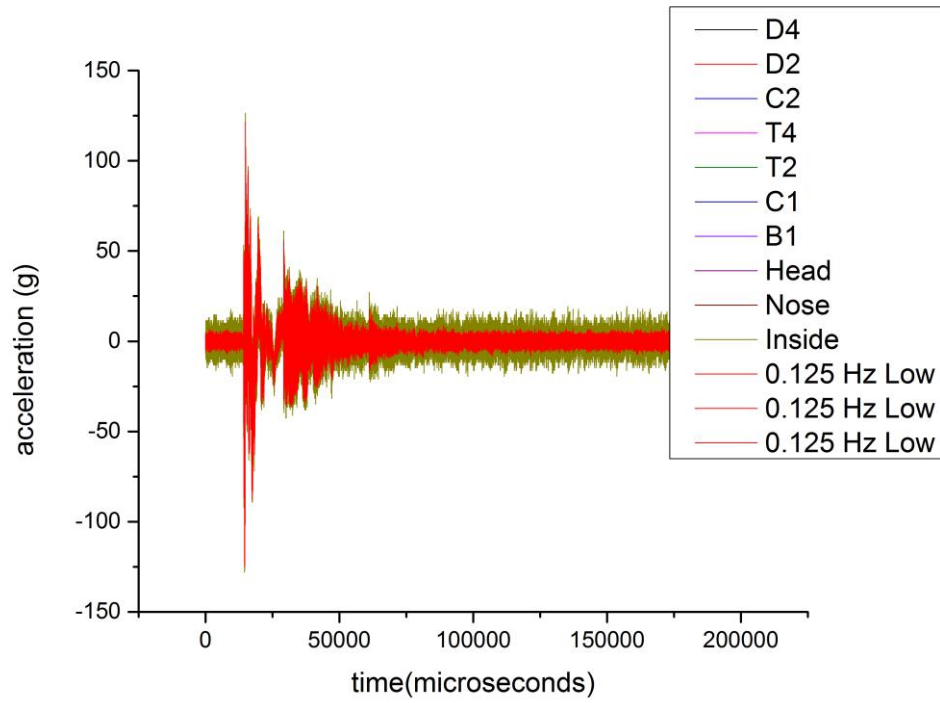


**Figure D.5** 1537 acceleration versus time of shot.

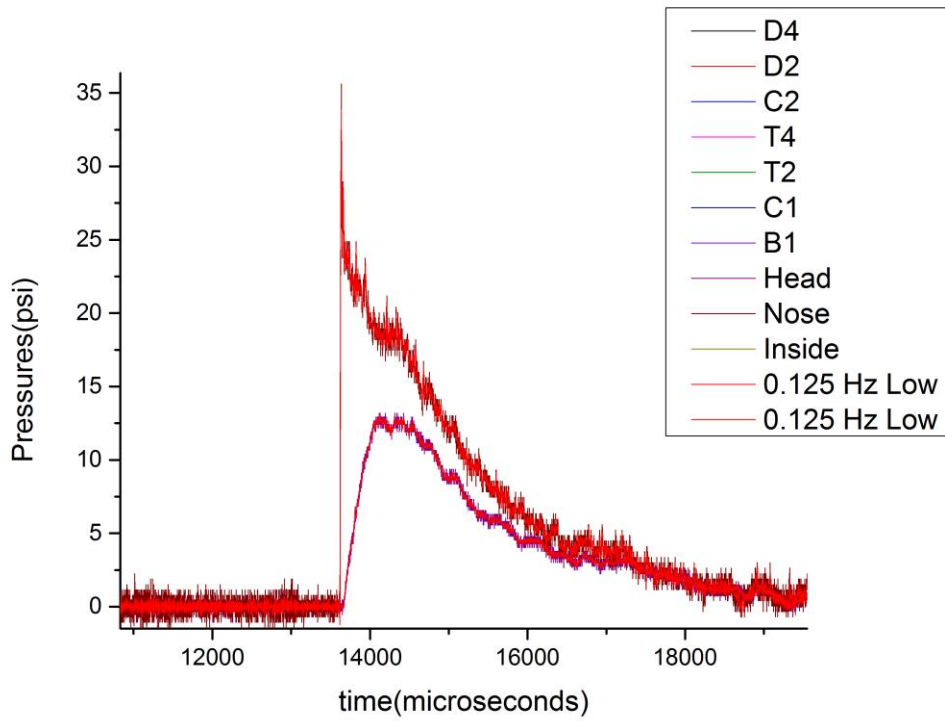


**Figure D.6** 1537 pressure versus time of nose, head and incident sensors.

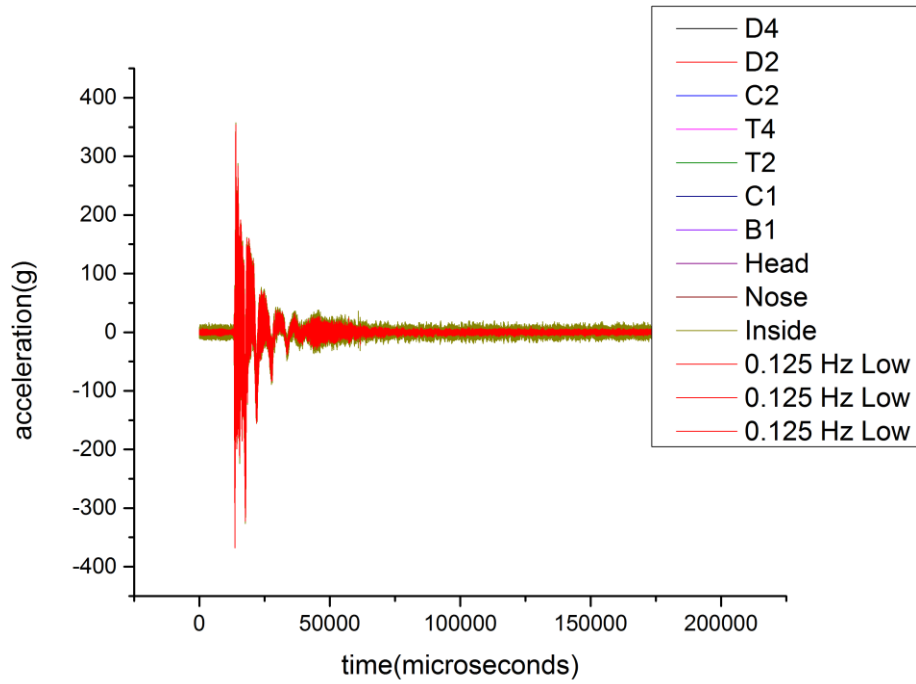


**Figure D.7** 1538 acceleration versus time of shot.

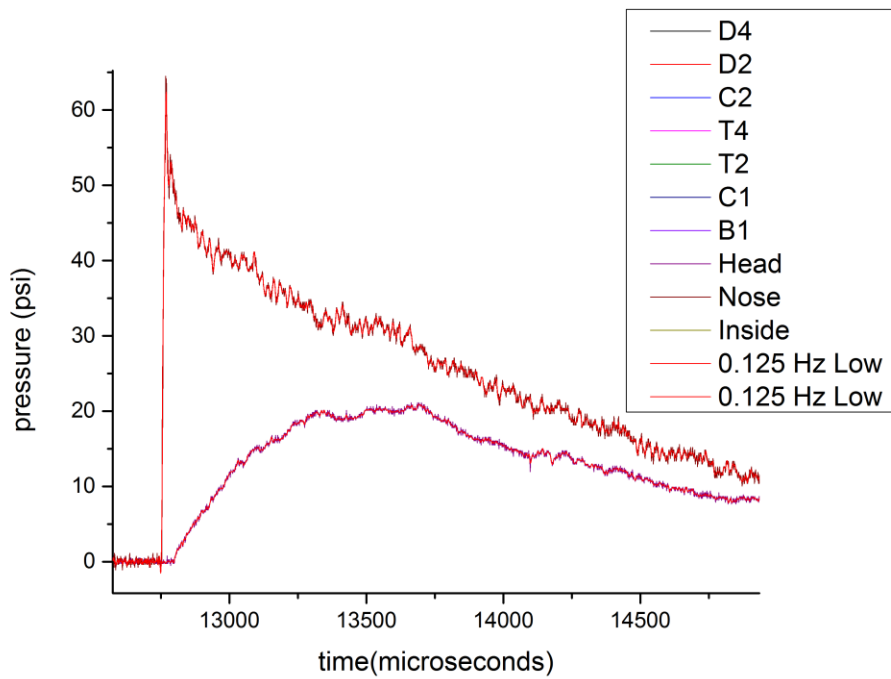


**Figure D.8** 1538 pressure versus time of nose, head and incident sensors.

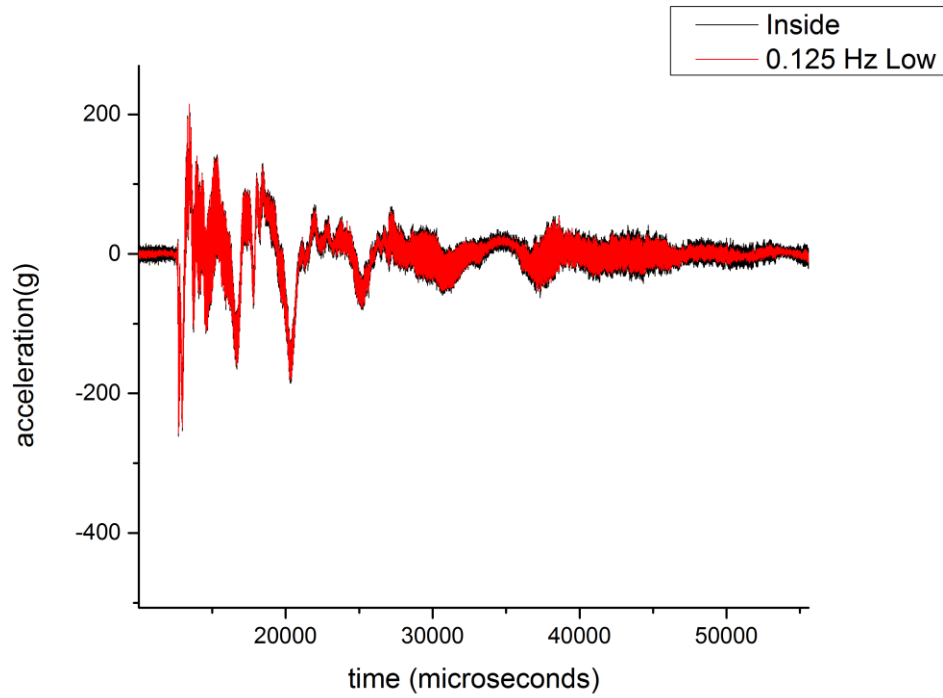


**Figure D.9** 1539 acceleration versus time of shot.

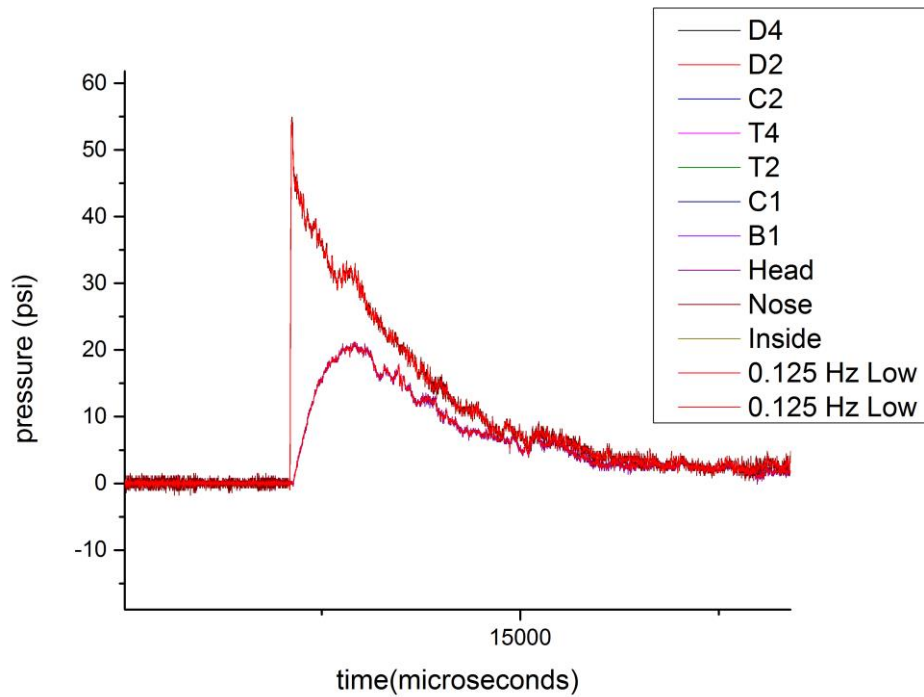


**Figure D.10** 1539 pressure versus time of nose, head and incident sensors.

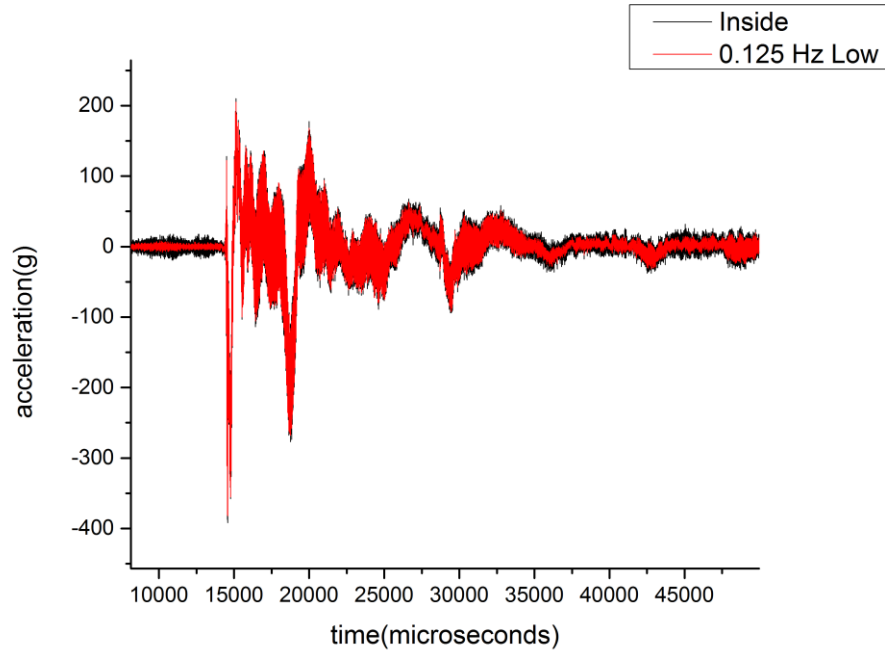


**Figure D.11** 1540 acceleration versus time of shot.

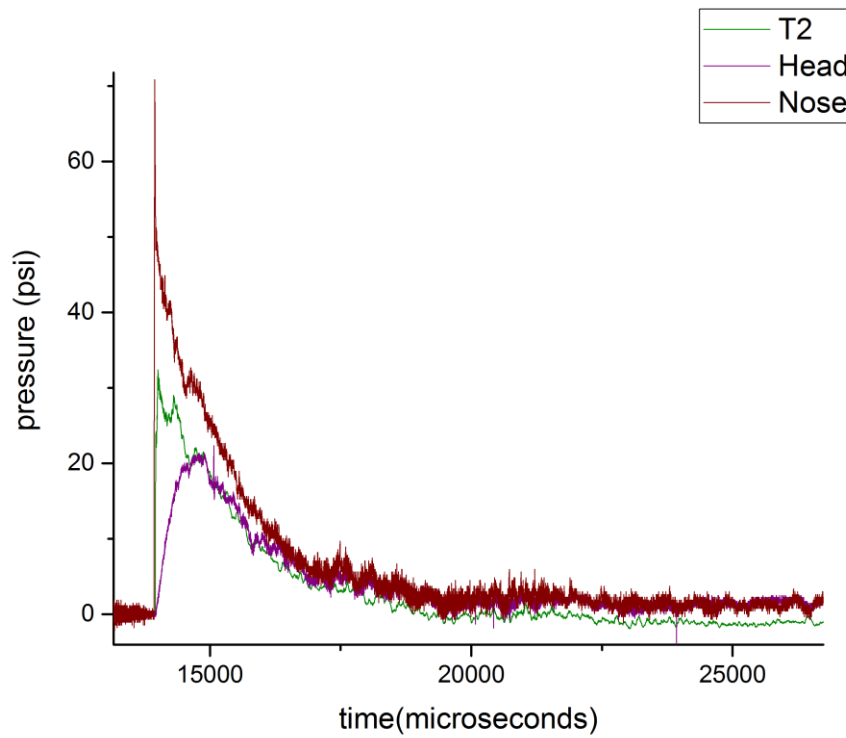


**Figure D.12** 1540 pressure versus time of nose, head and incident sensors.

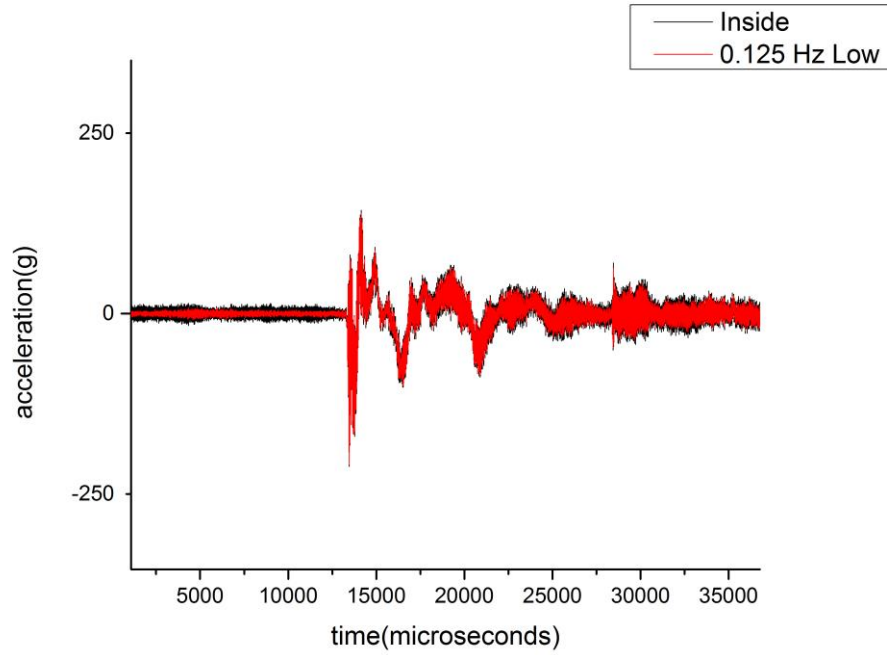


**Figure D.13** 1541 acceleration versus time of shot.

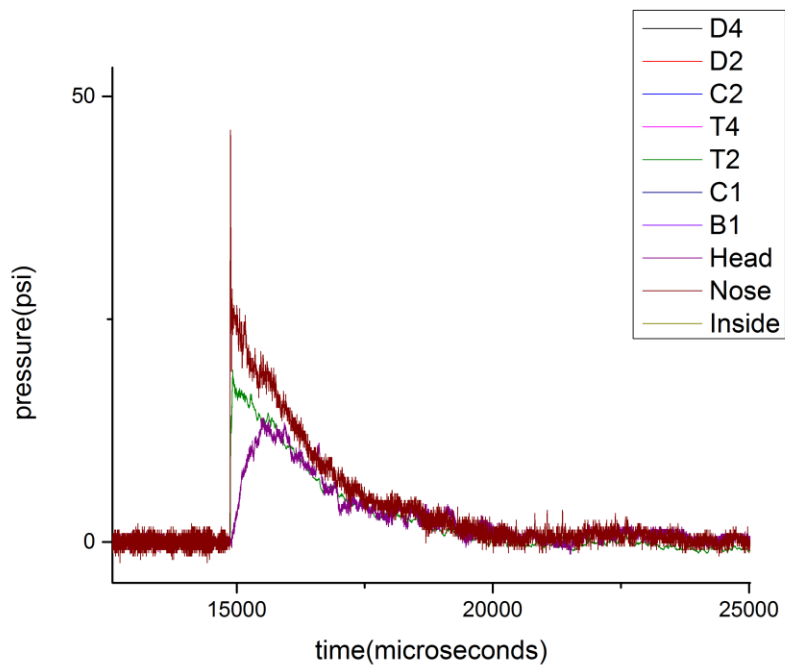


**Figure D.14** 1541 pressure versus time of nose, head and incident sensors.

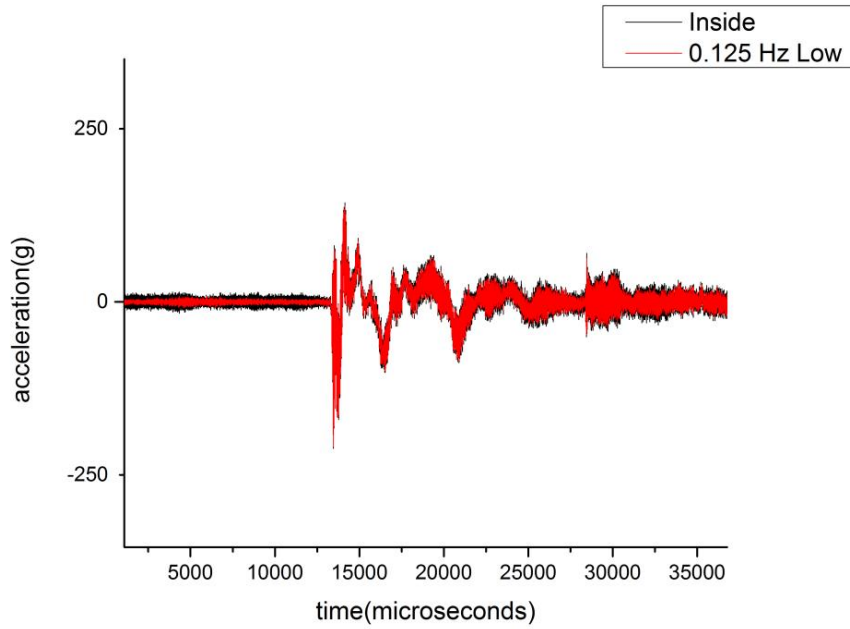


**Figure D.15** 1542 acceleration versus time of shot.

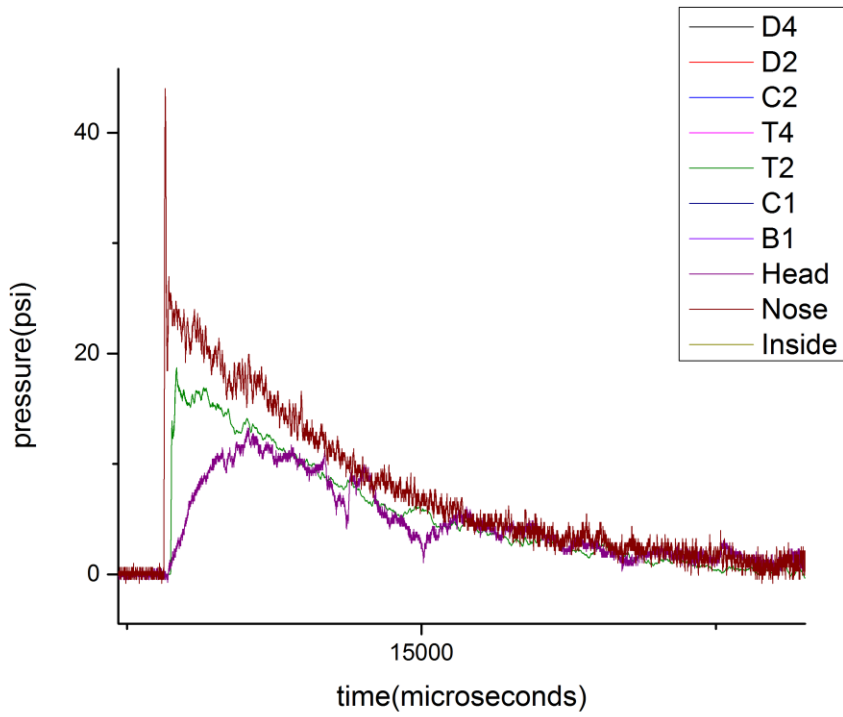


**Figure D.16** 1542 pressure versus time of nose, head and incident sensors.

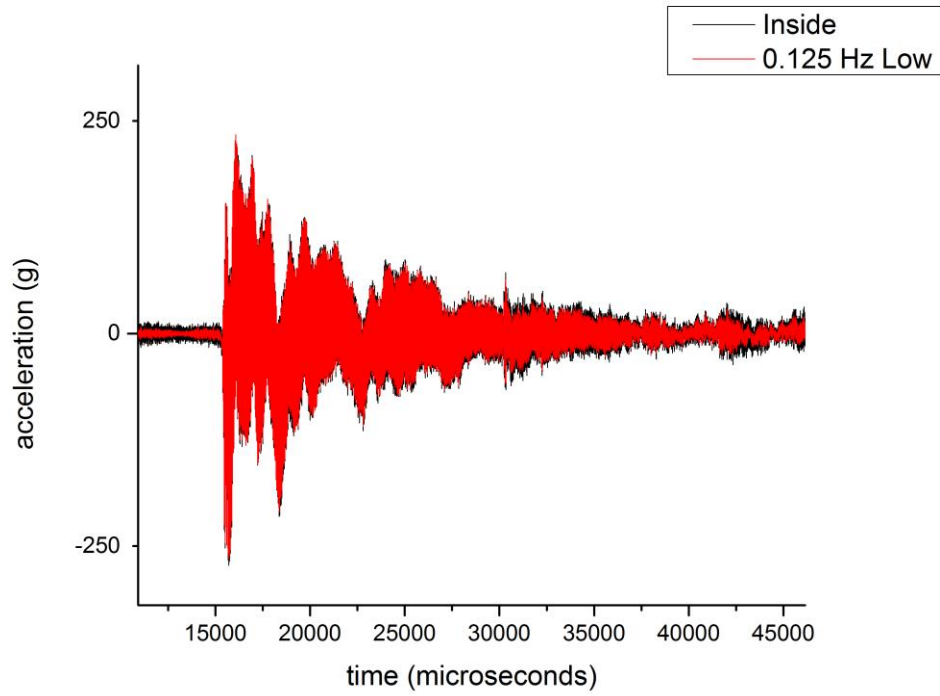


**Figure D.17** 1543 acceleration versus time of shot.

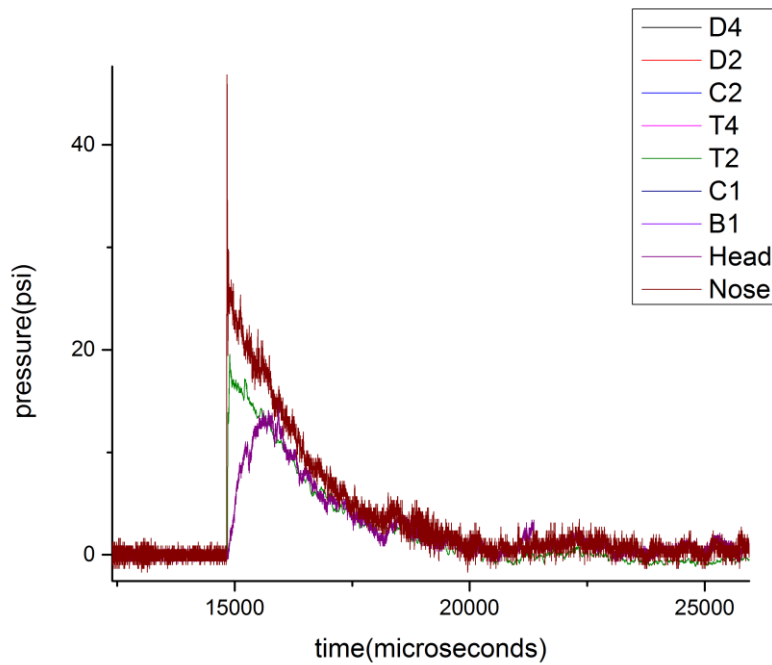


**Figure D.18** 1543 pressure versus time of nose, head and incident sensors.



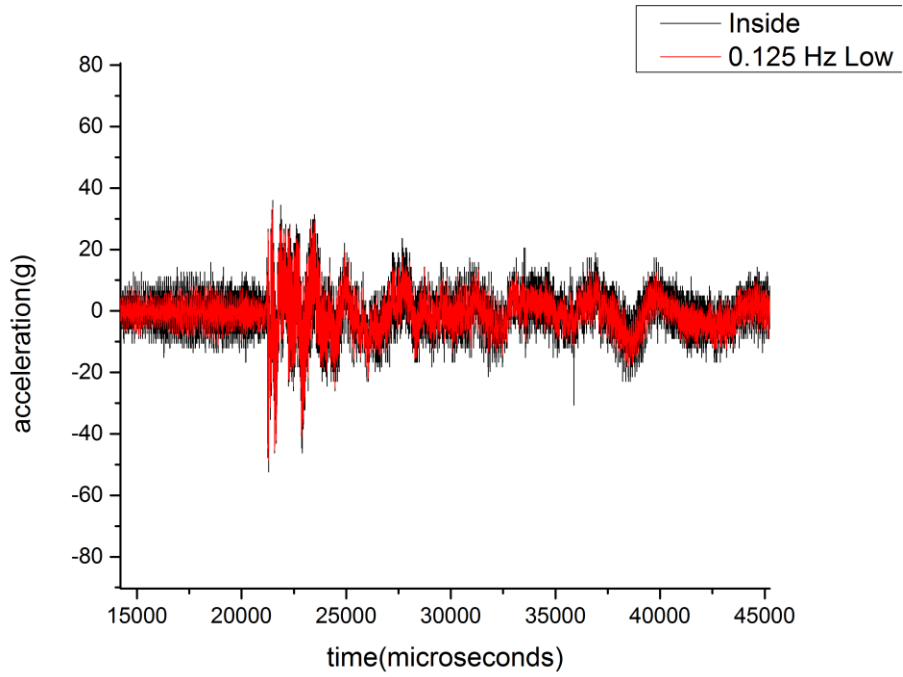


**Figure D.19** 1544 acceleration versus time of shot.

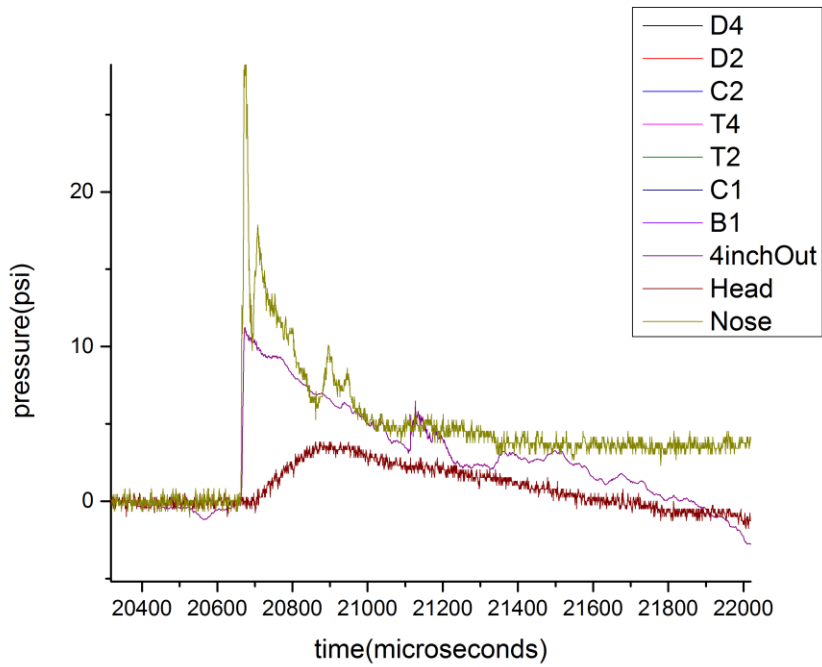


**Figure D.20** 1544 pressure versus time of nose, head and incident sensors.

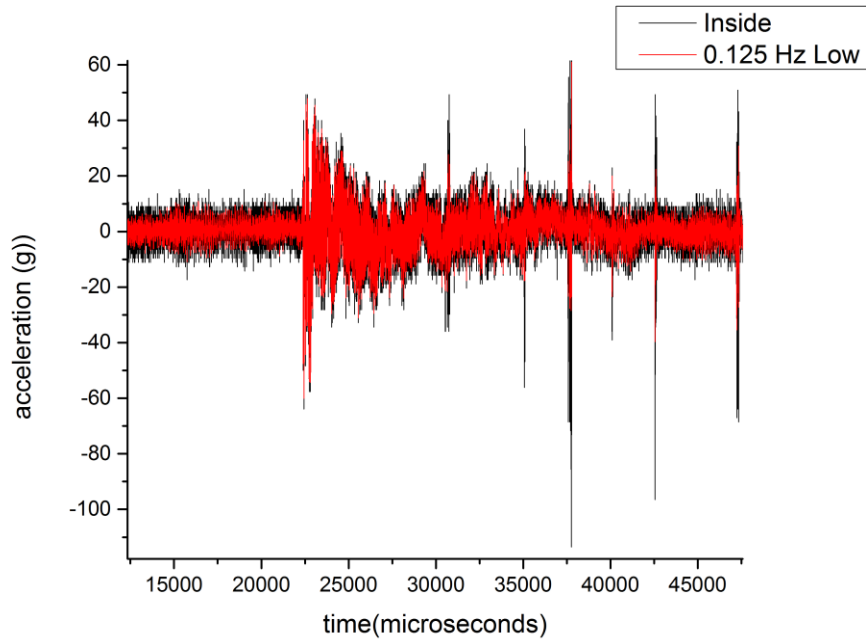


**Figure D.21** 1545 acceleration versus time of shot.

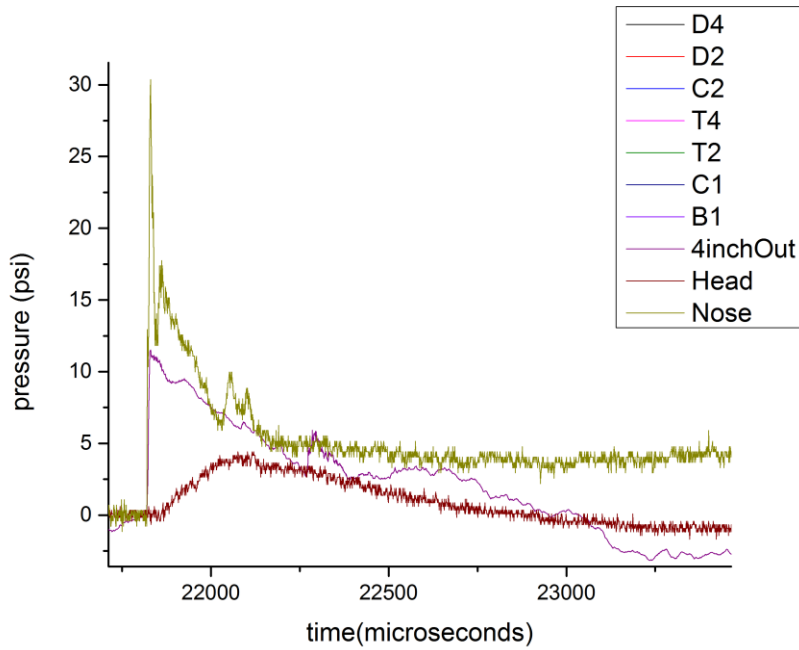


**Figure D.22** 1545 pressure versus time of nose, head and incident sensors.

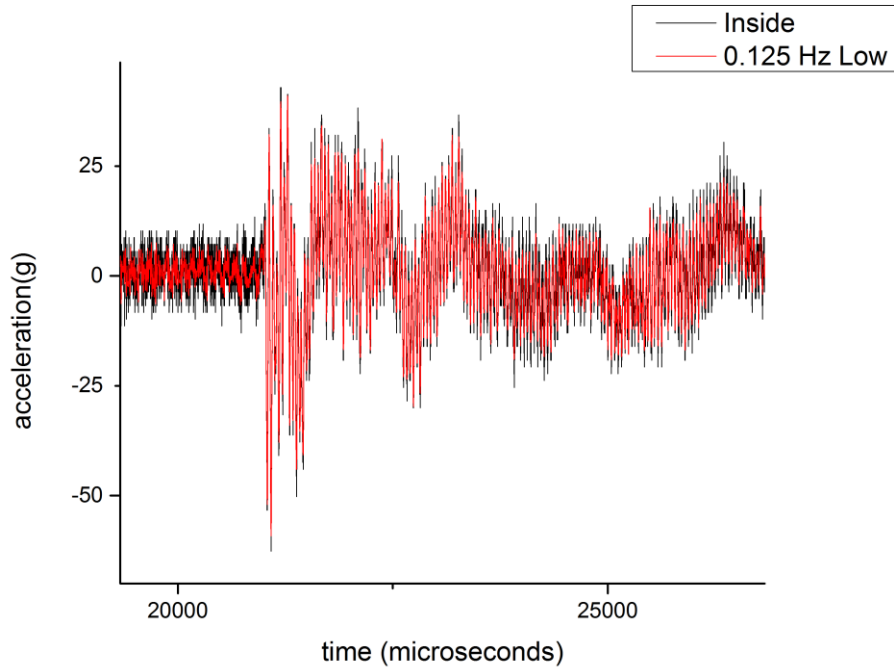


**Figure D.23** 1546 acceleration versus time of shot.

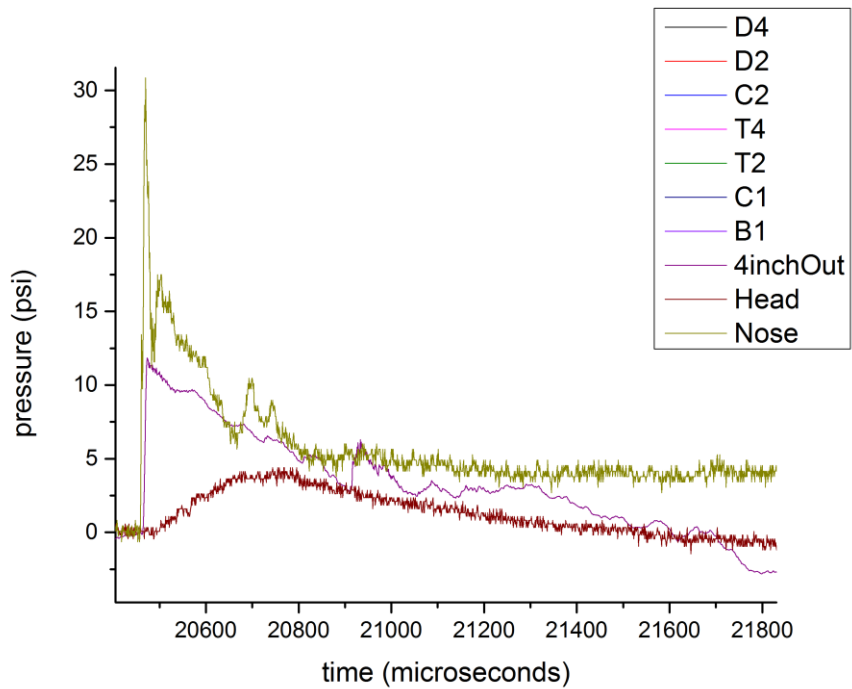


**Figure D.24** 1546 pressure versus time of nose, head and incident sensors.

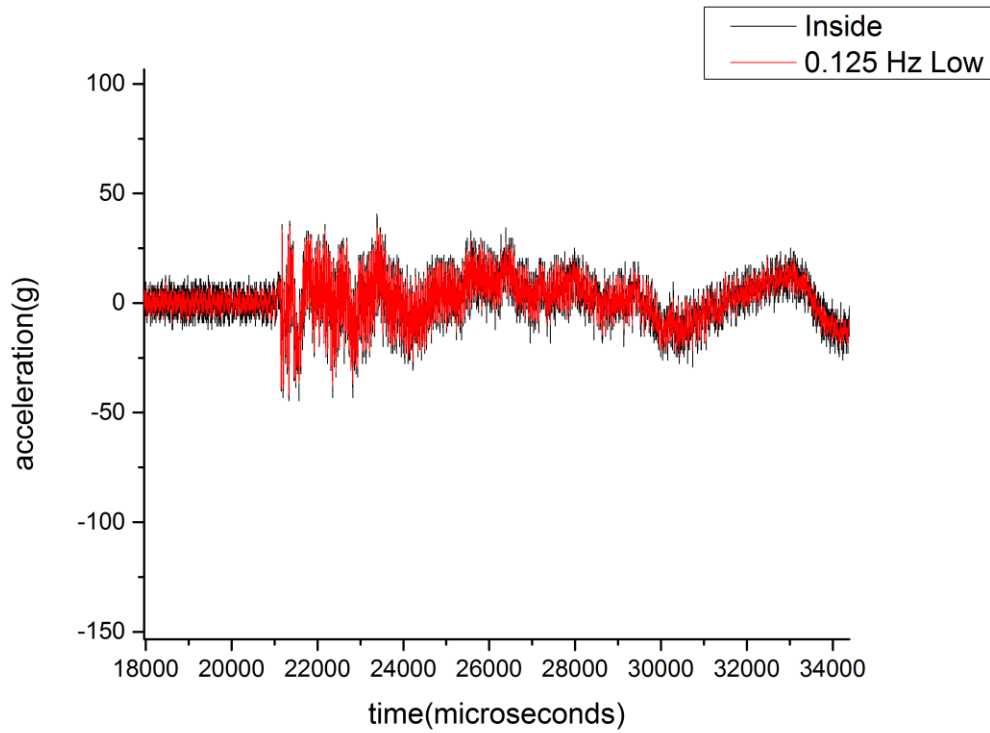


**Figure D.25** 1547 acceleration versus time of shot.

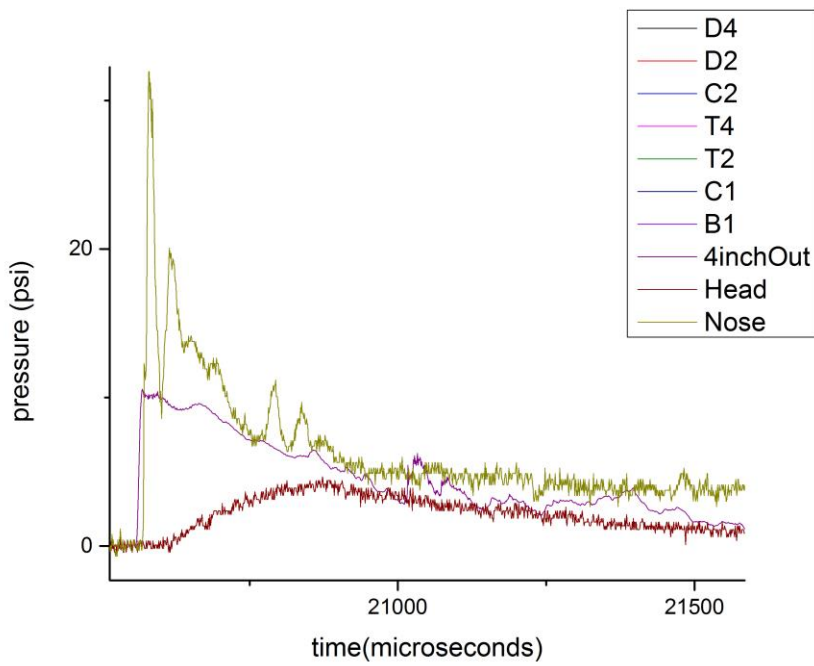


**Figure D.26** 1547 pressure versus time of nose, head and incident sensors.

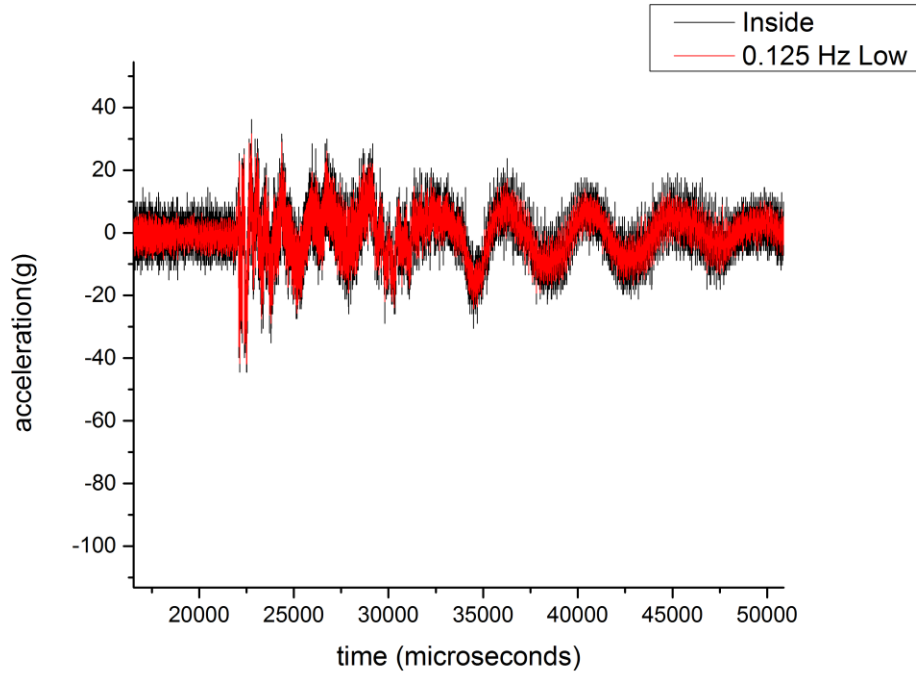


**Figure D.27** 1548 acceleration versus time of shot.

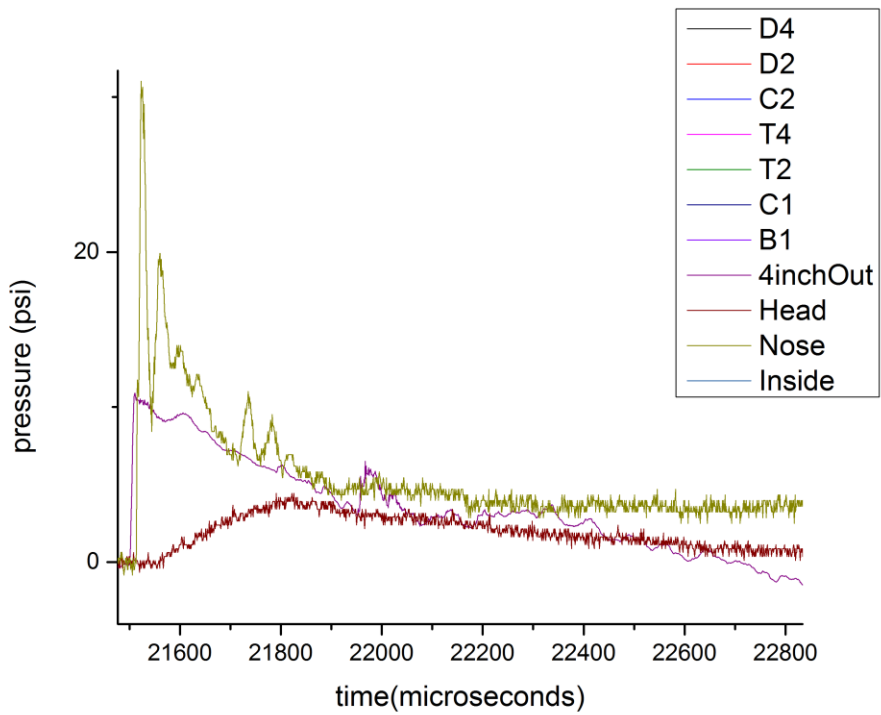


**Figure D.28** 1548 pressure versus time of nose, head and incident sensors.

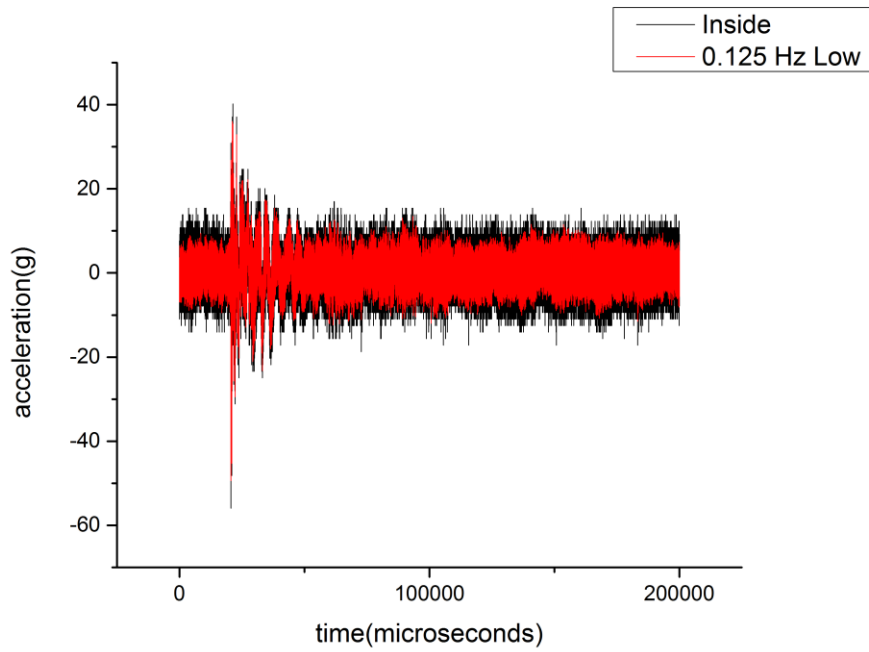


**Figure D.29** 1549 acceleration versus time of shot.

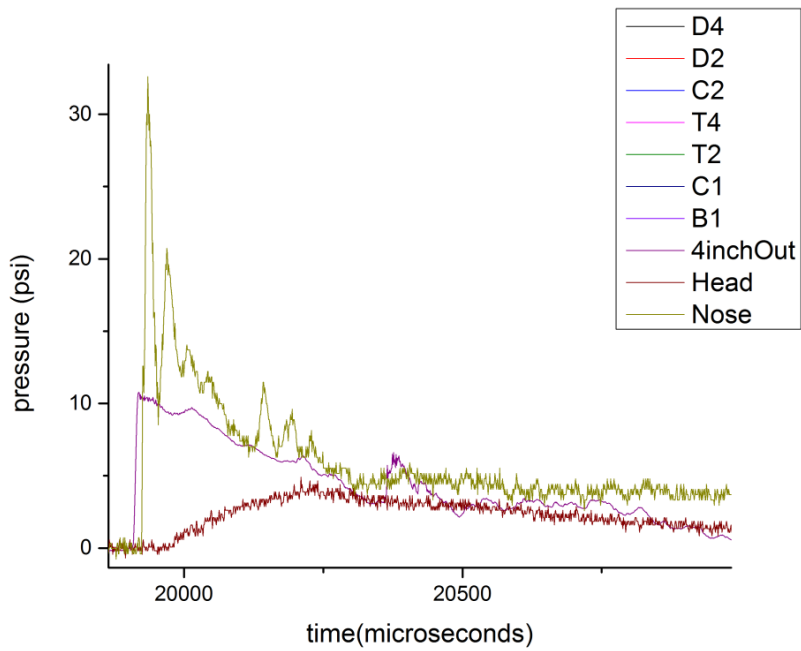


**Figure D.30** 1549 pressure versus time of nose, head and incident sensors.

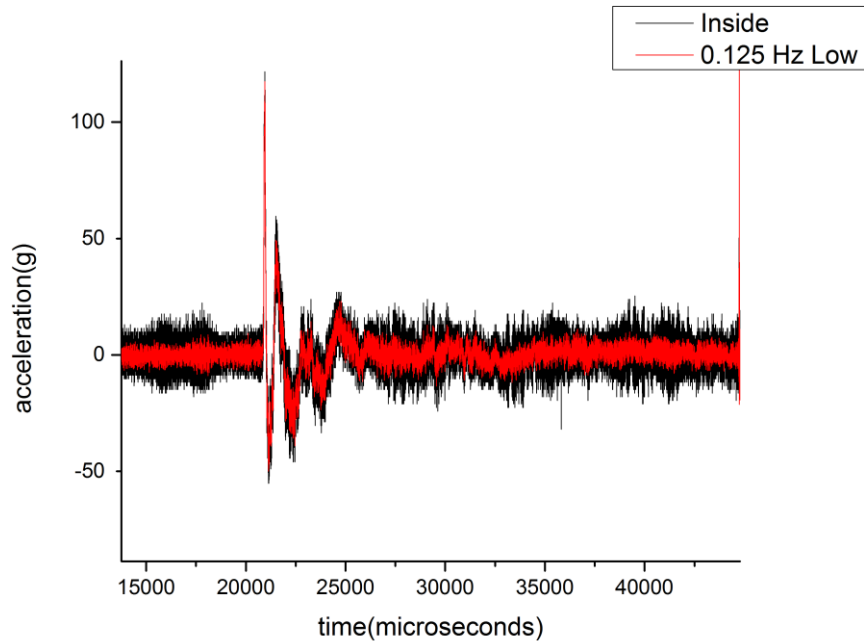


**Figure D.31** 1550 acceleration versus time of shot.

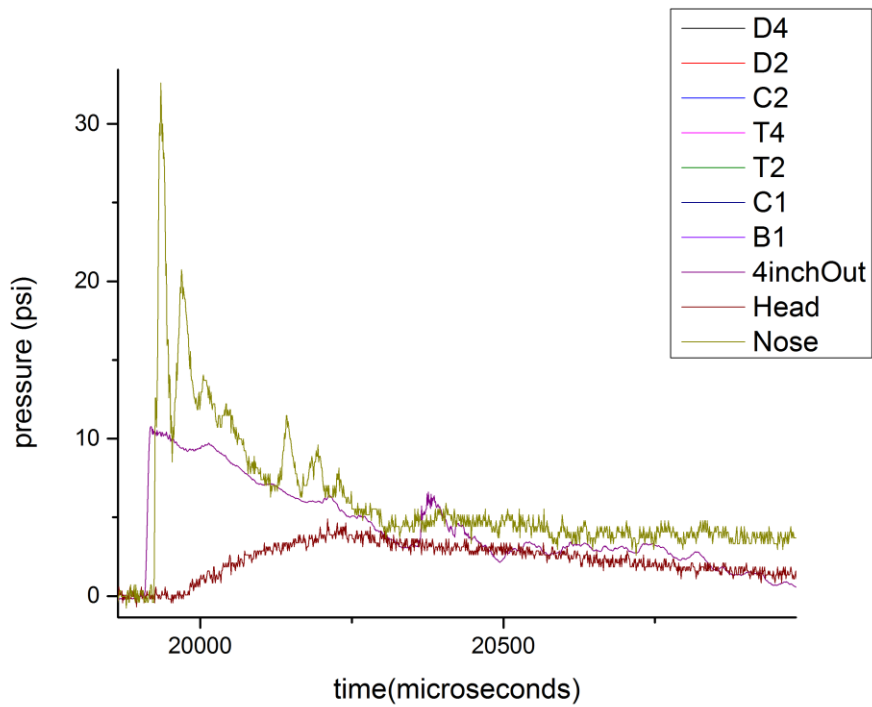


**Figure D.32** 1550 pressure versus time of nose, head and incident sensors.

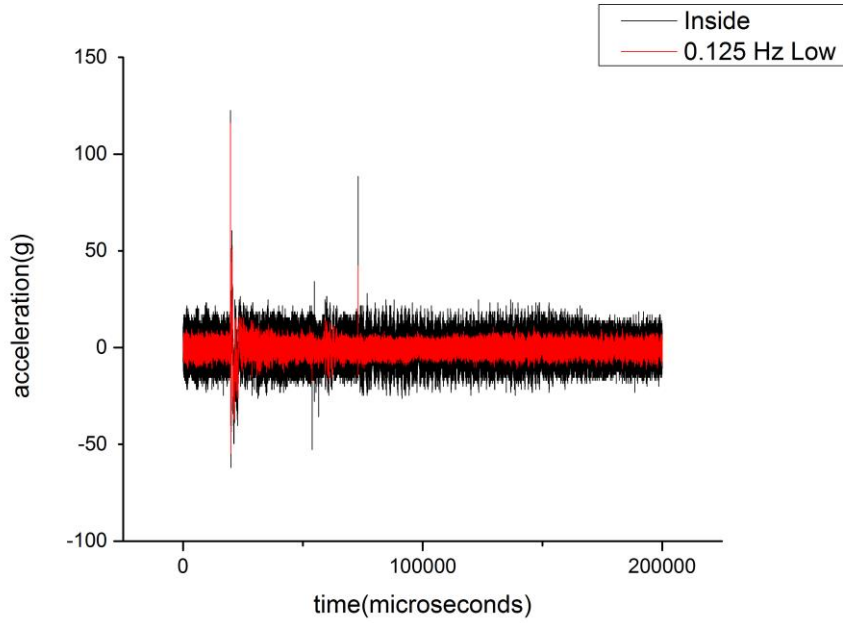


**Figure D.33** 1551 acceleration versus time of shot.

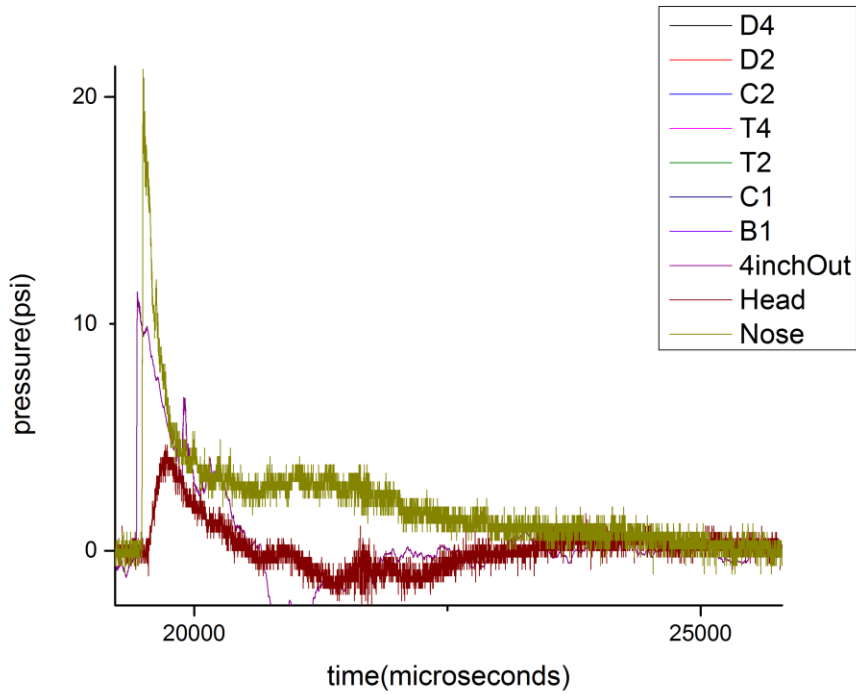


**Figure D.34** 1551 pressure versus time of nose, head and incident sensors.



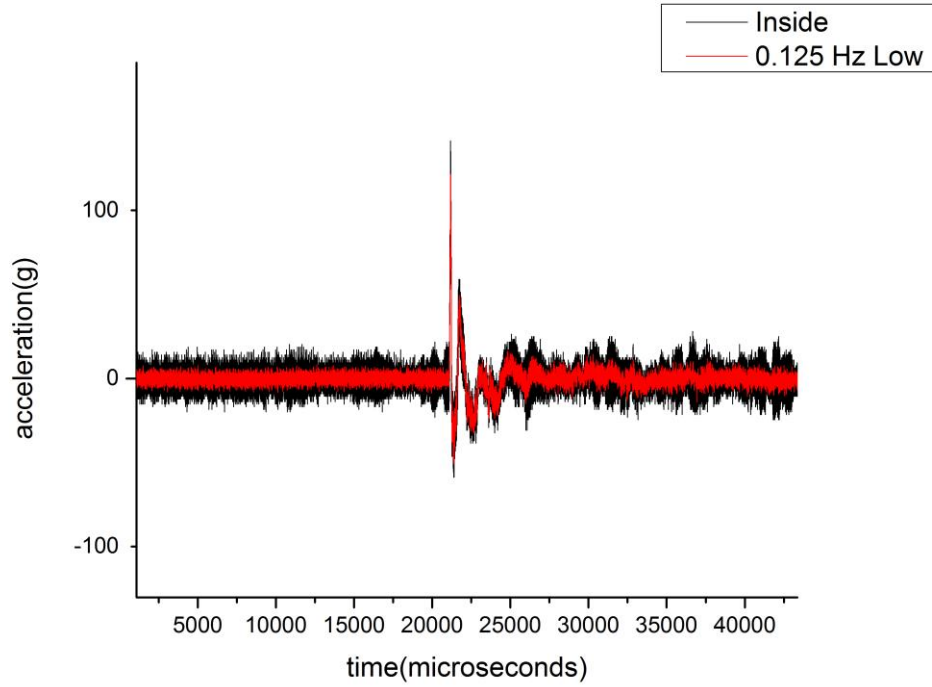


**Figure D.35** 1552 acceleration versus time of shot.

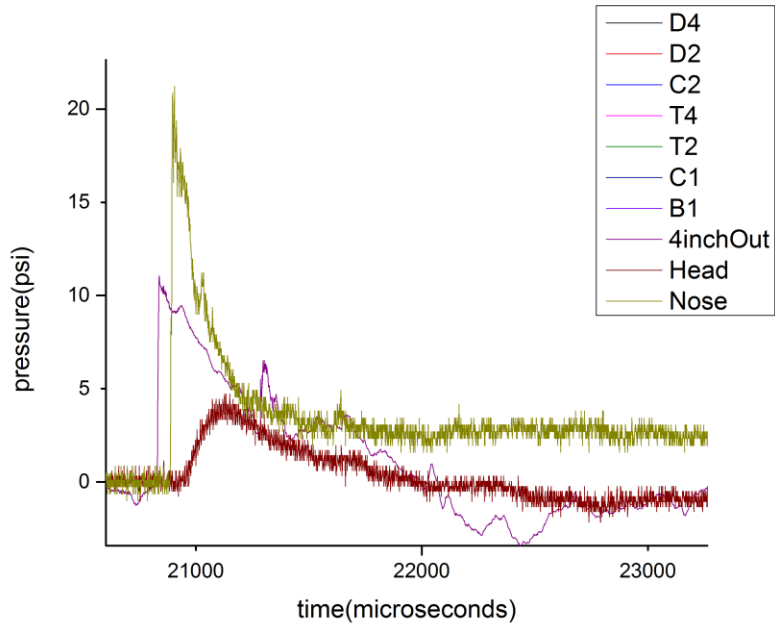


**Figure D.36** 1552 pressure versus time of nose, head and incident sensors.

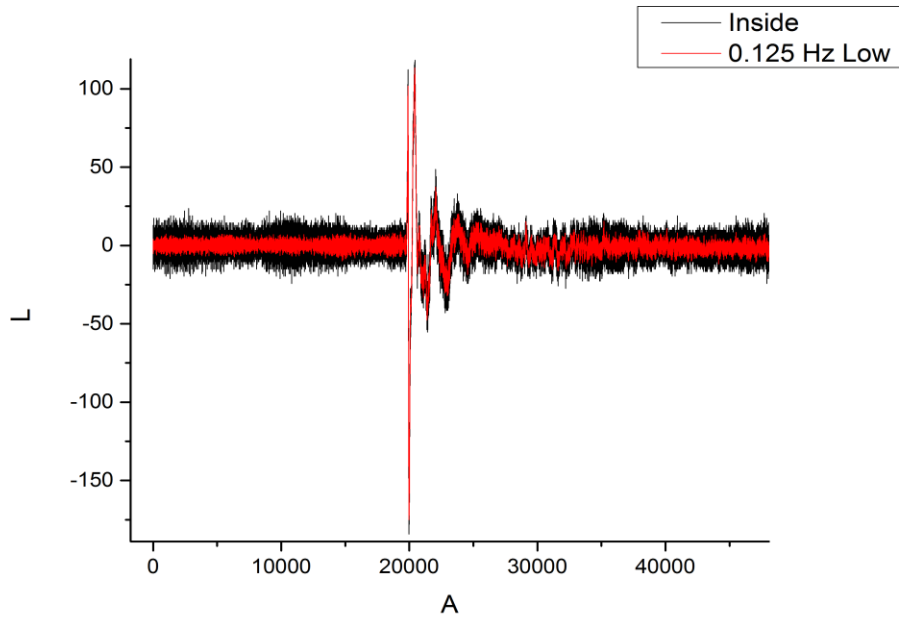


**Figure D.37** 1553 acceleration versus time of shot.

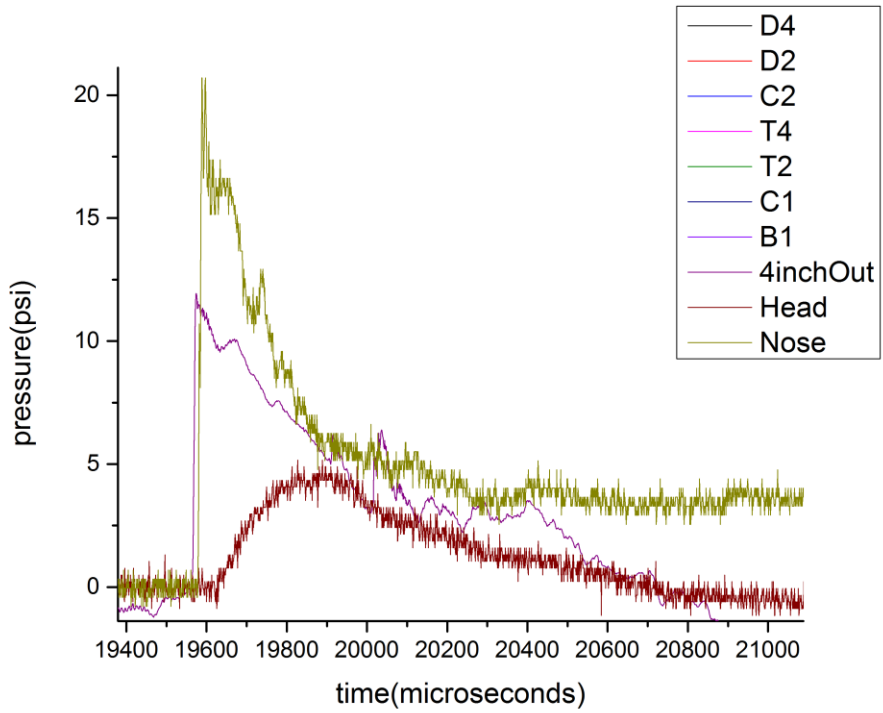


**Figure D.38** 1553 pressure versus time of nose, head and incident sensors.

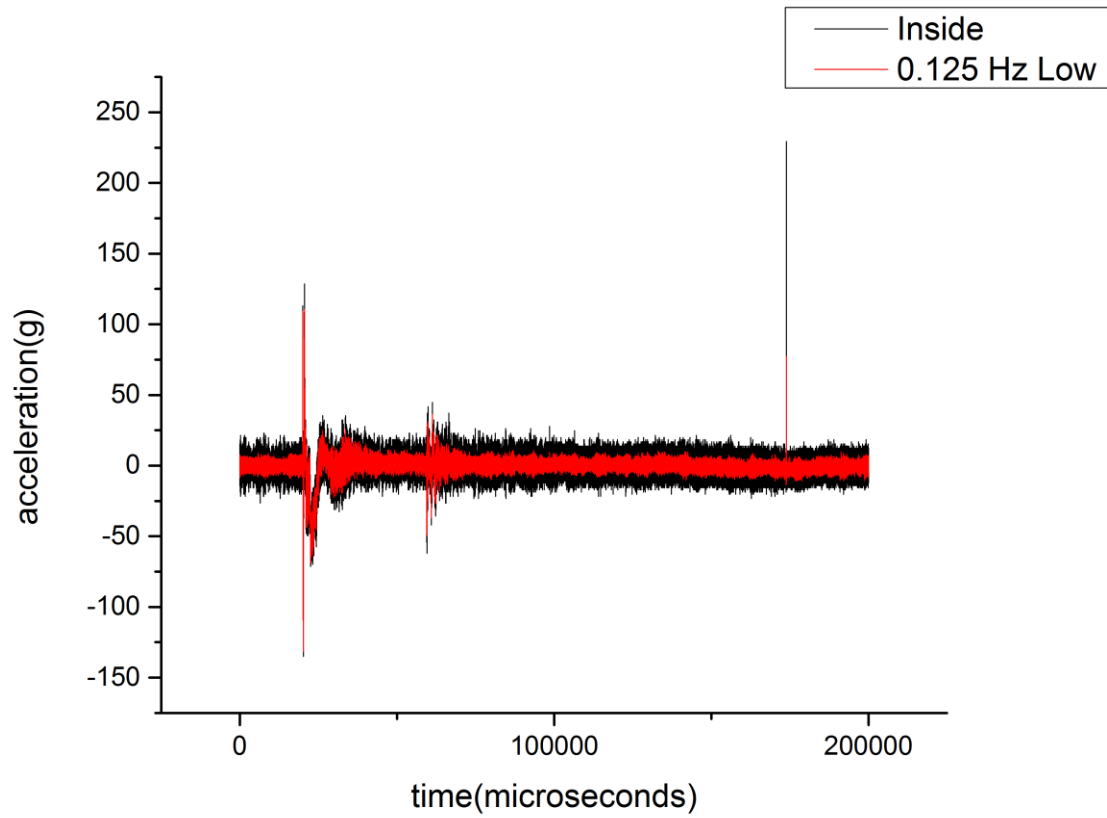


**Figure D.39** 1554 acceleration versus time of shot.

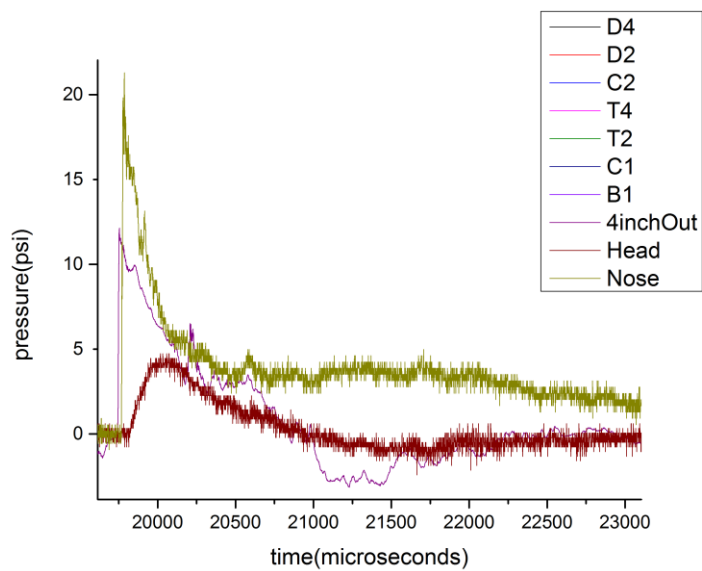


**Figure D.40** 1554 pressure versus time of nose, head and incident sensors.

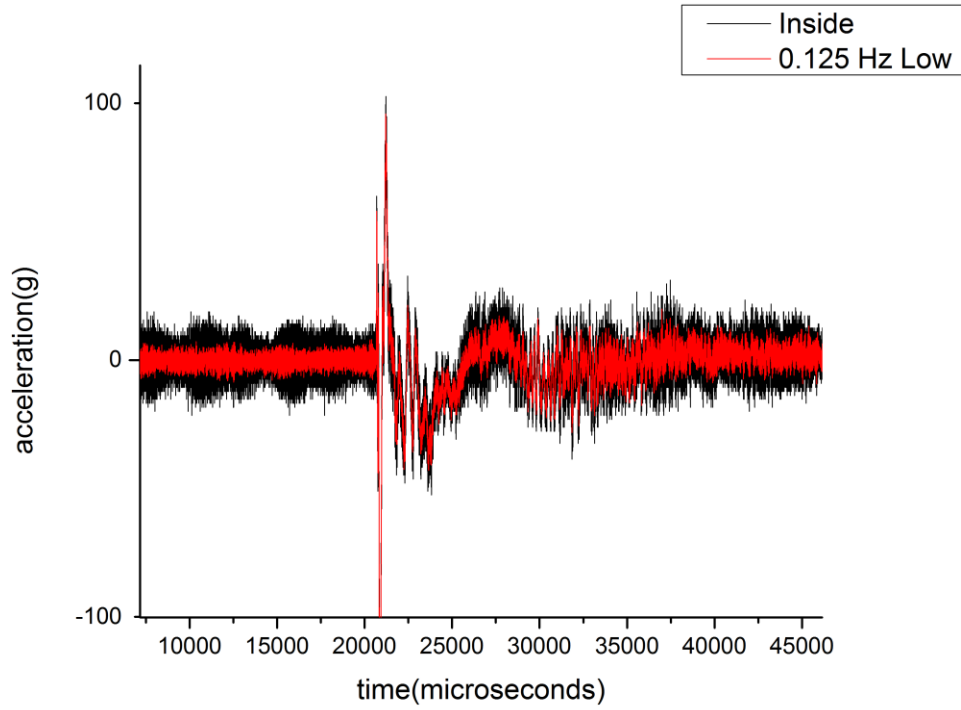


**Figure D.41** 1555 acceleration versus time of shot.

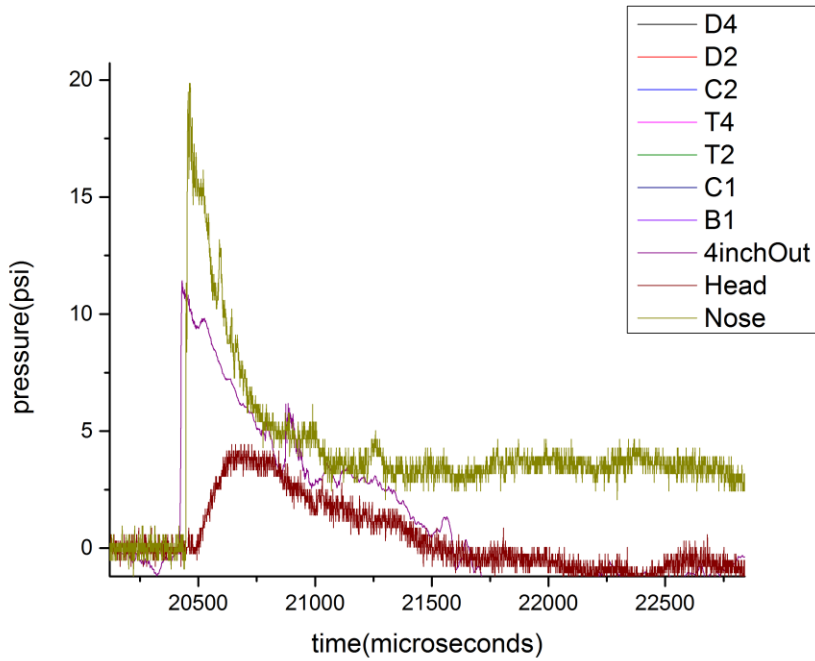


**Figure D.42** 1555 pressure versus time of nose, head and incident sensors.

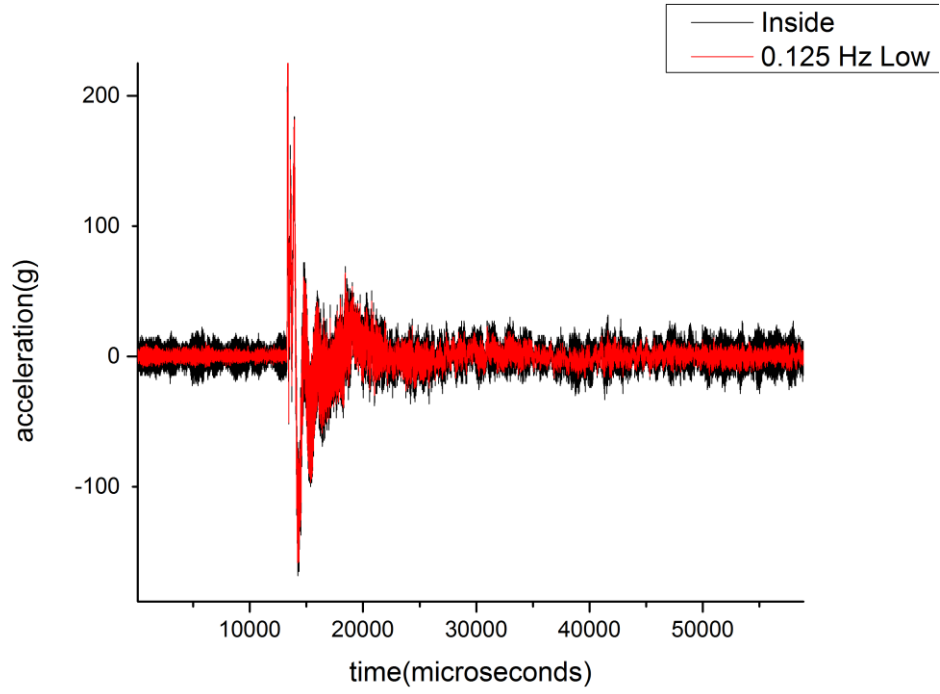


**Figure D.43** 1556 acceleration versus time of shot.

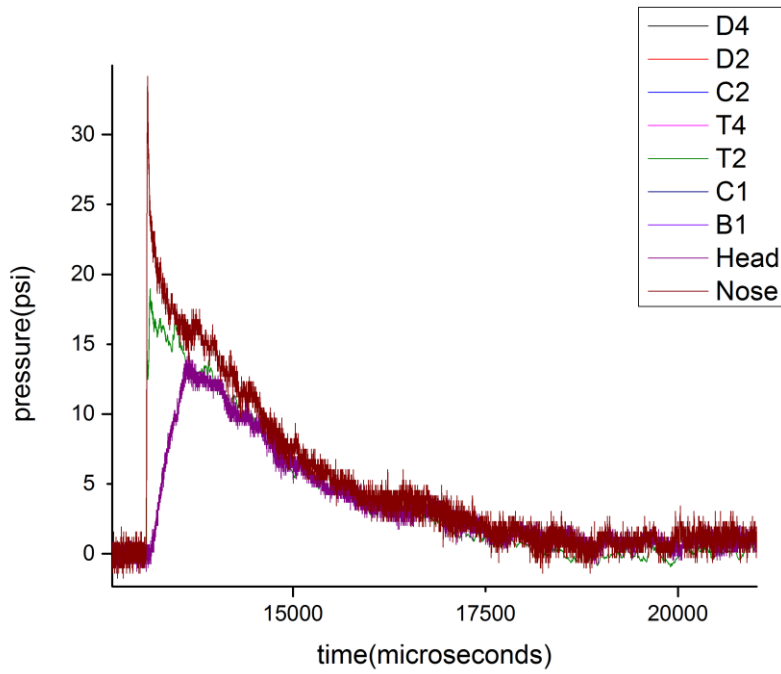


**Figure D.44** 1556 pressure versus time of nose, head and incident sensors.

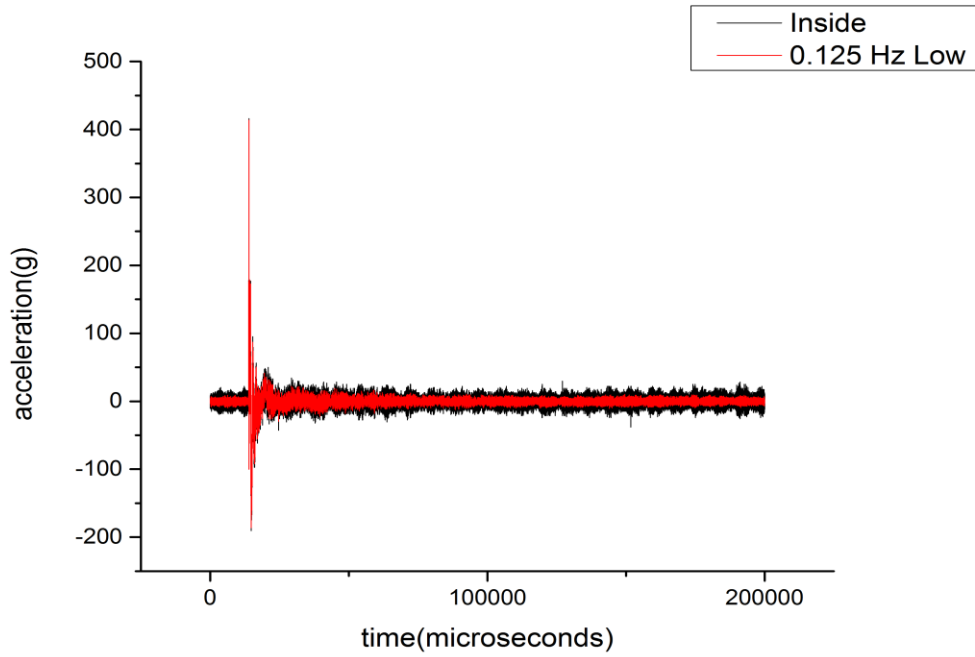


**Figure D.45** 1557 acceleration versus time of shot.

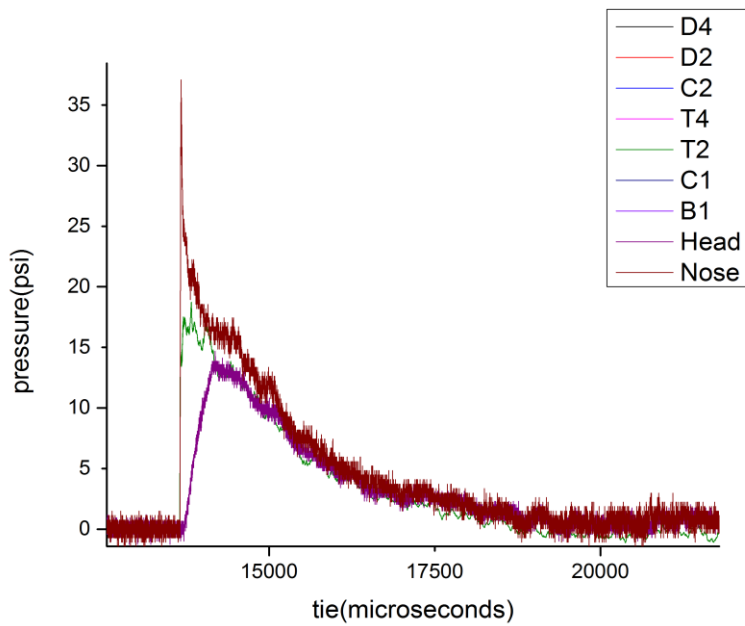


**Figure D.46** 1557 pressure versus time of nose, head and incident sensors.

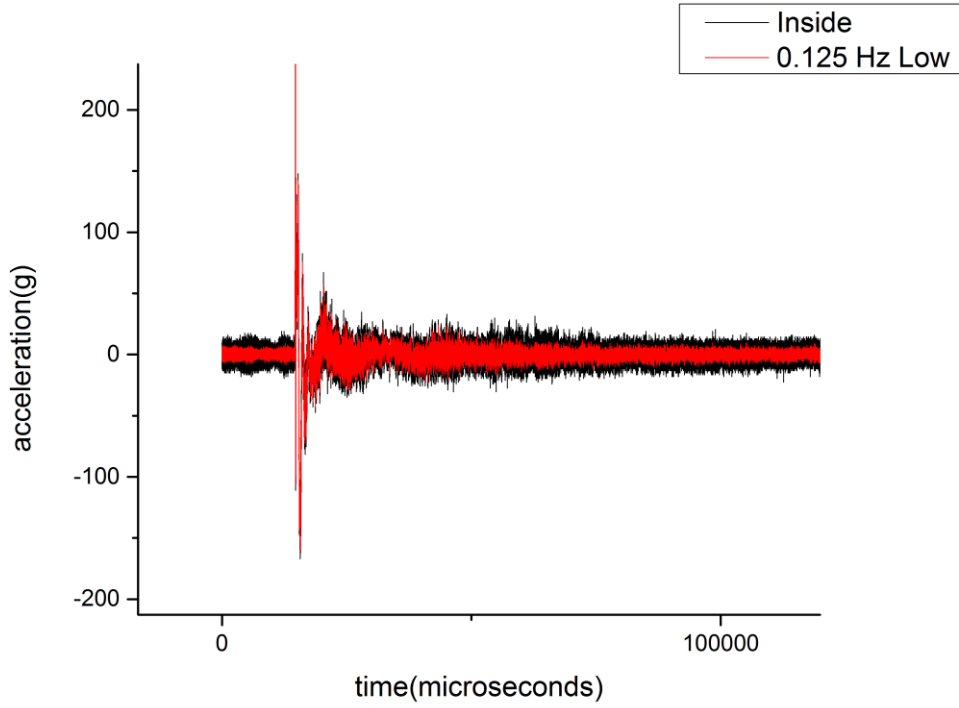


**Figure D.47** 1558 acceleration versus time of shot.

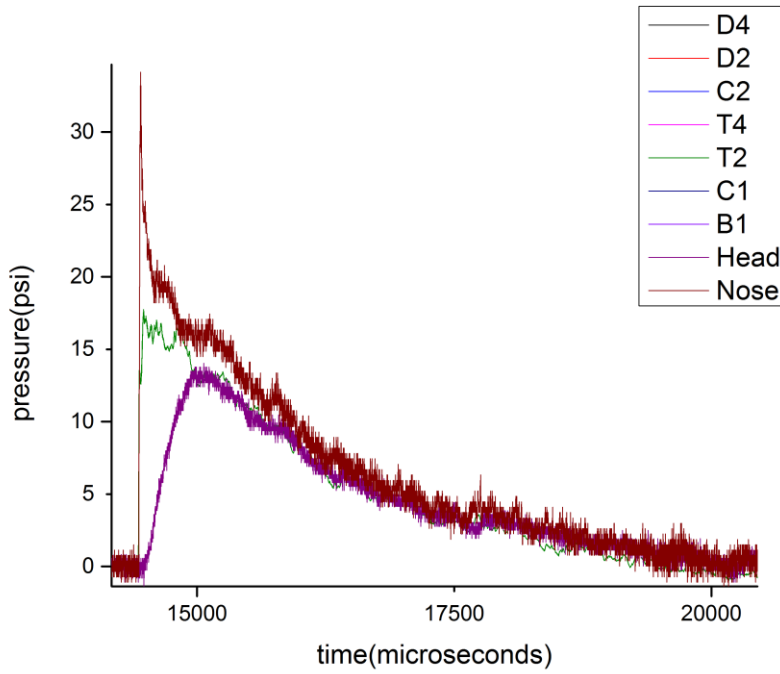


**Figure D.48** 1558 pressure versus time of nose, head and incident sensors.

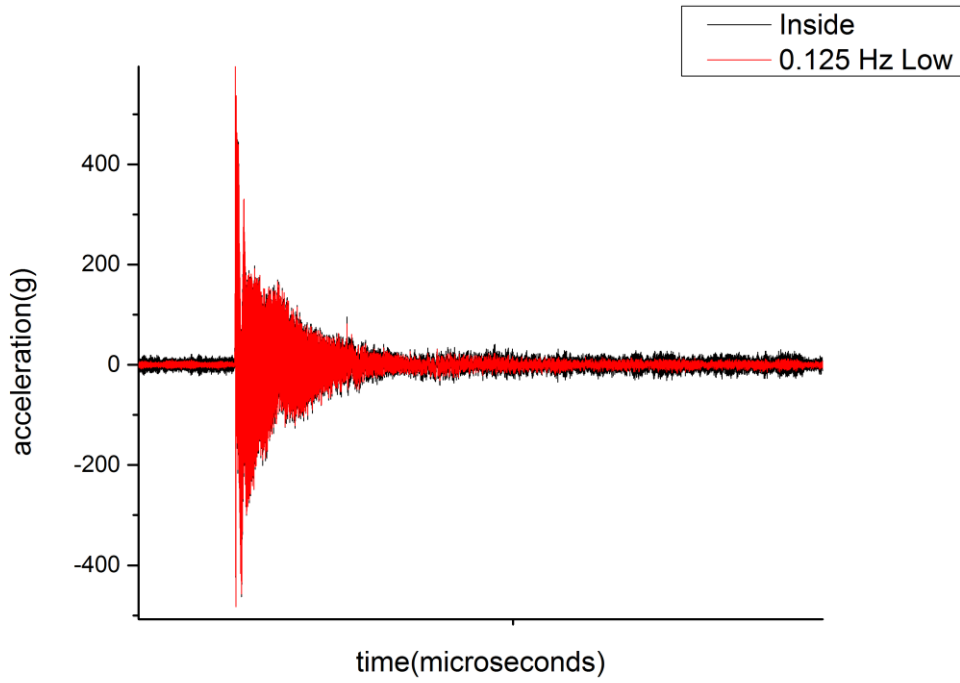


**Figure D.49** 1559 acceleration versus time of shot.

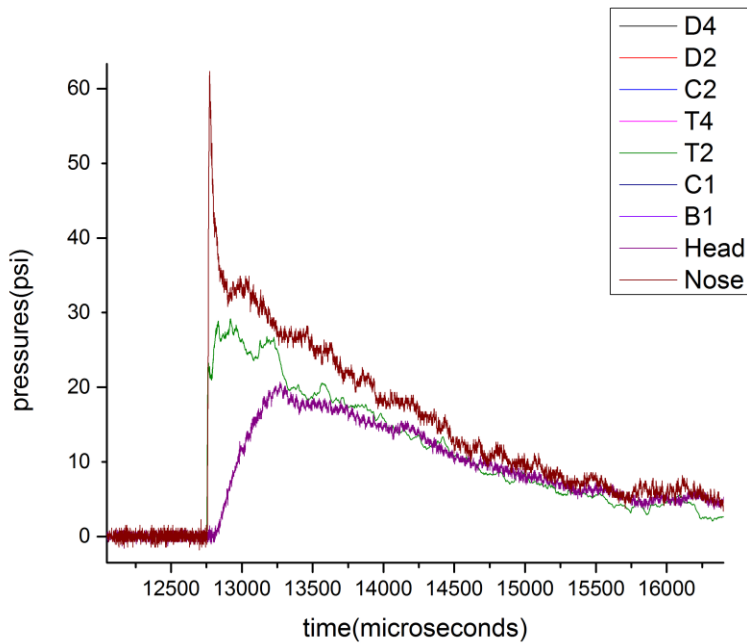


**Figure D.50** 1559 pressure versus time of nose, head and incident sensors.



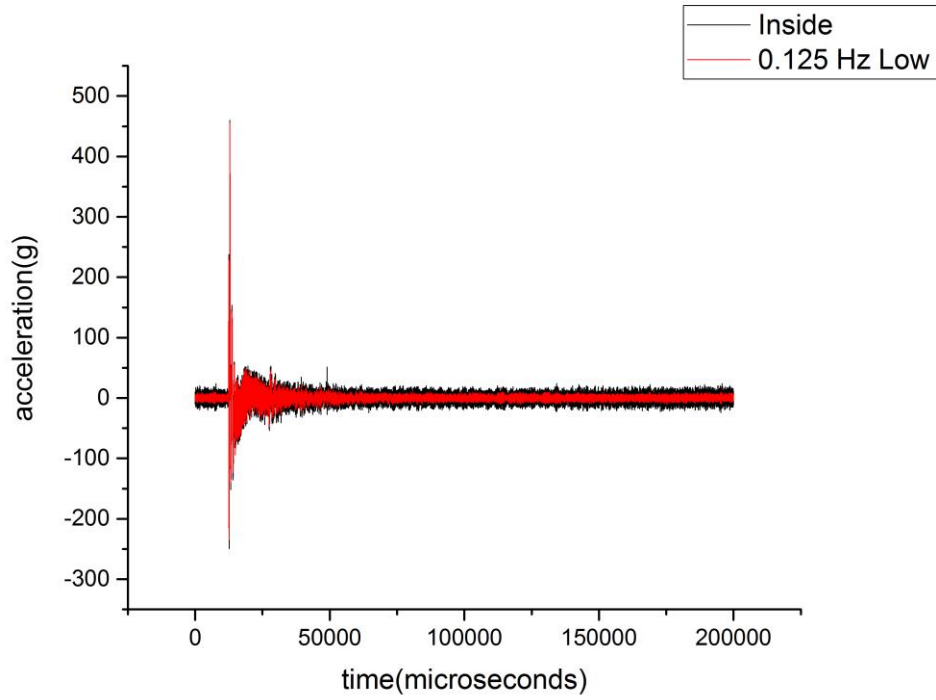


**Figure D.51** 1560 acceleration versus time of shot.

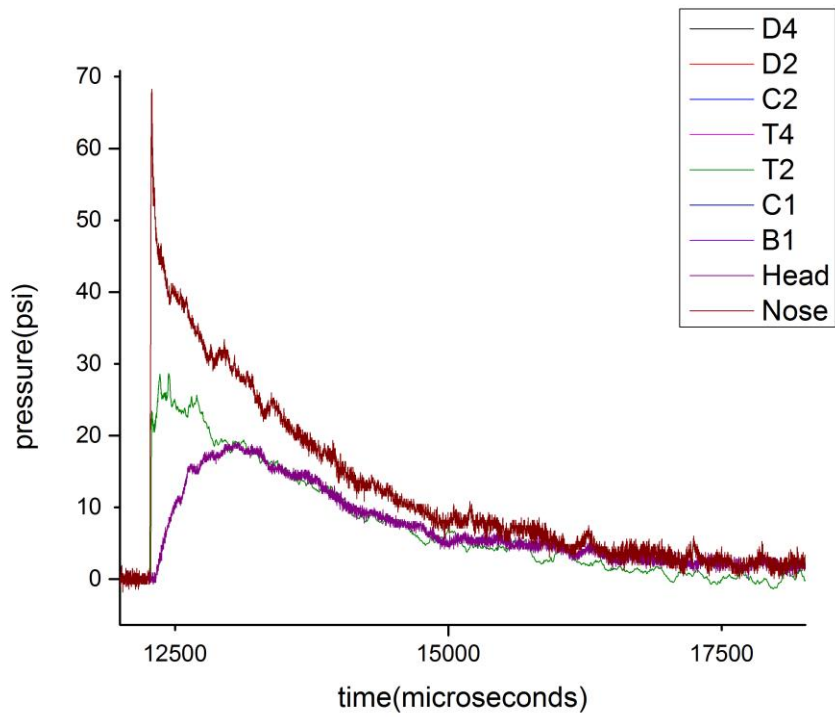


**Figure D.52** 1560 pressure versus time of nose, head and incident sensors.

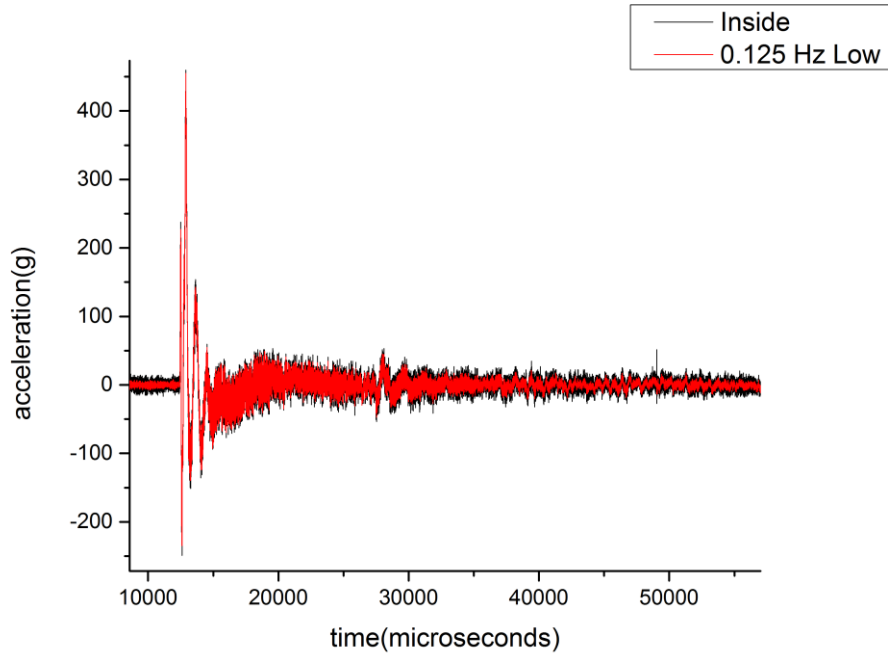


**Figure D.53** 1561 acceleration versus time of shot.

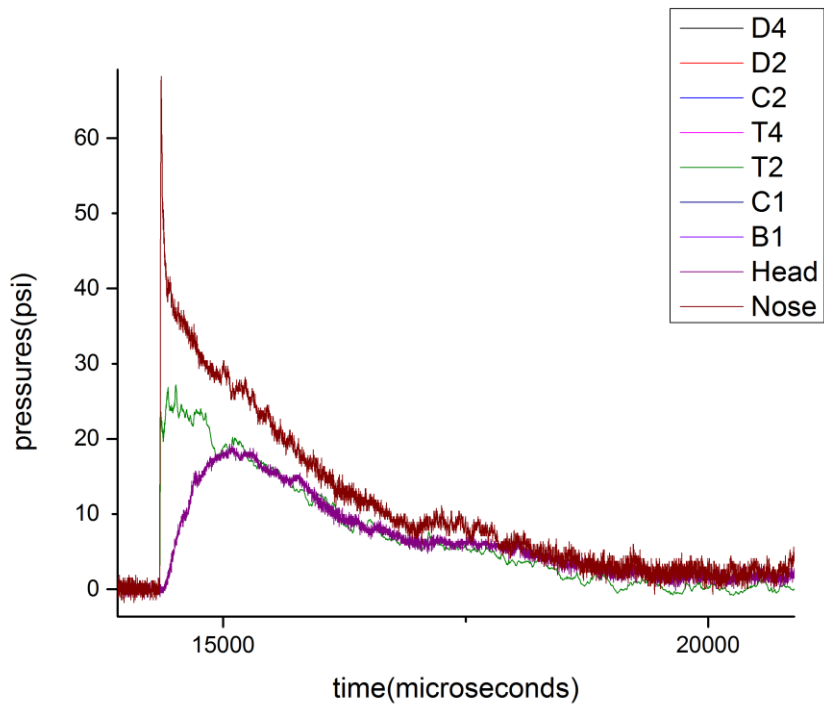


**Figure D.54** 1561 pressure versus time of nose, head and incident sensors.

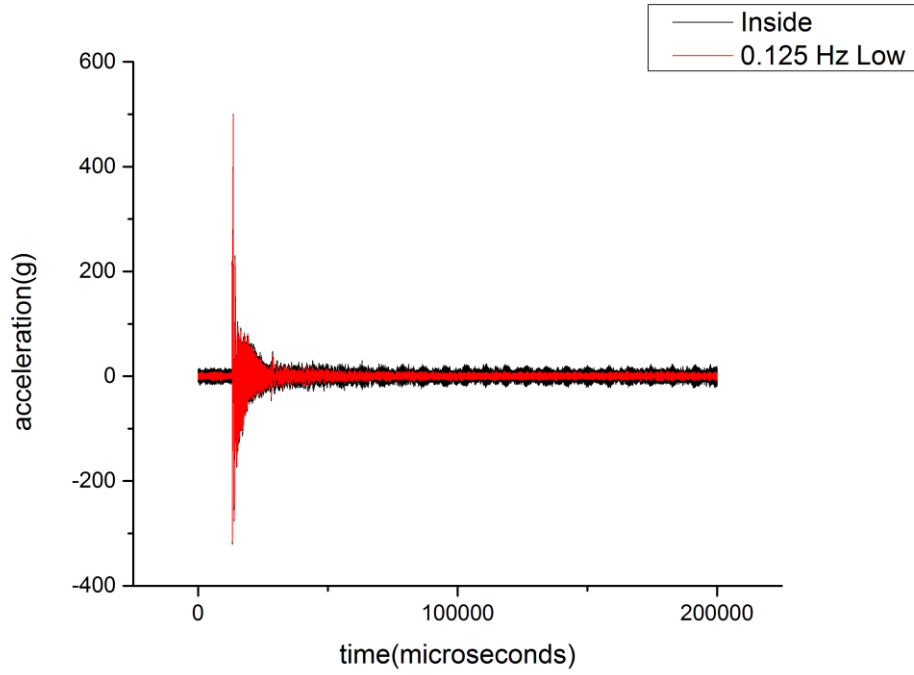


**Figure D.55** 1562 acceleration versus time of shot.

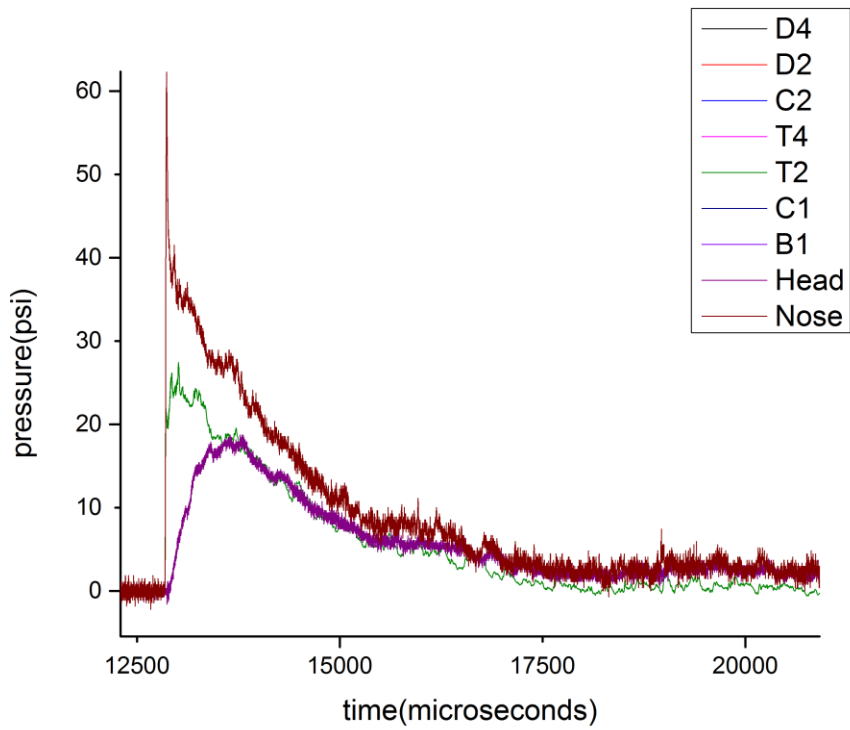


**Figure D.56** 1562 pressure versus time of nose, head and incident sensors.

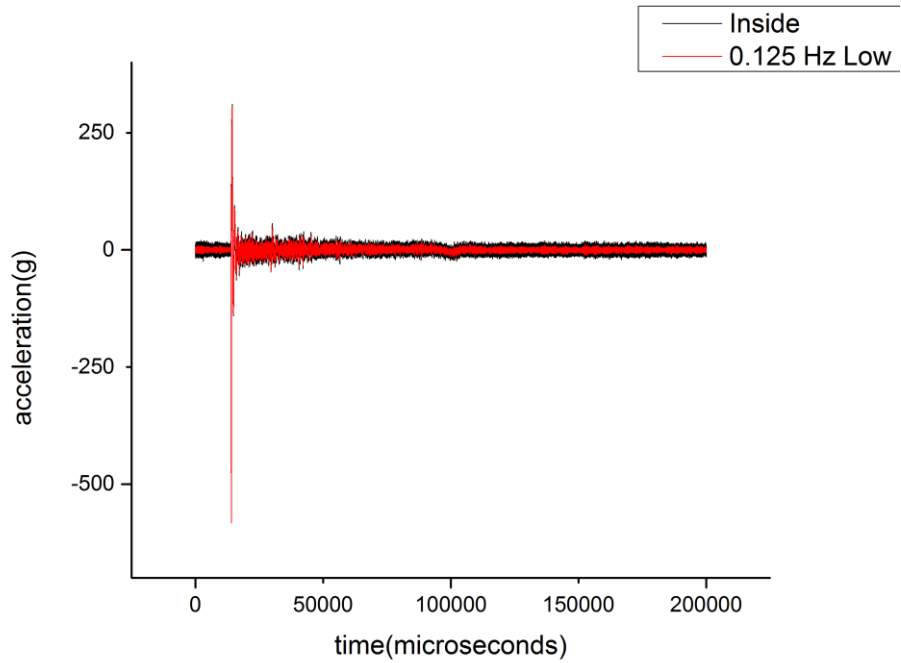


**Figure D.57** 1563 acceleration versus time of shot.

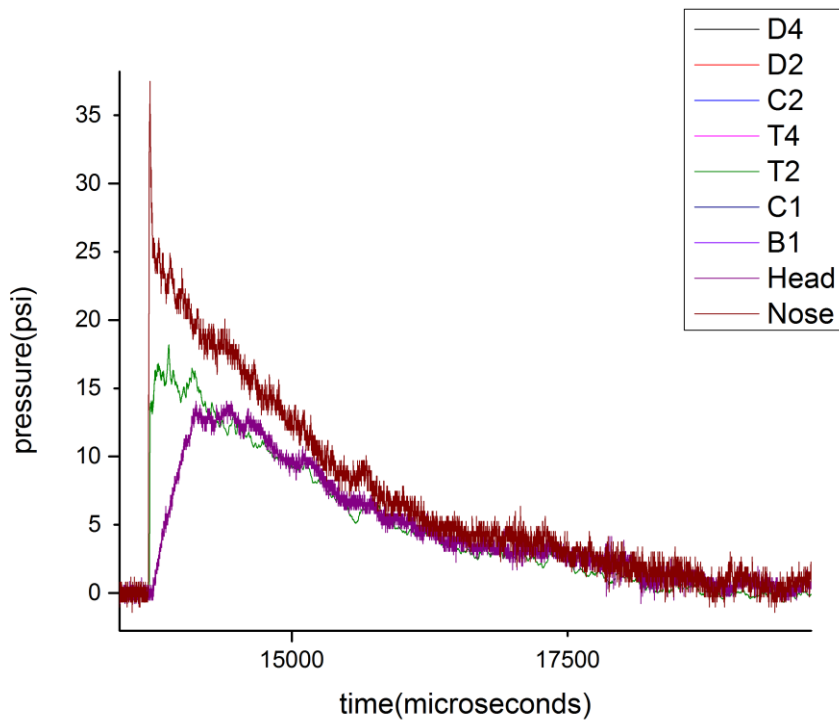


**Figure D.58** 1563 pressure versus time of nose, head and incident sensors.

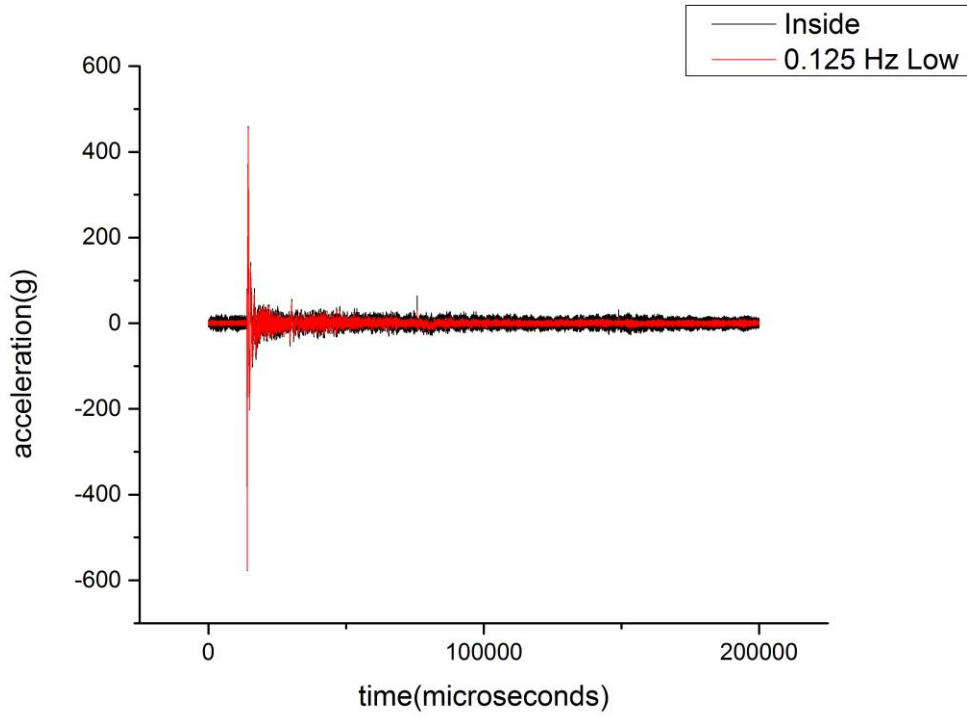


**Figure D.59** 1564 acceleration versus time of shot.

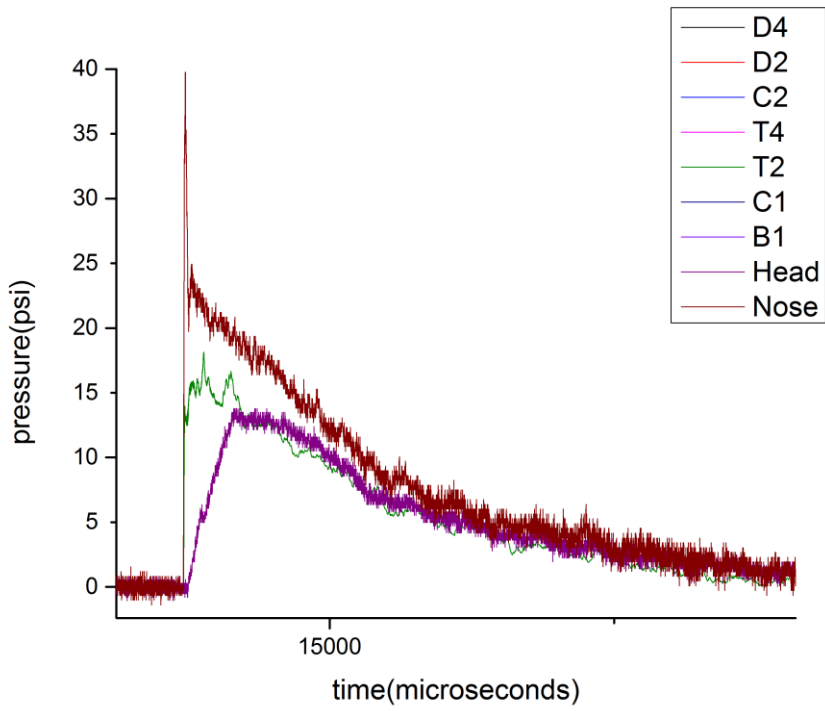


**Figure D.60** 1564 pressure versus time of nose, head and incident sensors.

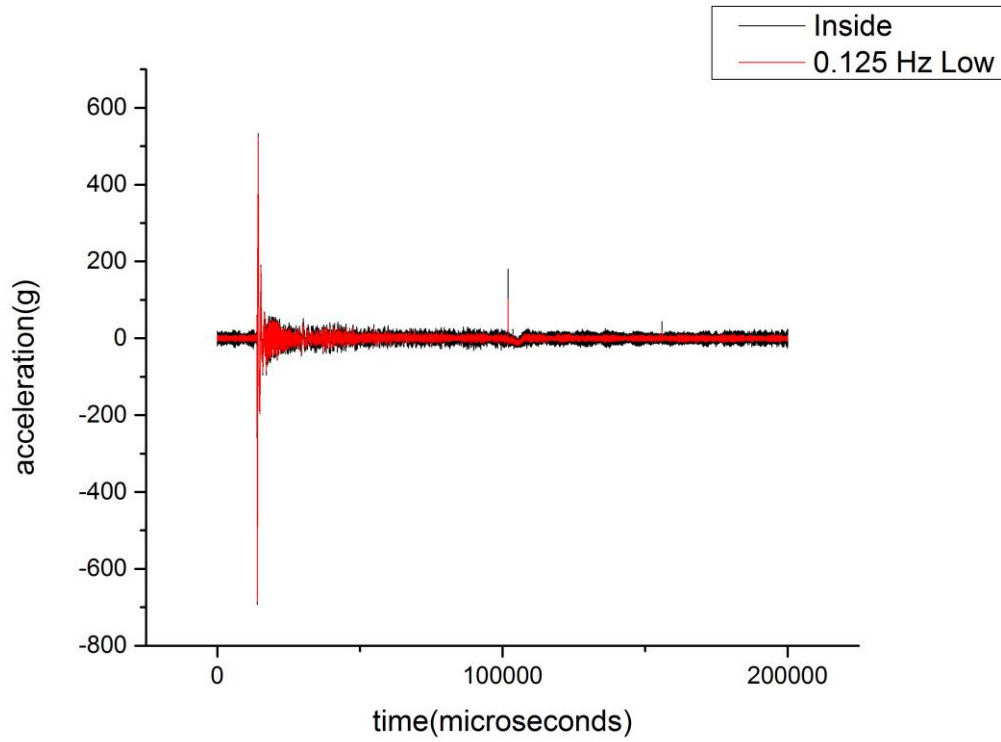


**Figure D.61** 1565 acceleration versus time of shot.

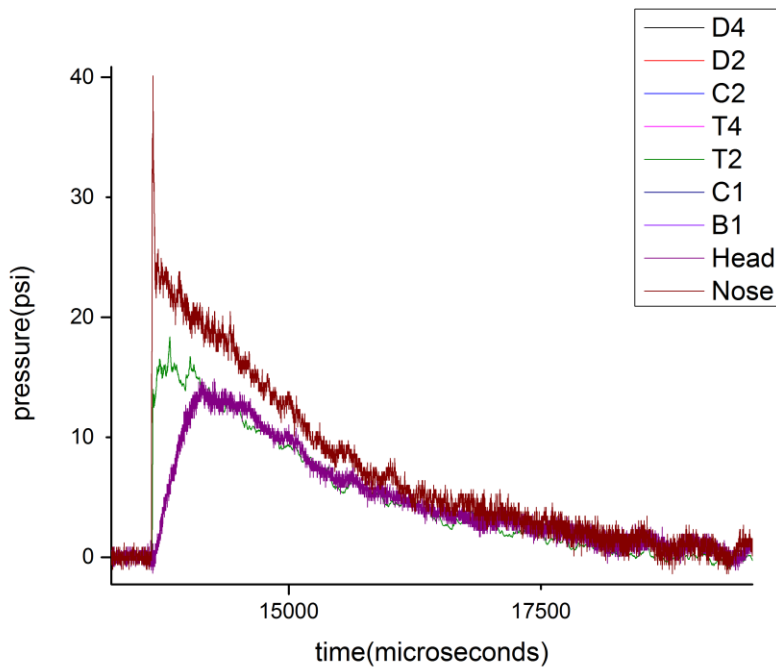


**Figure D.62** 1565 pressure versus time of nose, head and incident sensors.

## REFERENCES

- Budde, M. D., et al. "Primary blast traumatic brain injury in the rat relating diffusion tensor imaging and behavior." *Frontiers in Neurology* (2013): 1-12.
- Cernak, I. "The importance of systemic response in the pathobiology of blast-induced neurotrauma." *Frontiers in neurology* (2010): 1-9.
- Chandra, N. and A. Sundaramurthy. "Acute Pathophysiology of Blast injury." Kobeissy, Firas H. *Brain Neurotrauma: Molecular, neuropsychological and rehabilitation aspects*. Newark, NJ: CRC Press, 2014. 1-114.
- D'Agostino, R. B, Lisa M Sullivan and A. S. Beiser. *Introductory Applied Biostatistics*. Belmont, CA: Brooks/Cole Cengage Learning, 2006.
- DePalma, R. G., et al. "Blast Injuries." *The New England Journal of Medicine* (2005): 1335-1342.
- Elder, G.A and A. Cristian. "Blast-related mild traumatic brain injury: mechanisms of injury and impact on clinical care." *Mount Sinai Journal of Medicine* (2009): 111-8.
- Endevco. "Model 7264C Piezoresistive accelerometer." n.d.  
<https://www.endevco.com/product/prodpdf/7264C.pdf>. 2015.
- Kinney, G. F. and K. J. Graham. *Explosive Shocks in Air*. New York: Springer Science + Business Media, 1985.
- Kulite. "Miniature Leadless Pressure Transducer XCL-072 series." n.d.  
[http://www.kulitesensors.com.cn/pdf\\_Data\\_Sheets/XCL-072.pdf](http://www.kulitesensors.com.cn/pdf_Data_Sheets/XCL-072.pdf). 10 11 2015.
- . "Short Length Pressure Transducer XCL-152 Series." 2015.  
<http://www.kulite.com/docs/products/XCL-152.pdf>. 11 10 2015.
- Liu, L. and P.D. Katsabanis. "Development of a continuum damage model for blasting analysis." *International Journal of Rock Mechanics and Mining Sciences* (February 1997): 217-231.
- Ahlers, S.T., Vasserman-Stokes, E., Shaughness, M. C., Hall, A. A. , Shear D.A., Chavko M., McCarron R.M., Stone J.R. "Assessment of the effects of acute and repeated exposure to blast overpressure in rodents: toward a greater understanding of blast and the potential ramifications for injury in humans exposed to blast." *Frontiers in Neurology* (2012): 1-32.
- Seitz, M. W. and B. W Skews. "Effect of Compressible Foam Properties on Pressure Amplification During Shock Wave Impact." *Shock Waves* (July 2006): 177-197.
- Smooth-On. "OOMOO Series 1A:1B mix by volume silicone rubber." n.d.  
[http://www.smooth-on.com/tb/files/OOMOO\\_25\\_30\\_TB.pdf](http://www.smooth-on.com/tb/files/OOMOO_25_30_TB.pdf).

Sundaramurthy, A. and Chandra, N. "A parametric approach to shape field-relevant blast wave profiles in compressed-gas-driven shock tube." *Frontiers in Neurology* (2014): 1-10.

UMassAmherst Biology Department. "Rat Dissection Protocol." n.d.  
<http://bcrc.bio.umass.edu/intro/content/rat-dissection-protocol>.

Witkiewicz, W. and Andrzej Zielinski. "Properties of the Polyurethane (PU) light foams." *Advances in Material Science* (2006): 35-51.